Computer Simulations of the Structure, Stability and Phase Transitions of Diatomic Molecules Physisorbed on Ionic Surfaces: the CO/MgO(001), N_2/MgO(001) and N_2/NaCl(001) Systems

Abdulwahab K. Sallabi

A Thesis

in

The Department

of

Physics

Presented in Partial Fulfillment of the Requirements
for the Degree of Doctor of Philosophy at
Concordia University
Montréal, Québec, Canada

January 2002

ABSTRACT

Computer Simulations of the Structure, Stability and Phase Transitions of Diatomic Molecules Physisorbed on Ionic Surfaces: the CO/MgO(001), N_2/MgO(001) and N_2/NaCl(001) Systems

Abdulwahab K. Sallabi, Ph.D
Concordia University, 2002

Metropolis Monte Carlo simulations, using semiempirical potentials, are performed to study the structures, stability, and phase transitions of layers of CO and N_2 molecules physisorbed on the MgO(100) surface as well as a monolayer of N_2 physisorbed on NaCl(001) surface.

In agreement with experiments [35-37], our simulations show that the $c(4\times2)$ structure of CO on the MgO(001) surface is the most stable structure below 41 K. The unit cell contains three CO molecules; two bridging molecules tilted in opposite directions by the same polar angle of 31° with respect to the surface normal and a third molecule perpendicular to the surface. At 41 K the $c(4\times2)$ phase undergoes a transition into a less dense disordered phase accompanied by the desorption of some molecules. The density of this disordered phase is the same as for the $p(3\times2)$ phase. A model to compare the stability of the $c(4x2)$ and the $p(3\times2)$ phases is constructed and suggests that at sufficiently high pressures and temperatures the $p(3\times2)$ phase is more

stable than the c(4×2) phase as found by Panella *et al.* [35] . We propose that a sequence of transitions to a set of (n×2) structure with ever decreasing density is possible under suitable conditions of temperature and pressure. This sequence of transitions is an example of the devil's staircase phenomenon as has been suggested by LEED experiments.

Nitrogen molecules adsorbed on MgO(001) were studied and were also found to form a sequence of structures. A $\left(\sqrt{13}\times\sqrt{13}\right)R33.7^{\circ}$ structure is found to form the most stable phase at low temperatures (below 20 K). This structure undergoes a phase transition into a less dense phase at 20 K and in all likelihood evolves into the less dense $\left(\sqrt{25}\times\sqrt{25}\right)R36.9^{\circ}$ structure. The $\left(\sqrt{25}\times\sqrt{25}\right)R36.9^{\circ}$ structure is stable up to 25 K. These results are in agreement with HAS results. This system might also prove to be an example of the devil's staircase phenomena.

A monolayer of nitrogen molecules adsorbed on an NaCl(001) surface are used to test the validity of the theory of critical phenomena and its applicability to molecular systems. The simulations predict that this system undergoes a continuous order-disorder transition near 25 K with a logarithmically divergent heat capacity. The values of the critical exponents for the order parameter and susceptibility are calculated and found to deviate significantly from the Ising values but still satisfy

Rushbrooke's scaling law. This behaviour is typical of the universality class containing the XY model with cubic anisotropy where the critical exponents are functions of the anisotropy and are thus "nonuniversal".

ACKNOWLEDGMENTS

I wish to express my gratitude to my supervisor, Prof. David Jack, for his continual encouragement and precious guidance during the course of this study. This wok became much easier with his support and friendship.

I would like to express my thanks to Prof. Marina Frank for her support and encouragement.

I would like also to thank Nuria and Fatma for their support and patience

I am also grateful to Thanh Vu, Amine Benrehbouh and Jamal Dawoud who were always available to provide assistance and helpful discussions. I would like also to thank all the people whom I had the chance to work with them during my study in Concordia University.

To my parents,

my wife

and my daughter Fatma

Contents

List of Figures

List of Tables

Special Symbols

T	absolute temperature
T_c	transition temperature
t	reduced temperature
C	heat capacity
α	heat capacity critical exponent
Φ	order parameter
β	order parameter critical exponent
χ	susceptibility
γ	susceptibility critical exponent
ν	correlation length critical exponent
N	number of molecules
$L \times L$	size of a system
h_4	anisotropy strength
LEED	low energy electron diffraction
HAS	helium atom scattering
PIRS	polarization infrared spectroscopy
q	charge
e	electron
MC	Monte Carlo simulations
r	distance
q_{st}	isosteric heat of adsorption
k_B	Boltzmann constant

E_o	binding energy to the surface for a single molecule
μ	molecular dipole moment
Θ	quadrupole moment
Ω	octupole hexadecapole moment
Λ	hexadecapole moment
r_i	distances of the point charge at site i from the origin
q_i	point charges at site i
μ_i	point dipoles at site i
α_1	dipole polarizabilities
α_2	quadrupolar polarizability
A_{ij}	the Born-Mayer parameter (strength of the repulsion)
η_{ij}	the Born-Mayer parameter (range of the repulsion)
C_n	dispersion constants (n=6, 8, 10)
$\psi(\vec{r}_i)$	surface electrostatic potential
$\vec{E}(\vec{r}_i)$	electric field generated by the ionic surface
$\alpha_i^{\perp}$	perpendicular atomic polarizabilities
$\alpha_i^{\parallel}$	parallel atomic polarizabilities
θ	polar angle
φ	azimuthal angle.
ξ	random number
$C(\tau)$	autocorrelation function for a number τ of steps

U_L	Binder fourth order cumulant
Z_c	height of a C atom above the MgO(001) surface.
ΔG	difference in free Gibbs energy
A'	surface area covered by the film
μ'	chemical potential of the film which is in equilibrium with the gas reservoir above the surface,
$\tilde{\gamma}_j$	surface tension and N_j is the number of
Ξ	grand partition function
$\tilde{\gamma}^0$	surface tension of the clean surface
P_i^*	half coverage pressures P_i^*
m	mass of the molecule
I	the moment of inertia
h	Planck's constant
d	spatial dimension
WMIN	computer program (Crystal energy minimization program)
$V_{ij}^{(elc)}$	electrostatic energy
$V_{ij}(r_{ij})$	Potential energy between two sites i and j
V_{elc}^{m-s}	electrostatic energy between a molecule and the ionic surface

1. Introduction

The experimental and computational studies of adsorbed layers on various solid surfaces have been shown to provide a great deal of understanding of the fundamental processes in surface science such as the theory of interactions of gases with solid surfaces [1][2], orientational ordering of adsorbed layers, e.g. diatomic molecules on graphite [3][4][5], thin films on solid surfaces [6], surface diffusion [7], surface aligned photochemistry [8][9], phase transitions and critical phenomena, *e.g.* ^{4}He on graphite [10][11], ^{4}He on Kr-preplated graphite [12], and the structures and dynamics of molecules on ionic surfaces [13].

A wealth of information on structures (position and orientation) and phase transitions of adsorbed layers of molecules on solid surfaces at low temperatures have been made available by various experimental techniques such as low energy electron diffraction (LEED)[14] and helium atom scattering (HAS)[15][16]. These techniques provide information on the translational ordering (positions) of the adsorbed molecules through the presence of symmetries in diffraction spectra patterns. Knowledge of the orientations of adsorbed molecules can be obtained from polarization infrared spectroscopy (PIRS)[17], which is known to be sensitive to the orientations of the adsorbed molecules. Calorimetric experiments have

been used to study a variety of phase transitions in two dimensions (2D) through measurements of the heat capacity [18][19].

Parallel to the experimental techniques, computer simulations have been accepted as a useful tool in determining additional details of the structures of adsorbed molecules. Thus they help in understanding physics at surfaces [20][21], and have been used to substantiate and interpret experimental results [22-26]. Furthermore, computer simulations can be used to predict additional results and guide experiments to perform more experimental work [5][27]. The most widely known techniques in computer simulation are the Metropolis Monte Carlo (MC) [26-29] and Molecular Dynamics (MD) methods [21].

In this thesis the computer simulations using the Metropolis Monte Carlo method are performed to study the structures, stabilities and phase transitions of N_2 molecules physisorbed on an MgO(001) and NaCl(001) surfaces, as well as the CO molecules physisorbed on MgO(001) surface. This will shed some light on the many issues raised in previous experimental work on these systems [30-38]. The N_2/MgO and CO/MgO systems are of further interest because they may be considered as a realization of the so-called devil's staircase phenomenon [39-40].

Before any further review of the history and development of these systems we should discuss some of the general ideas of surface science and phase transitions in two dimensions (2D).

1.1 Adsorption

Adsorption can be most simply defined as the accumulation of atoms or molecules of a material at the surface of another material. When molecules are adsorbed on a solid surface the solid is referred to as the adsorbent and the adsorbed molecules as the adsorbate. The most important physical quantity that can be used to classify the adsorption phenomena is called the binding energy or "adsorption energy", which is defined as the energy liberated when a molecule strikes the surface and sticks on it. Generally, adsorption is classified as either physisorption (physical adsorption) or chemisorption (chemical adsorption), depending on the nature of the interactions involved [40-43].

Chemical adsorption usually involves the transfer of electrons between the molecules (adsorbate) and the surface (adsorbent), which leads to the formation of a chemical bond between the surface and the molecule or atom that strikes the surface. In this case the adsorbed molecule might not retain its identity. The binding energies in chemisorption processes are typically between 100 kJ/mol to 500 kJ/mol. Due to the chemical change in a chemical adsorption process,

one usually considers chemisorption to be irreversible and either a rapid or slow process like any chemical reaction. Because of the necessity to form chemical bonds between adsorbate and substrate, chemical adsorption leads only to the formation of a monolayer of adsorbed particles on the substrate. Carbon dioxide (CO_2) adsorbed on W(100), which has a binding energy of 456 kJ/mol [45], is an example of chemical adsorption.

In physical adsorption there is no sharing of electrons between adsorbate and substrate (surface) and thus there is no chemical bond between adsorbed molecules and the surface. Instead of chemical bonds, van der Waals and electrostatic forces dominate adsorbate-substrate interactions. Physisorption processes occur very rapidly even at very low temperatures. This kind of adsorption is regarded to be reversible. Physical adsorption may lead to the formation of multi-layers of adsorbed molecules on the substrate. In physical adsorption the binding energy is typically less than 50kJ/mol. The CO/LiF(001) [27], CO_2/NaCl(001) [25] and N_2/MgO(001) [34] systems are examples of physical adsorption as indicated by Secondary Ion Mass Spectroscopy, which shows that there is only a negligible chemical reaction of the ionic surfaces with any of constituents of air (N_2, O_2 and CO) [46]. In this thesis we will be concerned with physical adsorption.

1.2 Surface crystallography

1.2.1 Substrate crystallography

Solids are made up of particles arranged in a regular repeating geometrical patterns. The smallest section of the pattern that holds all the basic information about a given arrangement of points in a lattice is called the unit cell. The primitive surface unit cell is the smallest geometrical shape that can be used by repeating its translation, to construct the ordered arrangement of the entire surface. The unit cell's shape, size and symmetry can conventionally be defined using two vectors $\mathbf{b}_1$ and $\mathbf{b}_2$ along two sides of the unit cell and have a common origin as shown in Fig. 1.1.

Ionic crystalline solids have ions occupying the lattice points in the crystal, and are primarily held together by electrostatic forces. The fcc(001) surface of a cubic crystal has 4-fold rotational symmetry and its primitive unit cell is square in shape.

1.2.2 Overlayer crystallography

Many atoms and molecules form ordered layers (adlayers) on a surface at certain temperatures. These layers may be commensurate (well-defined relationship to substrate structure) or incommensurate (adsorbate structure independent of substrate) [40][47].

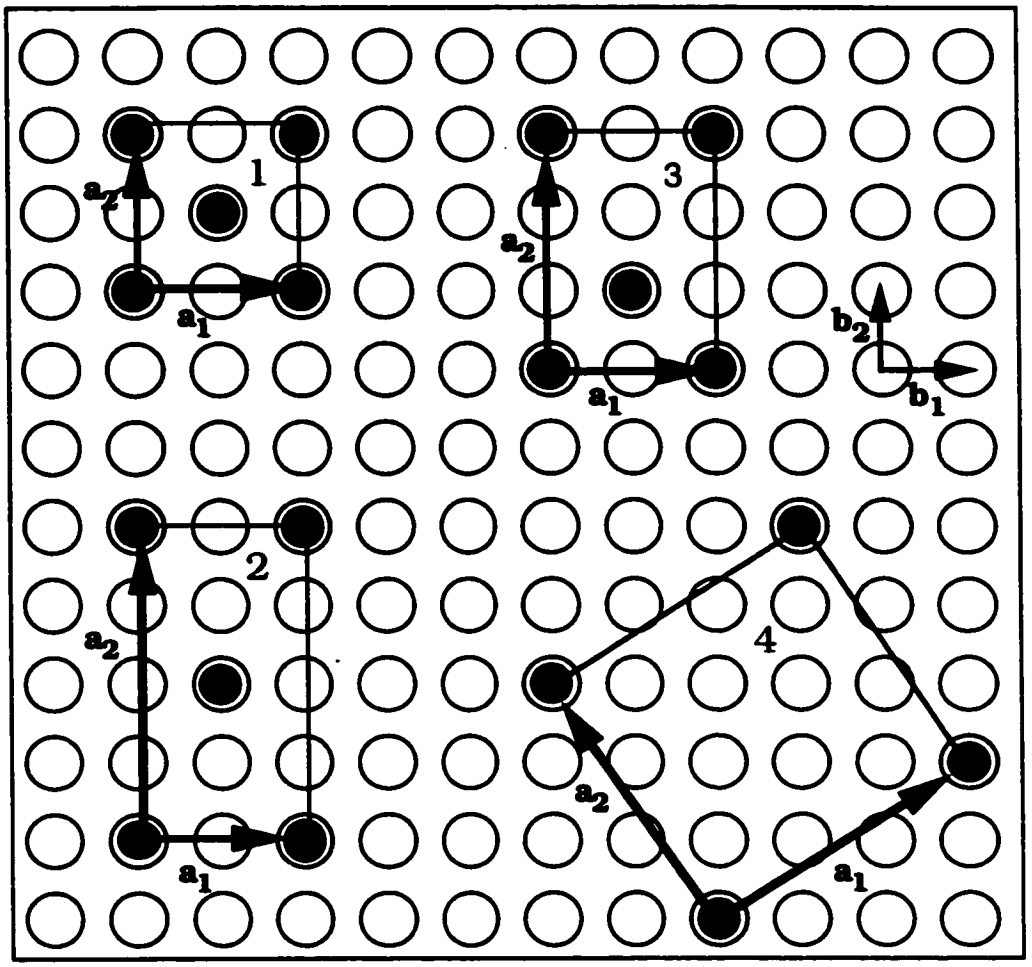

1) $c(2\times2)$
2) $c(4\times2)$
3) $p(3\times2)$
4) $\left(\sqrt{13}\times\sqrt{13}\right)R33.7^{\circ}$

Figure 1.1. Several unit cells and arrangements of adsorbed molecules on (001) face of ionic surfaces. The unit cell of the substrate is described by two vectors $\mathbf{b}_1$ and $\mathbf{b}_2$, while the adsorbate unit cell is defined by two vectors $\mathbf{a}_1$ and $\mathbf{a}_2$.

The same ideas in section 1.2.1 can be used to describe and define the structures of ordered overlayers of adsorbed molecules. The overlayer adsorbate unit cell is conventionally defined by the two vectors $\mathbf{a}_1$ and $\mathbf{a}_2$, where $\mathbf{a}_2$ is selected to be anticlockwise from $\mathbf{a}_1$. Wood's

notation defines the geometry of the overlayer structures in terms of the surface primitive unit cell, where the lengths of $\mathbf{a}_1$ and $\mathbf{a}_2$ are given as simple multiples of $\mathbf{b}_1$ and $\mathbf{b}_2$ respectively as follows ($|\mathbf{a}_1|/|\mathbf{b}_1| \times |\mathbf{a}_2|/|\mathbf{b}_2|$) i.e. a (2 x 2) structure has $|\mathbf{a}_1| = 2|\mathbf{b}_1|$ and $|\mathbf{a}_2| = 2|\mathbf{b}_2|$. This is followed by the angle of rotation of $\mathbf{a}_1$ from $\mathbf{b}_1$ (if this is non-zero). In Fig. 1.1 we show several possible structures of adsorbates overlayer on an fcc(100) surface [48][49].

1.3 Two dimensions phase transitions

The structures of adsorbed molecules on solid surfaces are governed by the competition between the laterally directed and orientationally dependent molecule-molecule interactions and the molecule-surface interactions. Molecule-molecule interactions try to force the molecules to adopt their natural bulk structure, while the molecule-surface interactions tend to force the molecules to occupy the favored adsorption sites.

The stability of the layer structures and the occurrence of possible phase transitions in these structures depends on the competition mentioned above and many other physical conditions *i.e.* ratio of the lattice constants of the substrate and the adsorbate, symmetries of the adlayer structures, coverage, surface temperature and spreading pressure. At low temperatures molecules may form well ordered phases

on solid surfaces. The degree of order can be measured by an order parameter, Φ, where the order parameter is equal to one when the system is very well ordered at low temperatures. If the temperature is increased the system will stay ordered until a certain temperature where the system becomes disordered. The order parameter will equal zero when this phase becomes fully disordered. This kind of change is called an order-disorder phase transition and takes place at the transition temperature T_c, which is also called the critical temperature [24][28].

The phase transitions are classified into two kinds, first order phase transition and second order or continuous phase transitions. In the first order transitions the order parameter is discontinuous at the transition temperature T_c. In general, there is a finite discontinuity in one or more of the first derivatives of the known thermodynamic quantities such as energy or order parameter. In the case of second order phase transitions the order parameter goes to zero continuously, and the first derivatives of the thermodynamic quantities such as energy and order parameter are continuous but the second derivatives are discontinuous [24].

The theories that describe phase transitions such as the devil's staircase phenomena and the theory of critical phenomena are summarized below.

1.3.1 Devil's staircase phenomena

Aubry [39] introduced this concept to describe structural phase transitions. According to this concept any incommensurate structures can be approximated by a "lock-in" high order commensurate (HOC) structures with a large unit cell. This commensurate unit cell contains several atoms/molecules. Some of these adsorbed atoms/molecules will be adsorbed on top of preferential adsorption sites, therefore these HOC structures will be energetically favored over any incommensurate structure [50].

Depending on the corrugation of the surface, the phase diagram will consist of several HOC phases if the corrugation is sufficiently large. The unit cell constant of these phases passes through a discrete series of commensurate values within a sequence of phase transitions from one HOC phase to the other. Such a phenomena is called the devil's staircase and it arises from the competition between the molecule-molecule and the molecule-surface interactions [35].

There are few experimental realizations for this phenomena and these are limited to rare-gases adsorbed on solid surfaces [50]. In molecular systems the devil's staircase phenomena results from the coupling of the translational and orientational changes. Recently, the

CO/MgO(001) system was suggested to be an example of this phenomena [35].

1.3.2 Order disorder phase transitions

1.3.2.1 Critical Phenomena

Critical phenomena are those phenomena observed in continuous transitions within the region around the critical temperature.

1.3.2.2 Critical exponents and their direct measurement

Suppose that the behaviour of some thermodynamic quantity such as order parameter, heat capacity or susceptibility can be described by a function $F(t)$ in terms of the reduced temperature, $t = 1 - T/T_c$, where T is the temperature and T_c is the critical transition temperature. A critical exponent δ associated with the function F(t) is the limit of $\ln[F(t)]/\ln(t) \approx \delta$ as $t \to 0$, and hence $F(t) \sim t^{\delta}$ [51-52]. The critical exponents related to the work of this thesis are α, β and γ, which govern the critical behavior of the specific heat, order parameter, and susceptibility respectively. From the above definition of the critical exponents the divergences of the heat capacity, order parameter and susceptibility typically follow a power law near the critical point.

The heat capacity diverges at the critical temperature T_c, according to

$$C = A^{\pm} t^{-\alpha} + [\text{less singular part}] \qquad (1.1)$$

where $A^{\pm}$ are the nonuniversal (their values differ from one system to another) amplitudes above (+) and below (-)the transition temperatures. The value of the ratio of the amplitudes A^{+} / A^{-} is, however, universal.

Below the critical temperature the order parameter disappears as follows,

$$\Phi = Bt^{\beta} \qquad (1.2)$$

where B is the amplitude. Above T_c, the order parameter is zero.

The susceptibility, χ, calculated from the fluctuations of the order parameter has a critical exponent, γ, also diverges at T_c, *viz.*

$$\chi = H^{\pm} t^{-\gamma} \qquad (1.3)$$

where $H^{\pm}$ are the amplitudes of the susceptibility above and below the transition temperature.

To directly measure these critical exponents, the data of the thermodynamic quantity of interest, such as the heat capacity or the order parameter, is fitted to the suggested asymptotic power law form. By plotting on a logarithmic scale (*i.e.* log-log plot) the data of the quantity versus the reduced temperature "t", we will get a straight line.

The slope of this straight line is then the critical exponent associated with the plotted quantity.

1.4.2.3 Exponent relations: The scaling laws

The critical exponents α, β, γ, and ν are not all independent. According to Rushbrooke, these exponents are related to each other via the following inequality

$$\alpha + 2\beta + \gamma \geq 2 \qquad \text{for } T<T_c \tag{1.4a}$$

as derived from general thermodynamic considerations [51-53]. Furthermore, Josephson's hyperscaling [51-53] law relates the spatial dimension d (at a solid surface $d = 2$) and critical exponents as follows

$$d\nu \geq 2 - \alpha \tag{1.4b}$$

If the scaling hypothesis holds these relations are satisfied as equalities.

1.4.2.4 Finite size scaling hypothesis: data collapse

Systems studied by computer simulations are limited to finite sizes, whereas the sizes of real systems in real experiments are much larger and effectively infinite. These finite systems in computer simulations cause the phase transition temperature to be shifted from its position in the case of real systems (thermodynamic limit) and leads to the rounding of thermodynamic quantities, *e.g.* the heat capacity. The shift and rounding in finite systems limits, and sometimes prevents, us from determining accurate values of the critical exponent. To overcome

this problem the finite size scaling hypothesis was developed. One of the consequences of this hypothesis is the invariance of certain quantities at the transition temperature T_c of the infinite system. In particular, the transition temperature T_c can be obtained correctly by using the fourth order Binder cumulant [26], which will be discussed in details in chapter 3.

The finite size scaling hypothesis has been developed to show how the measured quantities vary with the size (L) of the studied system, where in a 2-D system the number of particles is $N=L^2$. Knowledge of this behaviour allows one to extract accurate values of the critical exponent. Near the transition temperature T_c the following relations for the order parameter $\Phi(T,L)$ and susceptibility $\chi(T,L)$ are expected to be valid [26],

$$\Phi(T,L) = L^{-\beta/\nu}\hat{f}[(T-T_c)L^{1/\nu}] \qquad (1.5)$$

$$\chi(T,L) = L^{\gamma/\nu}\hat{g}[(T-T_c)L^{1/\nu}] \qquad (1.6)$$

where the functions $\hat{f}$ and $\hat{g}$ are called scaling functions.

The scaling of the order parameter can be done by plotting $(1-T/T_c)L^{1/\nu}$ versus $\Phi(T,L)L^{\beta/\nu}$. If the transition temperature T_c is correct and the exponents β and ν are well chosen then the data for various

system sizes will collapse onto a single curve determined by the scaling functions $\hat{f}$.

The finite size scaling analysis for the susceptibility can be done by plotting $(1-T/T_c)L^{1/\nu}$ versus $\chi(T,L)L^{-\gamma/\nu}$. Again, if T_c, γ and ν are well chosen then the data for various system sizes will collapse onto a single curve.

1.4.2.5 Universality

What makes the critical exponents interesting is the idea of universality. The critical exponents are found to be independent of the details of the interatomic interactions. According to the idea of universality, the critical exponents of all systems that exhibit a continuous phase transition near the critical temperature can be grouped into a small number of universality classes. Within each universality class, the critical behavior is remarkably similar. In Table 1.1 the universality classes, which are related to the order-disorder phase transitions in two dimensions are presented.

As can be seen in Table 1.1, in two dimensional systems there is a symmetry class whose critical exponents have nonuniversal values [54-56]. The values of the exponents in this class depend on the strengths of an anisotropic external potential h_4. In the N_2/NaCl(001) system this

anisotropy is provided by the substrate and perhaps the molecule-molecule interactions. As shown in Fig. 1.2, for infinite anisotropy the Ising exponents are recovered whereas in the limit of zero anisotropy Kosterlitz-Thouless (K-T) behaviour occurs. For example, the critical exponent β, has a value of 0.125 for the Ising model (infinite anisotropy) and will increase towards infinity as K-T behaviour is approached at zero anisotropy.

Table 1.1 Universality classes and its critical exponents.

Universality class Exponent	Ising	XY with cubic anisotropy	3-state Potts	4-state Potts
α	O (log)	Non universal	1/3	2/3
β	1/8	Non universal	1/9	1/12
γ	7/4	Non universal	13/9	7/6

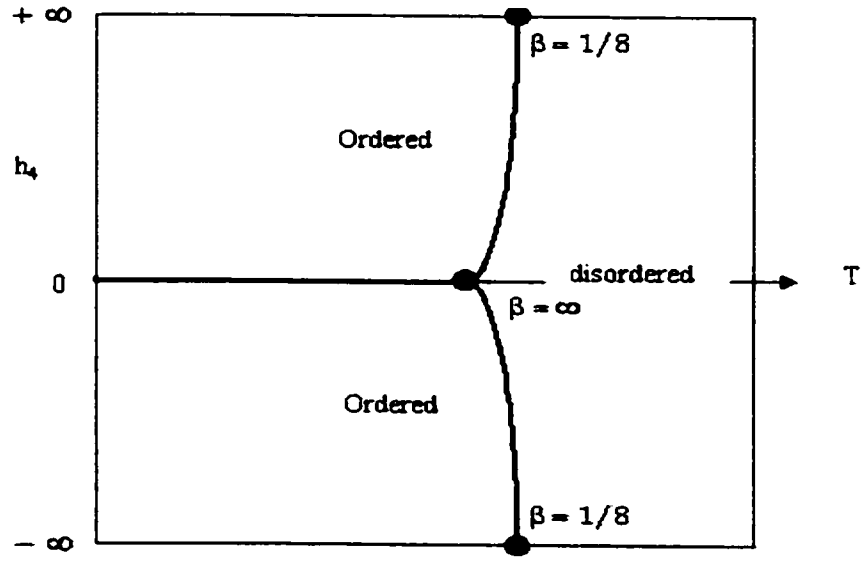

Figure 1.2. Phase diagram for the XY model in the h_4 –T plane shows how the critical exponent β varies with anisotropy strength h_4 (Ref. [54]).

1.4 Previous work on diatomic molecules adsorbed on ionic surfaces

Adsorption of atoms and molecules on a hexagonal surface such as graphite has received considerable attention in the past decades [57-60], as well as various ordered structures of molecules (N_2, CO,...) chemisorbed on surfaces such as Au, Ag *etc.* Molecules adsorbed on square ionic lattices have received less attention until recently [31][61]. Ionic surfaces, such as the MgO(001) surface, provide potential wells arrayed with square symmetry that are typically deeper than those on graphite [62], and with a periodic electric field that can strongly orient the admolecules and force them into structures not seen when only molecule-molecule interactions [34] are present. The interactions of the electric multipoles of the adsorbed molecules with the electric field generated by the ionic lattice of MgO(001) gives rise to a variety of ordered structures.

1.4.1 CO/MgO(001) system

Experimental studies show that CO molecules form ordered structures at low temperatures on a vacuum cleaved magnesium oxide (MgO(001)) crystal. The first experimental data on the structures and phase transitions of this system were reported by Panella *et al.*[33][35] where low energy electron diffraction (LEED) was used. The experiments were performed in the temperature range from 30 K to 55 K and at a CO

pressure of 1×10^{-7} mbar. From their data the authors concluded that the CO molecules form a $c(4\times2)$ ordered structure below 41 K. The $c(4\times2)$ phase was found to undergo a phase transition to a $p(3\times2)$ structure at 41 K. Above 51 K, this phase transforms by a series of phase transitions into a set of (n×2) structures, where n is an integer.

With helium atom scattering (HAS), Gerlach *et al.*[36] confirmed the $c(4\times2)$ structure observed by the LEED experiments [35]. They found that CO molecules form the $c(4\times2)$ pattern at temperatures between 35 K and 45 K. From phonon dispersion data, it is inferred that the unit cell of the $c(4x2)$ structure contains two types of CO adsorption sites with a ratio of 2:1. The experiment was performed at CO pressures of $>1\times10^{-8}$ mbar and $<1\times10^{-10}$ mbar. It was worth noting that this pressure is different from that of the LEED experiment [35]. It was found that, the $c(4\times2)$ phase undergoes a transition into a less dense (1×1) disordered structure at 45 K. Due to the desorption of some CO molecules during the transition and the observation that the phase transition was reversible only if gaseous CO was offered after the sample had been recooled to below the transition temperature, it was inferred that the (1×1) disordered phase has a density less than that of the $c(4x2)$ phase. It was proposed that the (1×1) disordered phase is a lattice gas in which the adsorbed CO molecules statistically occupy sites over top of the

magnesium cations but at a coverage less than that of the *c*(4×2) phase. The transformation of the *c*(4×2) phase into the *p*(3×2) or (n×2) phases, which had been observed by Panella *et al.*[35], was not observed in the HAS experiment. The authors mentioned that their HAS work was done at a pressure lower than that of Panella *et al.* [35] and speculated that this might be the origin of the discrepancy between the different methods. In other words the transformation of *c*(4×2) phase into different structures might be pressure dependent.

Knowledge of the orientation of the adsorbed CO molecules on MgO(001) in the unit cell was obtained by Heidberg *et al.* [37]. They performed polarization infrared spectroscopy (PIRS) experiments at a CO pressure of 5×10^{-9} mbar and temperatures above 36 K. The formation of a *c*(4×2) structure at temperatures below 45 K was indicated from the three p-polarized frequencies and a single s-polarized in the infrared spectra. These results corroborate the findings of Gerlach *et al.* [36] and Panella *et al.* [35] findings, where three CO molecules (6 in the full cell) in the primitive unit cell of the *c*(4×2) structure was suggested; one molecule perpendicular to the surface on top of the Mg^{2+} ion with the C atom down and two bridging molecules which are energetically equivalent and tilted with respect to the surface normal by 29° but are oriented in opposite azimuthal directions. When the *c*(4×2) phase is warmed up to 45 K, the infrared spectra shows only a single p-polarized

signal which is attributed to the transition into a (1×1) phase. The (1×1) phase was found to have dynamical dipoles oriented in the perpendicular direction only thus extinguishing the s-polarized signal. Again no evidence of the *p*(3×2) or (*n*×2) structures was found.

From the above discussion we can conclude that HAS [36] and PIRS [37] experiments corroborate the LEED [35] findings at low temperature where the *c*(4×2) geometry is found. At higher temperatures (above 45 K) the HAS and PIRS experiments show serious discrepancies with the LEED experiment. It was suggested that these discrepancies might be due to the different experimental conditions.

Extensive theoretical studies have been done on the CO/MgO(001) system. To the best of our knowledge all these studies were performed at zero temperature. From semi-empirical interaction potentials, Panella *et al.* [35] found that the most stable structure was the (4×2) structure with a coverage of 75% and lower in energy than the *p*(3×2) structure in keeping with their experimental findings. They proposed that the cell of the *c*(4×2) structure contains eight MgO units. This cell contains six CO molecules with three different binding sites, each with a different energy and CO orientation: two molecules are perpendicular on top of an Mg site, two are slightly displaced relative to a Mg^{2+} site and tilted by 20° with respect to the surface normal, and the last two are parallel to the

surface bridging two Mg sites. Three different possible configurations of the (4×2) phase, including that proposed by the Göttingen [36] and Hannover [37[groups as well as the one proposed by Panella *et al.* [35], were studied by Hoang *et al.* [63]. They found that the most stable structure was the one that contained three different binding sites with different molecular orientations at each site. Minot *et al.* [64] performed Hartree-Fock calculations to study the CO/MgO system and compared the structures proposed by Panella *et al.* [35] with that of the Göttingen-Hannover (G-H) groups [36-37]. They found that the G-H model was the most stable structure with two adsorption sites and three CO molecules per unit cell; one molecule sits perpendicular to the surface on top of a Mg^{2+} site, while the other two molecules are tilted at an angle of 43.5° with respect to the surface normal (which differs from the experimentally observed value of 29°). The findings of Minot *et al.* [64] were corroborated by semi-empirical molecular orbital calculation results of Jug *et al.* [65] who found that the c(4×2) phase, with two adsorption sites and three CO molecules in the unit cell, is energetically the most preferable structure at 0 K and contained molecules with a tilt angle of 24° in better agreement with the experimental result [37]. This work, however reported a binding energy with a value of -7.3 kcal/mol per molecule, which is more than twice the most recent experimental value of the heat of adsorption. Thus the Göttingen-Hannover (G-H) model for the c(4×2) structure was corroborated by theoretical work, although some

of the details of the theoretical work are not consistent with the experimental record.

The binding energy of CO on a MgO(001) surface still challenges the community of surface science. Unfortunately, no definite value for the binding energy of CO/MgO system has been yet obtained experimentally or theoretically. The different experimental and theoretical values of the binding energy, the various methods used to determine them, and the somewhat confusing state of affairs surrounding the value of the binding energy were summarized by Pacchioni [66] and Snyder *et al.* [67]. All the experimental binding energy values reported so far [68-72], range from 3.22 kcal/mol to 9.9 kcal/mol, while the theoretical *ab initio* values [66-67][73-78] range from 1.6 kcal/mol to 8.6 kcal/mol. The recent experimental work [79] indicates that the binding energy of the CO molecules on MgO surface probably around 3.6 kcal/mol. This value is very close to the earlier experimental data where values of 3.4-4.6 kcal/mol were reported.

1.4.2 N_2/MgO(001) system

There has also been considerable interest in studying the adsorption of monolayer nitrogen on the (001) face of MgO surface [80][81]. Experimental studies [30-32, 34] showed that N_2 molecules form ordered structures on the MgO(001) surface. Using neutron

diffraction techniques within the range of temperatures of 10-60 K, Trabelsi *et al.* [32][34] found that at submonolayer coverage, N_2 adopts a sequence of semi-commensurate $p(n\times2)$ type structures. At the completion of 70 % coverage, the N_2 molecules form a highly ordered $\left(\sqrt{13}\times\sqrt{13}\right)R33.7^\circ$ structure, which is commensurate with the surface. In attempting to model this structure Trabelsi *et al.* [34] assume that all molecules have the same tilt angle of 30° with respect to the surface normal. A single azimuthal angle of 15° (in our nomenclature) was proposed. They found that this structure is stable at 10 K and continued to be stable up to temperatures less than 30 K. At higher temperatures (T >50 K) they observed the formation of an ordered hexagonal incommensurate structure. The hexagonal structure is expected for a solid structure of the nitrogen molecules at low temperatures.

Recently Traeger *et al.* [38] performed HAS experiments at 12 K to study the structures and dynamics of nitrogen monolayers physisorbed on the MgO(001) surface. In these studies they confirmed the $\left(\sqrt{13}\times\sqrt{13}\right)R33.7^\circ$ structure observed by Trabelsi *et al.* [34], and observed a new commensurate ordered structure with $\left(\sqrt{25}\times\sqrt{25}\right)R36.9^\circ$ symmetry. The coverage of this new structure is lower than that of the $\left(\sqrt{13}\times\sqrt{13}\right)R33.7^\circ$ case. These two structures are both found to be stable around 12 K. An incommensurate phase was also observed at 12 K and

has a coverage less than that of the $(\sqrt{13}\times\sqrt{13})R33.7^{\circ}$ structure and greater than that of the $(\sqrt{25}\times\sqrt{25})R36.9^{\circ}$ phase. The stabilities and phase transitions of these systems as a function of temperature were not systematically studied in the HAS experiments, but the $(\sqrt{13}\times\sqrt{13})R33.7^{\circ}$ phase was found to be thermally stable up to 18 K. Furthermore, at 36 K they observe a new phase that has a density lower than that of the $(\sqrt{25}\times\sqrt{25})R36.9^{\circ}$ structure, but the symmetry of this new structure was not obtained. They did not find any evidence for the presence of the $c(4\times2)$ structure or any kind of (n×2) phases observed by Angot *et al.* [30] and Trabelsi *et al.*[32][34].

Theoretical work on this system using semi-empirical potentials was limited to a single molecule. Lakhlifi *et al.* [1] had found that a N_2 molecule lies down on the surface and aligned along Mg-Mg channels. However the charge of the Mg was only 1 q/e in their work, which is lower than the known value of +2 q/e. To the best of our knowledge there is no computational work on the structures or stabilities of the N_2/MgO(001) system.

1.4.3 N_2/NaCl(001) system

Due to the intense electric field of the NaCl(001) surface, dipoles are induced in the N_2 molecules. These dipoles are infrared active and

hence induced infrared experiments have been performed to study the N_2/NaCl(001) system. According to polarization (induced IR) studies, the nitrogen molecules were found to adsorb perpendicular to the surface directly over the Na^+ ions. This result is similar to that for CO molecules adsorbed on NaCl(001). As with the CO/NaCl(001) system, the N_2/NaCl(001) system exhibits epitaxy and the nitrogen molecules are found to form a full monolayer where every adsorption site is occupied by N_2 molecule [82].

The two diatomic molecules N_2 and CO have similarities in many bulk properties [83-89]. The main difference between these two molecules is that CO has a permanent dipole moment while N_2 does not. These similarities make it reasonable to expect that N_2 molecules will behave similarly to that of CO molecules on NaCl(001), and that the experimental results concerning CO/NaCl(001) could well be a model for N_2/NaCl(001). Recent HAS [90] and PIRS [91] experimental studies of the structure and dynamics of CO adsorbed on NaCl(001) indicate that the CO molecules form a $p(2\times1)$ structure at low temperatures, which undergoes an orientational order-disorder phase transition to a $p(1\times1)$ phase at temperatures around 30-35 K.

Details of the low temperature phase of CO/NaCl were obtained by the use of Monte Carlo simulations and the phase transition was

reproduced at temperatures similar to that observed experimentally [92,93]. It was argued that the phase transitions of CO/NaCl(001) [93] as well as the CO/LiF(001) [27] systems fall in the universality class of that of the XY model with cubic anisotropy and thus will have nonuniversal critical exponent. As reported in Ref. [92] the authors concluded that it was not possible to obtain the critical exponent computationally in these systems (CO/NaCl and CO/LiF) due to the presence of the small dipole moment on the CO molecule. Dipolar interaction can lead to long relaxation times for energy and order parameter equilibration. In order to avoid this difficulty, N_2 molecules could be substituted for the CO molecules. In the case of N_2 only the short-range quadrupole-quadrupole ($\sim r^5$) interactions are present.

Recent computational work [94] suggests that in order to get the short range Ising exponents, the molecules should have only quadrupole or higher electric multipole moments but not lower than that. This study supports our choice of N_2 molecules adsorbed on NaCl(001) to test the theory of critical phenomena.

1.5 Research objectives

1.5.1 CO/MgO(001) system

The experimental findings of the orientations of the adsorbed CO molecules have not been confirmed by previous theoretical work by other researchers. As was discussed in section 1.4.1, it is clear that there is less understanding of the physics behind the formation of these interesting structures and that more work is needed to correctly interpret the experiments. The main cause of the failure of previous theoretical studies in resolving the discrepancy in the observed experimentally structures between 30 K and 55 K is that the theoretical studies were performed only at a temperature of 0 K. These studies can confirm the low temperature structures but cannot resolve the discrepancy in the experimentally observed structures at 45 K.

Part of our work is to construct an interaction potential to study the CO/MgO(001) system and reproduce the known experimental data for this system. We are going to shed some light on some of the discrepancy between the different experimental studies of the adsorption of CO molecules on MgO(001) and to give details on these ordered structures such as the orientations and positions of the adsorbed CO molecules. Also, we will study possible phase transitions versus temperature. We will show that these phase transitions are an example

of the devil's staircase phenomenon and try to reconcile the findings of the LEED experiments with those of the HAS and PIRS experiments. In particular, we will determine under what conditions the $c(4\times2)$ phase transforms into either the $p(3\times2)$ phase or a disordered (1×1) phase.

1.5.2 N_2/MgO(001) system

Recently, this system was the subject of an extensive experimental study. There has been no theoretical work reported on the structures and stabilities of this system. Part of this thesis reports on the construction of a surface potential for this system and Mont Carlo simulations that give details on the structures and stabilities of this system. This part of the thesis is done with access to the experimental data of Professor J.P. Toennies' group [38]. This system is expected to undergo a sequence of phase transitions as in the CO/MgO system and hence provide another realization of the devil's staircase phenomena.

1.5.3 N_2/NaCl(001) system

As has been discussed in section 1.4.3, monolayer nitrogen adsorbed on the NaCl(001) surface is an ideal candidate to substitute for the CO/NaCl(001) system in order to study and test the validity of the theory of phase transition and critical phenomena and its applicability to molecular systems.

We will report on the results of a Monte Carlo study that predicts an orientational order-disorder phase transition in N_2/NaCl system. N_2 molecules are expected to behave similarly to that of CO molecules adsorbed on NaCl(001) and hence N_2 molecules are expected to form a $p(2\times1)$ structure that is expected to undergoes a continuous phase transition, similar to that observed in CO/NaCl system at low temperatures.

Roelofs and Estrup [53] pointed out that it is very interesting to examine how the value of the order parameter critical exponent β varies between the four-state-clock ($\beta=1/8$ and $h_4=\infty$) and the Kosterlitz-Thouless ($\beta=1/8$ and $h_4=0$) values. The N_2/NaCl(001) system is expected to exhibit critical behaviour with nonuniversal critical exponents which depend on the anisotropy of the molecule-molecule and molecule-substrate interactions. Thus this system will allow us to examine how the critical exponents differ from the Ising results. Finite size scaling analysis will be applied to obtain the critical exponents.

2. Potentials and parameters

The choice of interaction potentials and their parameters determines the adsorption energy and molecular orientation of the adsorbed molecules.

2.1. Adsorption energy

Because semi-empirical potentials are used in the simulations presented in this thesis, the experimental values of quantities such as the heat of adsorption are used to put limits on the values of the interaction parameters. Experimental values of the adsorption energy are measured at temperatures above 0 K. In order to calculate the binding energy E_0 at 0 K, for a diatomic molecule with five degrees of freedom (3 translational and 2 rotational) we can use the following relation [1][92][96][97].

$$q_{st}=-E_0-\frac{3}{2}k_BT \tag{2.1}$$

where q_{st} is the isosteric heat of adsorption, k_B is the Boltzmann constant, T is the absolute temperature, E_0 is the binding energy to the surface for a single molecule. Note that the isosteric heat of adsorption depends on temperature.

As discussed in section 1.4.1 the experimental values of the heat of adsorption for CO molecules adsorbed on the MgO(001) surface range from 3.22 to 9.9 kcal/mol. The higher of the experimental values of the binding energy are attributed to the adsorption on defects. The value we chose for the binding energy of CO molecule on the MgO surface is the recent experimental value 3.6 kcal/mol [79], which is similar to the low experimental values (3.22-4.0 kcal/mol). These values are the most recent results obtained from MgO(001) substrates prepared by cleavage in a vacuum, and thus exhibit a very small defect density. By using Eq. 2.1, the binding energy of 3.6 kcal/mol obtained at 45 K yields a binding energy of 3.73 kcal/mol at 0 K. This latter value will be used to put limits on CO/MgO(001) surface potential.

The experimental binding energy of N_2 on MgO(001) was found to have values of 2.6 kcal/mol at 10 K and 2.65 kcal/mol at 77 K for a monolayer coverage [31][32]. The most recent experimental result is 2.86 kcal/mol at 43 K for a monolayer of N_2/MgO(001) [38], which by using Eq. 2.1 yields a binding energy of 2.98 kcal/mol at 0 K.

A monolayer of nitrogen molecules is found to bind to NaCl(001) surface with a binding energy of 2.65 kcal/mol at 77 K [82]. This value yields a binding energy of 2.88 kcal/mol at 0 K.

2.2. Interaction Potentials

To simulate the systems of interest, the potential energy functions must be constructed to calculate the total potential energy of the system under study. The total potential consists of two parts, molecule-molecule and molecule-surface potentials. Accurate potentials will allow us to reproduce most of the known experimental data of a system. The method used to construct the total potentials in this thesis is similar to that used by Polanyi's group [61][98]. Atom-atom/ion potentials with summation over a two body interactions is applied to describe the repulsion and dispersion interactions. In addition to these interactions, electrostatic contributions are also considered.

2.2.1 Molecule-molecule interactions

In this study a site-site model is used to construct the intermolecular potential. The parameters governing the potentials are chosen so as to reproduce various experimental molecular properties of CO and N_2 molecules. The WMIN computer program [99] is used to calculate the repulsion parameters so that the molecule-molecule interactions will yield the crystal structures of the α-phases of solid CO and solid N_2. The program accomplishes this by adjusting some of the potential parameters (chosen by the user) so as to minimize the energy of

a molecular crystal while the positions of the molecules are fixed in their crystal structure.

2.2.1.1 Electrostatic interactions

The electrostatic interactions are mediated by point charges q_i and point dipoles $\vec{\mu}_i$ that are distributed around the molecule (on the atomic sites) in such a way that the known multipole moments of the molecule can be reproduced through the following linear equations [92],

$$q_1 + q_2 = 0 \tag{2.2}$$

$$\mu = \sum_{i=1}^{2} q_i r_i + \sum_{i=1}^{2} \mu_i \tag{2.3}$$

$$\Theta = \sum_{i=1}^{2} q_i r_i^2 + 2\sum_{i=1}^{2} \mu_i r_i \tag{2.4}$$

$$\Omega = \sum_{i=1}^{2} q_i r_i^3 + 3\sum_{i=1}^{2} \mu_i r_i^2 \tag{2.5}$$

$$\Lambda = \sum_{i=1}^{2} q_i r_i^4 + 4\sum_{i=1}^{2} \mu_i r_i^3 \tag{2.6}$$

where μ, Θ, Ω and Λ are the molecular dipole, quadrupole, octupole and hexadecapole moments respectively. The r_i are the distances of the point charges q_i and point dipoles μ_i at site i from the molecular center of mass. The faithful reproduction of the molecular multipole moments up

to the octupole for CO and the hexadecapole for N_2 in these simulations is necessary since they are known to make important contributions to the molecule-surface interaction [100].

The values of the distributed point charges and dipoles at the atomic sites can be determined by using the above equations. The known values of the dipoles, quadrupoles and polarizabilities of CO and N_2 molecules are given in Table 2.1. The calculated values of the distributed point charges and point dipoles at the atomic sites of the N_2 and CO are presented in Table 2.2.

Using the point charges and point dipoles at the atomic sites of diatomic molecules has an advantage over using the purely point charge model used in Ref. [101]. By using the latter model we cannot correctly reproduce more than the dipole moment in the case of CO molecules, unless we allow additional point charges at non-atomic sites. By using point charges and point dipoles at atomic sites we can reproduce molecular multipole moments up to the octupole level. The inclusion of these multipole moments in the CO-NaCl interactions is known to be very important [100]. The idea of assigning additional charges at non-atomic sites is physically difficult to justify.

The electrostatic interactions between an atom i (with charge q_i and dipole μ_i) of a molecule "m" with an atom j of another molecule "n" (with charge q_j and dipole μ_j) can be written as follows [96],

$$V_{ij}^{(elc)} = \frac{q_i q_j}{r_{ij}} - \frac{q_i \mu_j}{r_{ij}^3}(\hat{u}_j \cdot \vec{r}_{ij}) + \frac{q_j \mu_i}{r_{ij}^3}(\hat{u}_i \cdot \vec{r}_{ij}) + \frac{\mu_j \mu_i}{r_{ij}^5}[(\hat{u}_i \cdot \hat{u}_j) r_{ij}^2 - 3(\hat{u}_i \cdot \vec{r}_{ij})(\hat{u}_j \cdot \vec{r}_{ij})] \quad (2.7)$$

where $\vec{r}_{ij}$ is the vector position of i^{th} atom of the n^{th} molecule with respect to the j^{th} atom of the m^{th} molecule. In other words, $\vec{r}_{ij}$ points from atom j to atom i. And $\hat{u}_i$ is an orientation unit vector at atom "i" of the n^{th} molecule. Fig. 2.2 illustrates the atom-atom or site-site potential for diatomic molecules.

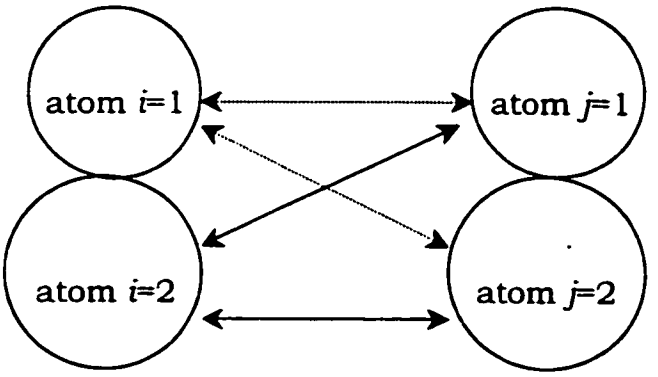

Figure 2.2. An atom-atom model for a diatomic molecule.

TABLE 2.1: dipole, quadrupole, octapole and hexadecapole of CO and N_2 molecules as well as their dipole polarizabilities (α_1) and quadrupolar polarizability (α_2).

	CO	N_2
dipole (D)	0.11[a]	0.0
quadrupole (D. Å)	-1.9[b]	-1.41[b]
ocutpole (D. Å^2)	2.77[c]	0.0
hexadecapole(D.Å^3)	-3.7[c]	-3.01[f]
polarizability (α_1) (Å^3)	2.1[d]	1.74[g]
polarizability $\parallel$ (Å^3)	2.32[d]	2.19[h]
polarizability $\perp$ (Å^3)	1.79[d]	1.513[h]
(α_2) (Å^5)	5.09[e]	77.96[f]

[a] Ref. 102
[b] Ref. 103
[c] Ref. 104
[d] Ref. 105
[e] Ref. 106
[f] Ref. 107
[g] Ref. 108
[h] Ref. 109

TABLE 2.2: Summary of the electrostatic model of the CO and N_2 molecules. The positions are calculated with respect to the centre of mass of the molecule. The dipoles are oriented along the molecular axis with the carbon to oxygen direction defining the positive sense of orientation. The molecular axis also defines the sense of direction for the parallel and perpendicular polarizabilities $\alpha_{\parallel}$ and $\alpha_{\perp}$ respectively.

	C atom (in CO)	O atom (in CO)	N atom (in N_2)	N atom (in N_2)
position (Å)	-0.6446	0.4834	-0.5472	0.5472
charge ($\times 10^{-10}$ esu)	3.036	-3.036	0.0	0.0
dipole (D)	2.655	0.880	0.664	-0.664
polarizability (Å^3)	1.44[a]	0.66[a]	1.078[b]	1.078[b]
polarizability $\parallel$ (Å^3)	1.59[a]	0.73[a]	1.096	1.096
polarizability $\perp$ (Å^3)	1.23[a]	0.56[a]	0.756	0.756

[a]From Ref. 92
[b]From Ref. 110.

2.2.1.2 van der Waals interactions

Once again the atomic site model is used to model the van der Waals interaction (repulsion and dispersion interaction) between molecules so that, the molecular interaction may be expressed in terms of the atom-atom interactions by the modified Buckingham potential,

$$V_{ij}(r_{ij}) = A_{ij}\exp(-\eta_{ij}r_{ij}) - \frac{C_6^{ij}}{r_{ij}^6} - \frac{C_8^{ij}}{r_{ij}^8} \qquad (2.8)$$

where the variable r_{ij} is the distance between atom sites i and j of different molecules. The Born-Mayer parameters, A_{ij} and η_{ij}, characterize the strength and the range of the repulsion respectively. C_6 and C_8 are dispersion constants that represent the strength of the leading terms in the dispersion series, these constants are well known for molecules and are easy to determine for atomic sites. In contrast, the repulsive parameters are difficult to obtain experimentally in most cases and hence we assume that repulsive parameters can be adjusted so as to reproduce certain experimentally known quantities such as the crystal structure and cohesive energy of bulk CO and N_2. The values of these parameters can be manipulated by using the WMIN program [99] where the crystal structure (position, orientation, lattice constant) of the α–phase of the solid CO and solid N_2 along with the interaction parameters for the electrostatic and dispersion forces were used as input parameters (see below). Then the cohesive energy of the crystal is minimized

through the variation of the radii (a_i) and softness (b_i) parameters. The resulting parameters a_i, and b_i are used to construct the Born-Mayer parameters as follows [111],

$$\eta_{ij} = \frac{1}{b_i + b_j} \tag{2.9}$$

$$A_{ij} = (b_i + b_j) exp\left(\frac{a_i + a_j}{b_i + b_j}\right) \tag{2.10}$$

The calculated values of the atomic Born-Mayer parameters for CO and N_2 molecules are presented in Table 2.4. For N_2 we have used, the atomic Born-Mayer parameters of $\eta_{NN} = 3.48\,\text{Å}$ and A_{NN}=2900 kcal/mol used by Westerhoff *et al.* [112] and Boham *et al.* [113] to model N_2-N_2 interaction, as an initial values in the WMIN program, the final values are very similar to the initial values and presented in Table 2.4.

In order to use the site-site model, the molecular dispersion interaction parameters, available in the literature for N_2 and CO molecules and given in Table 2.3, must be broken up into atomic based ones. The following relation and combining rule were used to estimate the atom-atom dispersion parameters from the values for molecular quantities [114] [115],

$$C_6^{CO\text{-}CO} = C_6^{C\text{-}C} + C_6^{O\text{-}O} + 2C_6^{C\text{-}O} \tag{2.11}$$

$$C_6^{C\text{-}O} = (C_6^{C\text{-}C} C_6^{O\text{-}O})^{1/2} \tag{2.12}$$

The same relations hold for an N_2 molecule. The values of the atomic C_6 were obtained by using the program WMIN [99] under the constraint that the value of C_6 for a CO molecule be preserved. The atomic C_8 and C_{10} were determined by multiplying the atomic C_6 with the ratios C_8 / C_6 and C_{10} / C_6 as calculated from values of dispersion parameters for CO and N_2 molecules. The atomic C_6, C_8, and C_{10} for N_2 and CO are presented in Table 2.4.

2.2.2 Molecule-surface interaction

The pairwise sum of two-body interactions (atom-ion interactions) is used to model the electrostatic, dispersion and repulsion interactions between a molecule and the substrate. Because we are dealing with physisorbed systems where there is no noticeable reconstruction or distortion of the (001) ionic surface [117], it reasonable to assume that the surface of the substrate is not perturbed by adsorbed molecules and hence has the same lattice constant as the bulk. Ions of the surface are considered to be periodic in two dimensions and regular (the substrate is regarded as a semi-infinite solid) in the third dimension.

TABLE 2.3: Repulsion and dispersion parameters for the CO-CO and N_2-N_2 interactions. C_6, C_8 and C_{10}

	CO	N_2
C_6 (Å^6 • kcal/mol)	1218[a]	1010[b]
C_8 (Å^8 • kcal/mol)	10231[a]	9354[c]
C_{10} (Å^{10}• kcal/mol)	94516[a]	-

[a] *ab initio* Ref. 115
[b] Ref. 110
[c] Ref. 116

TABLE 2.4: Atomic repulsion and dispersion parameters for the CO-CO and N_2-N_2 interactions. C_6, C_8 and C_{10}

	C atom (i=1)	O atom (i=2)	N atom in N_2
a_i (Å)	1.656	1.762	1.666
b_i (Å)	0.1356	0.1711	0.1437
A_{ii} (kcal/mol)	1.193×10^5	5.465×10^3	3.100×10^4
η_{ii} (Å^{-1})	3.687	2.922	3.48
C_6 (Å^6 • kcal/mol)	3.236×10^2	2.860×10^2	2.528×10^2
C_8 (Å^8 • kcal/mol)	2.718×10^3	2.402×10^3	2.340×10^3
C_{10} (Å^{10} • kcal/mol)	2.511×10^4	2.219×10^4	4.954×10^4

2.2.2.1 Electrostatic interactions

The electrostatic energy (V_{elc}^{m-s}) of a single diatomic molecule on the ionic surface can have the following form

$$V_{elc}^{m-s} = \sum_{i=1}^{2} \left(\psi(\vec{r}_i) q_i + \vec{E}(\vec{r}_i) \cdot \vec{\mu}_i - \frac{1}{2} \alpha_i^{\perp} E_{\perp}^2(\vec{r}_i) - \frac{1}{2} \alpha_i^{\parallel} E_{\parallel}^2(\vec{r}_i) \right) \qquad (2.11)$$

Where q_i, $\vec{\mu}_i$ are point charges and point dipoles at the atomic sites of the molecule. $\psi(\vec{r}_i)$ and $\vec{E}(\vec{r}_i)$ are the electrostatic potential and electric field generated by the ionic crystal at position $\vec{r}$, the location of the interacting atom with respect to the origin of the coordinate system. The induction energy, which depends upon the "atomic" polarizabilities (perpendicular ($\alpha_i^{\perp}$) and parallel ($\alpha_i^{\parallel}$) to the molecular axis), is included in our calculations.

The sum in the above equation is over the two atomic sites of the diatomic molecule. The electrostatic potential above the surface of a FCC ionic crystal is well known [118] and may be written as a two dimensional Fourier series whose leading term is [2]

$$\psi(\vec{r}_i) = -\frac{4e}{a}\left[\frac{\exp\left(-\frac{2\pi z}{a}\right)}{1+\exp\left(-\sqrt{2}\pi\right)}\right]\left(\cos\left(\frac{2\pi x}{a}\right)+\cos\left(\frac{2\pi y}{a}\right)\right) \qquad (2.12)$$

where e is the absolute value of the electronic charge on an individual ion (for NaCl e=±1 and for MgO e=±2) and a is the lattice constant of the surface mesh (a_{NaCl}=3.99 Å and a_{MgO} =2.969 Å). The electric field at the crystal surface is readily calculated from the gradient of the electrostatic potential,

$$\vec{E}(\vec{r}) = -\vec{\nabla}\psi(\vec{r}) \tag{2.13}$$

The distributed charges, dipoles and polarizabilities for CO and N_2 molecules are listed in Table 2.2.

2.2.2.2 van der Waals interactions

The Tang-Toennies potential is used to describe the repulsion and dispersion interaction of an atom of an adsorbed molecule with an ion of the substrate,

$$V_{ij}^{m-s}(r_{ij}) = A_{ij}\exp(-\eta_{ij}r_{ij}) - \sum_{n=3}^{\infty} f_{2n}(r_{ij})\frac{C_{2n}^{ij}}{r_{ij}^{2n}} \tag{2.14}$$

where r_{ij} is the distance of atom i to ion j and C_6, C_8 and C_{10} are the atom-ion dispersion coefficients. The mathematical singularities at r=0 are removed by the presence of the phenomenological damping functions

$$f_{2n}(r_{ij}) = 1 - \sum_{k=0}^{2n} \frac{(\eta_{ij} r_{ij})^k}{k!}\exp(-\eta_{ij} r_{ij}) . \tag{2.15}$$

The dispersion series is in principle infinite but for practical reasons is truncated at the k=5 term, *i.e.* only the C_6, C_8 and C_{10} terms are included. To fully describe the potential it was necessary to estimate all interaction parameters A_{ij}, η_{ij}, C_6, C_8 and C_{10} for each of the atom-ion interactions.

2.2.2.2.1 Dispersion parameters

Values of C_6, C_8 and C_{10} for the molecule-ion interactions were estimated from combining rules derived [119] [120]. For example, the C_6 are assumed to obey the following relation

$$C_6^{ij} = \frac{2C_6^{ii}C_6^{jj}\alpha^i\alpha^j}{C_6^{ii}\left(\alpha^j\right)^2 + C_6^{jj}\left(\alpha^i\right)^2} \tag{2.16}$$

where the index *i* refers to the molecule and *j* refers to either the positive or negative ion in the substrate, and α is average polarizability.

The values of C_8 can be found using the following relations [119]:

$$C_8^{ij} = C^{ij}(1,2) + C^{ij}(2,1) \tag{2.17}$$

where,

$$C^{ij}(1,2) = \frac{15}{4}\left[\frac{\alpha_1^i\alpha_2^j Y_1^i Y_2^j}{Y_1^i + Y_2^j}\right] \tag{2.17a}$$

$$Y_1^i = \frac{4}{3}\frac{C_6^i}{\left(\alpha_1^i\right)^2}, \quad Y_2^i = \frac{2C_8^i Y_1^i}{15\alpha_1^i\alpha_2^i - 2C_8^i} \tag{2.17b}$$

The values of the C_{10} coefficients for each of the molecule-ion pairs were estimated using the approximate relation [121]

$$C_{10} = 49(C_8)^2/40\ C_6 \tag{2.18}$$

These values of the molecule-ion dispersion coefficients C_6, C_8, and C_{10} were used to calculate the atom-ion dispersion coefficients

$$C_6^{\text{atom-ion}} = \left(\alpha_{\text{atom}} / \alpha_{\text{molecule}}\right) C_6^{\text{molecule-ion}} \qquad (2.19)$$

It is worth noting that the C_8/C_6 and C_{10}/C_6 ratios for each atom-ion pair are assumed to be the same as the corresponding ratios for the molecule-ion pairs. The C_8, and C_{10} for atom-ion pairs can then be obtained by multiplying the values of C_6 of atom-ion by the appropriate ratio (C_8/C_6 (molecule-ion) and C_{10}/C_6 (molecule-ion)). The resulting values of the atom-ion dispersion coefficients for CO/MgO and N_2/MgO are given in Table 2.6, and for the N_2/NaCl system are given in Table 2.7

TABLE 2.5: Polarizabilities (dipolar α_1 and quadrupolar α_2) and dispersion coefficients of (C_6 and C_8) of in-crystal Mg^{2+} and O^{2-} ions .

	Mg^{2+}	O^{2-}	Na^+	Cl^-
C_6(Å^6·kcal/mol)	7.385[a]	833.5[f]	1.588[a]	180.3[a]
C_8(Å^8· kcal/mol)	11.687[b]	5813.66[f]	12.92[j]	6115.77[j]
Dipole polarizability α_1 (Å^3)	0.0724[c]	1.681[g]	0.150[k]	3.13[l]
Quadrupolar polarizability α_2 (Å^5)	0.0107[d]	1.081[h]	0.0316[n]	2.597[m]
A_{ii} (kcal/mol)	1.0133[e]	1.802[e]	467443[o]	19579[o]
η_{ii} (Å^{-1})	0.052[e]	0.250[i]	5.857[o]	2.491[o]

[a] From Ref. 122.
[b] From Ref. 123.
[c] From Ref. 124 and Ref. 125.
[d] From Ref. 126.
[e] From Ref. 127.
[f] From Ref. 128
[g] From Ref. 129
[h] From Ref. 130
[i] From Ref. 131
[j] From Ref. 99.
[k] From Ref. 132.
[l] From Ref. 133.
[n] From Ref. 134.
[m] From Ref. 135.
[o] From Ref. 136.

2.2.2.2.2 repulsion parameters

The method used to obtain Born-Mayer parameters for the atom-ion interactions are identical to that used in Ref. 137. The values for the like-like ion (Na^{+}-Na^{+}, Cl^{-}-Cl^{-} in NaCl and Mg^{+2}-Mg^{+2}, O^{-2}-O^{-2} in MgO) interactions were obtained or extracted from published data and are listed along with references in Table 2.5. The Born-Mayer parameters for atom-ion interactions are estimated by using the combining rules of Gilbert [138] [139] and Smith [140],

$$A_{ij} = \left[\frac{\eta_{ii} + \eta_{jj}}{2\eta_{ii}\eta_{jj}}\right](A_{ii}\eta_{ii})^{c}(A_{jj}\eta_{jj})^{d} \tag{2.20}$$

$$\eta_{ij} = \frac{2\eta_{ii}\eta_{jj}}{(\eta_{ii} + \eta_{jj})} \tag{2.21}$$

where the exponents c and d are defined as

$$c = \frac{\eta_{jj}}{\eta_{ii} + \eta_{jj}} \tag{2.22}$$

$$d = \frac{\eta_{ii}}{\eta_{ii} + \eta_{jj}} \tag{2.23}$$

$$\eta_{ij} = 1/(b_i + b_j) \tag{2.24}$$

$$A_{ij} = (b_i + b_j)\exp\left[(a_i + a_j)/(b_i + b_j)\right] \tag{2.25}$$

The resulting surface potential bound the molecule too strongly to the surface overtop of the positive ion site so that adjustments in the pre-

exponential factors A_{ij} were necessary. These adjustments are needed due to systematic shortcomings of the combining rules when applied to combinations of atom/ions with a large differences in size. It was found that by multiplying the A_{ij} by 1.9 then decreasing the {C,O}-O^{2-} factors by 10% and increasing the {C,O}-Mg^{2+} factors by 10% the experimental binding energy of single CO molecule adsorbed on MgO(001) could be reproduced. In order to reproduce the experimental binding energy at 0 K for N_2/MgO and N_2/NaCl systems, the repulsion parameters (A_{ij}) were multiplied by 1.81 and 1.67 for both systems respectively. Values for repulsion parameters of atom-ion pairs are given in Tables 2.6 and 2.7.

TABLE 2.6: Repulsion and dispersion parameters for the N(atom)-NaCl and N(atom)-MgO interactions.

	N-Na^+	N-Cl^-	N-Mg^{2+}	N-O^{2-}
η(Å^{-1})	4.37	2.90	5.11	2.54
A_{rep} (kcal/mol)	133,200	38,240	29,9500	4673
C_6(Å^6·kcal/mol)	64.57	784.8	34.03	458.1
C_8(Å^8·kcal/mol)	372.4	4063	175.20	3862
C_{10}(Å^{10}·kcal/mol)	2632	25770	1105	39880

TABLE 2.7: Calculated atomic repulsion and dispersion parameters for the CO-MgO and CO-CO interactions.

Interaction	A (kcal/mol)	η ($Å^{-1}$)	C_6($Å^6$. kcal/mol)	C_8($Å^8$. kcal/mol)	C_{10} ($Å^{10}$. kcal/mol)
C(atom)-Mg^{2+}	314,430	5.32	47.6	187.5	903
C(atom)-O^{2-}	5,399	2.59	689.9	5,130	46,745
O(atom)-Mg^{2+}	93,087	4.48	21.8	85.9	414
O(atom)-O^{2-}	2,108	2.37	316.2	2,351.6	21,425
C-C	119,300	3.69	323.6	2,718	25,110
O-O	5,465	2.92	286	2,402	2,2190
C-O	21,176	3.26	304.2	2,555	-

It is obvious that the above atom-ion potentials are for one atom that interacts with one ion. It is inefficient to calculate the summation of all pair atom-ion potentials over all lattice ions. Instead of explicitly performing these summations, we take advantage of the stability and periodicity of the ionic substrate and replace the direct summation with a Fourier series of the periodic potential.

3. Simulation methods

3.1 Introduction

Nicolas Metropolis introduced the Metropolis Monte Carlo method at the dawn of the computer era in 1953 [141]. The rapid development in computer technology has increased the applicability and accuracy of the Monte Carlo method and is now used routinely in many diverse fields, such as economics, physics and chemistry as a powerful numerical technique. As we know, it is easy to solve equations of interaction between two atoms or molecules and get an exact solution for a specific problem while in the case of large systems, where the number of particles involved in a problem is large, solving the problem in a deterministic way becomes impossible due to the large number of equations and variables that are needed to study the problem. Monte Carlo (MC) methods are stochastic (random) techniques in which random numbers and probability statistics are used to examine scientific problems in a probabilistic fashion rather than a deterministic one. To study the physical properties of a system with a large number of atoms or molecules interacting with each other, MC methods can be readily applied whereby possible configurations of the system can be sampled according to their Boltzmann probability distribution via the use of random numbers [21] [28] [142] [26].

Metropolis Monte Carlo simulations have been performed to study the structures and phase transitions of adsorbed molecules on solid surfaces such as HBr/LiF(001) [61], CO_2/NaCl [25], CO/NaCl [93] and CO/LiF [27]. They have also been used to study critical phenomena near their transition temperatures for many models such as the Ising, XY, and Heisenberg models [26]. MC methods have proved to be useful tools since they allow for the sampling of a large number of possible configurations at nonzero temperatures. In this study we use the Metropolis Monte Carlo method to simulate the structures and phase transitions of CO and N_2 molecules physisorbed on the (001) surface of MgO, as well as the N_2/NaCl (001) system.

3.2 Metropolis Monte Carlo method

By using the Metropolis Monte Carlo (canonical ensemble or Q(N,V,T)) technique [143], we can simulate the interaction of adsorbed molecules on ionic surfaces, where the number of molecules N, the simulation volume V, and temperature T are fixed during any simulation. In other words, during a simulation the positions and the orientations of molecules are allowed to change while the number of molecules, volume and temperature are not allowed to change. The surface is not allowed to move but provides a potential in which the molecules move. The adsorbed molecules are considered to be rigid bodies; the bond length is not allowed to change during the simulation. A MC simulation is

typically broken down into cycles. In every cycle, each adsorbed molecule is allowed to move in a random fashion. In each move a randomly chosen molecule is moved to a new random position or orientation. Then the computer decides whether to accept or reject this move with a Boltzmann probability $\exp(-\Delta E/k_B T)$ that depends on the change in energy ($\Delta E = E_{new} - E_{old}$) of the new ($E_{new}$) and old ($E_{old}$) configuration. In Fig. 3.1 we show the general steps of the Metropolis Monte Carlo simulation [144]. This process is repeated many times until there is no further change in the average energy and other computed properties of the system, at which point the system is deemed to have reached thermodynamic equilibrium. After this point is reached, a large number of configurations (geometries) are accumulated and the data are averaged to obtain thermodynamic properties of the system, such as the energy and angular distributions. The coordinate system of adsorbed molecules is shown in Fig. 3.2, where the position of an adsorbed molecule is described by the position vector $\mathbf{r}(x,y,z)$ with respect to the origin which is taken in the plane z=0 (the surface of the substrate) and at the anion site with the x and y axes running along the [1,-1,0] and [1,1,0] crystallographic directions respectively and with the z axis set perpendicular to the surface. The orientation of an adsorbed molecule is described by a polar angle θ and an azimuthal angle φ.

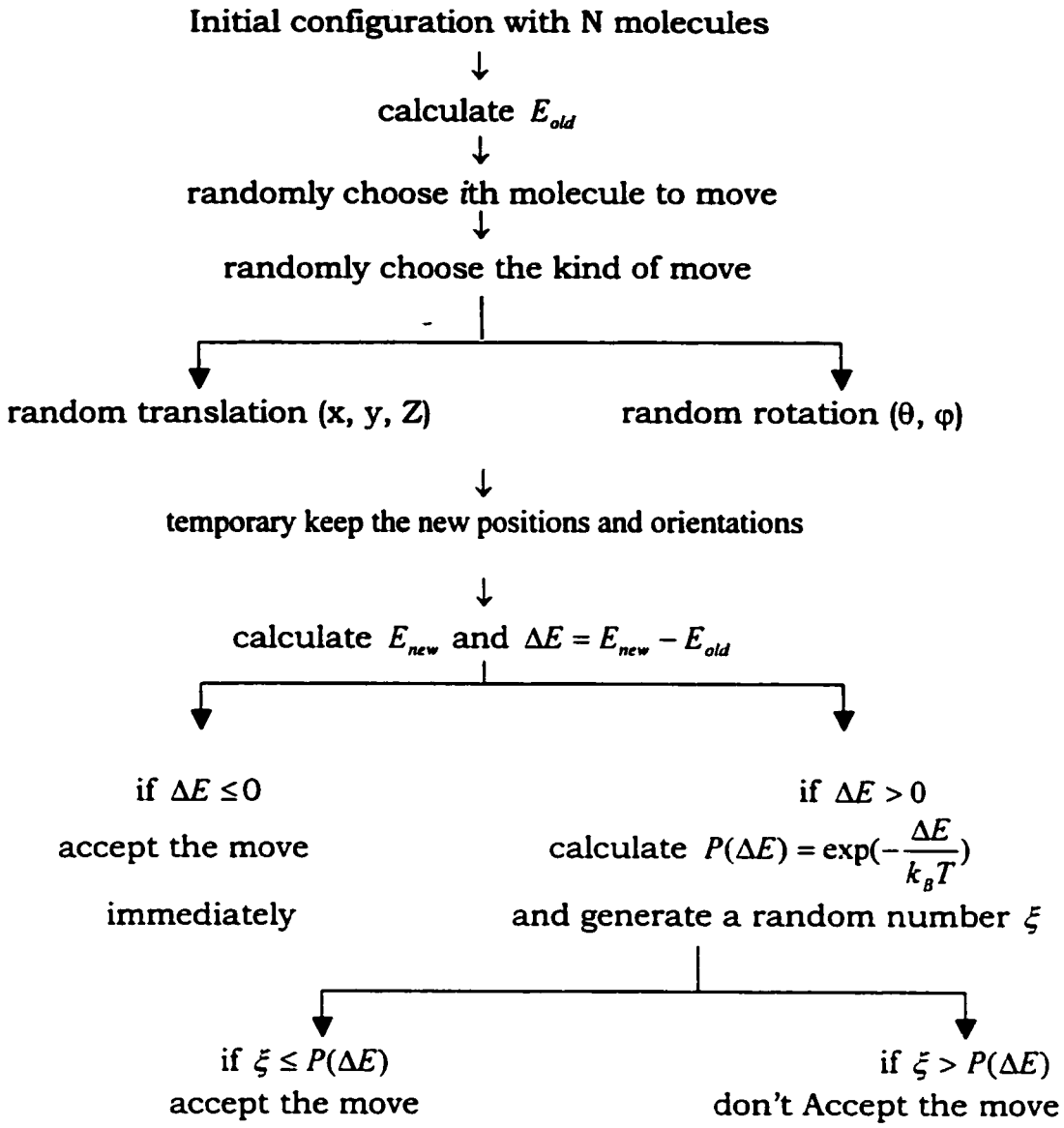

Figure 3.1 Flow chart of general steps of Metropolis Monte Carlo method

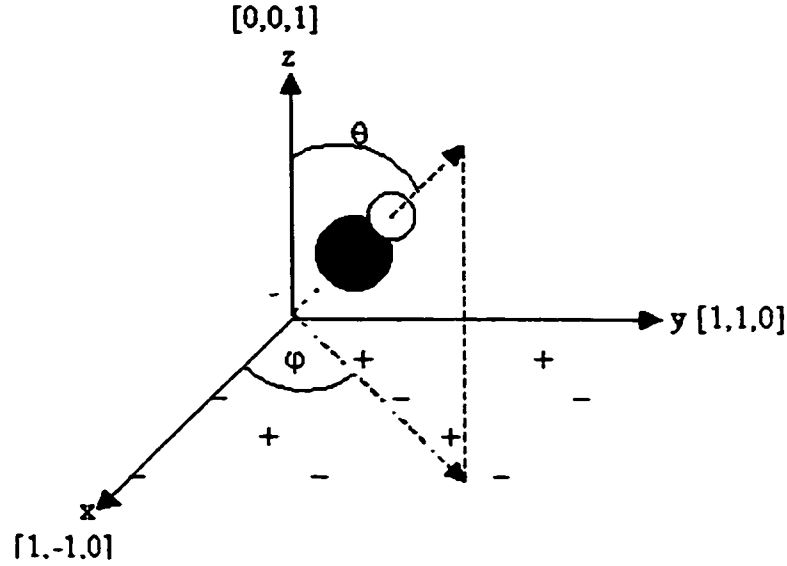

Figure 3.2. A top view of the (001) face ionic surface e.g. MgO(100) surface showing the x and y coordinate axes in terms of the crystallographic directions. The z-axis is perpendicular to the surface pointing out of the page. The (+) symbol represents the Mg^{2+} ion while the (-) symbol represents the O^{2-} ion. The origin is centered on a O^{2-} ion. The polar angle θ is the tilt of the molecular axis (carbon to oxygen) with respect to the surface normal (z-axis) while the azimuthal angle φ is the angle between the x-axis and the projection of the molecular axis onto the plane of the surface (xy-plane).

During the simulations an ensemble of N adsorbed molecules are placed in the surface potential of the ionic substrate. The surface potential is fixed in the space. If all of the positive sites of the surface are occupied then a monolayer of adsorbed molecules is formed. Periodic boundary conditions in the lateral directions (x and y) were imposed as well as a cutoff radius for the molecule-molecule interactions. Although no restrictions were placed on the motion of the molecules in the z

direction (away from the surface) the molecules nonetheless stayed in the vicinity of the surface due to the attraction by the surface potential and the cold temperatures at which the simulations were run. Each move is subjected to the usual Boltzmann weighted acceptance criterion. The amplitudes of the moves were adjusted independently and maintained a 50% acceptance probability. Statistics were collected from about 60 kcycles after the system is equilibrated. In the case of studying critical phenomena, analysis near the critical temperature needs longer runs to obtain good results.

3.2 Statistics

In order to study the continuous phase transition expected for the N_2 adsorbed on NaCl we need to calculate statistically the average energy (E), heat capacity (C_v), order parameter (Φ) and susceptibility (χ) for a monolayer of adsorbed molecules on a square lattice with $L \times L = N$ sites. To do that the order parameter and the energy per molecule were collected every cycle and have been kept for further analysis.

The heat capacity per particle is obtained from the fluctuations in the monolayer energy E *via* [24],

$$C_v=(\langle E^2\rangle-\langle E\rangle^2)/Nk_BT^2 . \qquad (3.1)$$

The order parameter Φ tells us how well the system is ordered. When the system is perfectly ordered the order parameter has a value of one while it has a value of zero when the system is fully disordered. The order parameter Φ for an anti-ferromagnetic like ground state is defined in terms of the azimuthal angle φ through the following relations and transformations [145].

$$\Phi = \sqrt{\Phi_x^2 + \Phi_y^2} \tag{3.2}$$

$$\Phi_x = \mathrm{N}^{-1} \sum_{i=1}^{N} (-1)^{n_{yi}} \cos(\varphi_i) \tag{3.3}$$

and

$$\Phi_y = \mathrm{N}^{-1} \sum_{i=1}^{N} (-1)^{n_{xi}} \sin(\varphi_i), \tag{3.4}$$

where $n_{xi} = 1,2,3,\ldots,L$ and $n_{yi} = 1,2,3,\ldots,L$ label the x and y positions of the adsorption sites of molecule i on the lattice. The summations are taken over all the localized adsorption sites of the molecules on a square lattice from 1 to $\mathrm{N} = L^2$. The transformed order parameter [146] Φ is obtained by using the phase factors $(-1)^{n_{xi}}$ and $(-1)^{n_{yi}}$. If the configuration of the adsorbed molecules is of the antiferro-type then the transformed configuration will be ferro-type where all the adsorbed molecules are oriented in the same direction. It is worth noting that these transformations do not affect the orientation of the adsorbed molecules in the Monte Carlo program. The process of transformation is

temporarily made after every Monte Carlo move when the order parameter is calculated.

The susceptibility is constructed from fluctuations in the order parameter, *via*

$$\chi = \left[\left\langle \Phi^2 \right\rangle - \left\langle \Phi \right\rangle^2\right] N / k_B T . \tag{3.5}$$

To determine how often we should sample a set of available data $\{X\}$, in order to calculate quantities such as the average energy, heat capacity and order parameter, an examination of the autocorrelation function [142] of data $\{X\}$ can be used,

$$C(\tau) = \frac{\left\langle X_i X_{i+\tau} \right\rangle - \left\langle X_i \right\rangle^2}{\left\langle X_i^2 \right\rangle - \left\langle X_i \right\rangle^2} \tag{3.6}$$

where X_i is the value of X at cycle i. The autocorrelation function for a number τ of steps can be calculated. It has a value of one when the data are completely correlated ($\tau = 0$) and decays exponentially to zero as τ becomes large enough that the data became uncorrelated. We can then find the number of steps (τ_e) required for the autocorrelation function

$C(\tau)$ to decay to 0.367 (1/e) of its value at τ=0. The data X can then be sampled every (τ_e) steps and still be uncorrelated.

Phase transitions in real systems (in experiments) are considered to be in the thermodynamic limit and thus effectively infinite in size. In computer simulations, the sizes of adsorbed systems are finite and small compared to the sizes of the real systems. It has been proved that in finite systems used in computer simulations the phase transition temperature is shifted compared to that in real systems. Hence, the transition temperature $T_c(L)$ changes as the 2-d size $L \times L$ of the system changes. This, plus the presence of large fluctuations due to finite size effects, makes it difficult to determine $T_c(\infty)$. In order to overcome these problems in determining the transition temperature for a system of infinite size, the Binder fourth order cumulant [147] [148]

$$U_L(T) = 1 - \frac{\langle \Phi^4 \rangle_L}{3\langle \Phi^2 \rangle_L^2} \tag{3.7}$$

for several values of L can be used to locate the transition point for a system of infinite size. When U_L is plotted as a function of temperature for a several systems of different sizes, we will get a set of curves that intersect at the infinite size transition temperature where they are independent of the lattice size. The fourth order cumulant has two

limiting values, for a completely ordered system $U_L = 2/3$, while $U_L = 0$ when the system is completely disordered. As the system size is increased, the fourth order cumulant will have values close to these limits.

4.0 CO molecules physisorbed on the MgO(001) surface

4.1 Introduction

From the experimental data reported on the CO/MgO(001) system, which has been discussed in section 1.4.1, it was concluded that HAS [36] and PIRS [37] experiments corroborate the LEED [35] findings at low temperature where the $c(4\times2)$ geometry is found. At higher temperatures (above 45 K) the HAS and PIRS experiments show serious discrepancies with the LEED experiment. LEED experiments showed that the $c(4\times2)$ phase undergoes a phase transition into a $p(3\times2)$ phase at 41 K and at 51 K the $p(3\times2)$ phase undergoes a sequence of transformations into $(n\times2)$ phases, while HAS experiments showed that $c(4\times2)$ undergoes a phase transition into a low density (1×1) disordered phase. It was suggested that these discrepancies might be due to the different experimental conditions.

One of our objectives, as discussed in section 1.5.1, is to reconcile the findings of the above experimental results and obtain more details on the structures and stabilities of CO/MgO system. In order to fulfill this objective we made use of the constructed surface potential (see chapter 2) for the CO/MgO(001) system and ran MC simulations using these potentials. This work is the first finite temperature simulations performed on this system. Most of the results presented in this chapter

were already published previously in The Journal of Chemical Physics [149].

4.2 Simulation methods and setup

To simulate CO molecules adsorbed on an MgO(001) surface, an ensemble of "N" CO molecules (where N=144, 108, 96 and 72 for monolayer, $c(4\times2)$, $p(3\times2)$ and $c(2\times2)$ structures respectively) was placed over top of an MgO surface with different initial configurations of the adsorbed molecules. A 12×12 patch of surface of MgO (in terms of surface unit cells) was used. Since the lattice constant of bulk MgO is 4.20 Å the patch of simulated substrate had a surface area of $(2.97 \times 12)^2 = 1270$ Å^2. A cutoff radius of 13.5 Å is imposed for the CO-CO interactions. Although no restrictions were placed on the "motion" of the molecules in the z direction (away from the surface) the molecules nonetheless stayed in the vicinity of the surface due to the attraction by the surface potential and the cold temperatures at which the simulations were run. The simulations were typically run for 50 kcycles with the first 10 kcycles being thrown away; statistics were collected for the remaining 40 kcycles. The coordinate system is similar to that shown in Fig. 3.2. The unit cell of several possible configurations of adsorbed CO molecules on MgO(001) are shown in Fig. 1.1. For example the periodicity of the

c(4×2) phase is twice the substrate unit cell along the x axis and four times the substrate unit cell in y axis.

4.3 Simulation Results

4.3.1 Single CO molecule adsorbed on the MgO(001) surface

In order to test the ion-atom parameters presented in chapter 2 that describe the surface potential of CO adsorbed on MgO(001) surface, we ran an energy minimization program at 0 K, (using the method of steepest descent) for a single CO molecule. Our data shows (as shown in Fig. 4.1) that a single CO molecule is bound to the MgO(001) surface with a binding energy of -3.69 kcal/mol and sits perpendicular to the surface over top a Mg^{2+} ion at a height of 2.58 Å (C-Mg^{2+} distance). These results are in a good agreement with available experimental and theoretical data [66-69].

The experimentally measured heat of adsorption is obtained from low coverage adsorption isotherm measurements [69] at 100 K and was found to be 4.0 kcal/mol. The infrared properties of CO adsorbed on MgO(001) surface at 77 K had been investigated in detail and reported by Escalona-Platero *et al.*[128]. This work showed that CO molecules are adsorbed perpendicular to the (001) planes of the MgO surface on the surface cations [128].

Dovesi *et al.*[73] had reported, based on their *ab initio* Hartree-Fock calculations using the CRYSTAL computer program, that the adsorption energy has a value of - 4.48 kcal/mol at a coverage of 0.25 of a monolayer. CO molecules were found to sit perpendicular to the MgO(001) surface with their C atoms down. The height of a C atom above the MgO(001) surface (Z_c) was found to have a value of 2.44 Å. The orientation with the O atom down was found to be not favorable with respect to the C-down orientation. Pacchioni *et al.* [95] reported that their computational work using cluster HF wave functions yielded an adsorption energy of -4.6 kcal/mol for CO adsorbed on MgO(001) with the C atom down [95].

According to the above discussion and the agreement of our energy minimization results with experimental and theoretical data, we conclude that our ion-atom parameters are reasonable and hence our CO-MgO surface potential is well characterized. An additional metastable orientation was found whereby the molecule is still localized above the Mg^{2+} site and is perpendicular to the surface but is inverted (oxygen down). In this case the oxygen atom sits at a height of 4.72Å above the surface and the molecule has a binding energy with the surface of only - 0.56 kcal/mol.

Our Monte Carlo simulations of a single CO molecule on MgO(001) surface at nonzero temperatures (1 K - 45 K) show that a single molecule

is adsorbed over top of Mg^{+2} with a carbon atom down (see Fig. 4.1). The total binding energy of the CO molecule to the MgO(001) surface was found to have a value of -3.88 kcal/mol. The electrostatic interaction of -6.21 kcal/mol is the main contribution to the surface binding energy. The polar angle distribution shown in Fig. 4.2 has a gaussian-like distribution centered on $\theta=0^{o}$, which means that CO molecule remains oriented perpendicular to the surface. From the distribution in the azimuthal angle (shown in Fig. 4.3) we can see that the CO molecule does not have a preferred azimuthal orientation. This result is the same as that obtained from Monte Carlo simulations of a single molecule of CO adsorbed on the NaCl(001) surface [93].

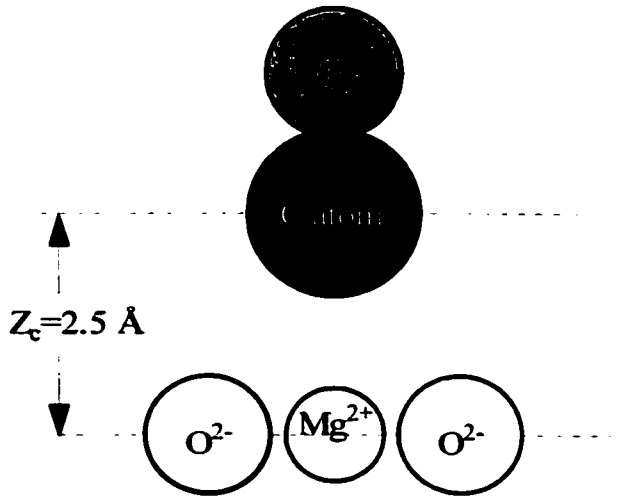

Figure 4.1. Schematic illustration of the adsorption of a single molecule over top a Mg^{2+} ion in MgO(001) surface as results from the method of steepest descent. Z_c is the height of a C atom above the MgO(001) surface.

4.3.2 CO monolayer on MgO(001)

At monolayer coverage, every Mg^{2+} site of the MgO surface is occupied by one CO molecule. Monte Carlo simulations are started with 144 molecules placed vertically on top of the MgO surface and run for at least 50 kcycles with the first 10 kcycles discarded. The final configuration form multiple domains of a $p(2\times1)$ structure with an average tilt angle of 17° with respect to the surface normal. This suggested that Monte Carlo simulations start with an initial configuration of a single domain of the $p(2\times1)$ structure. Although the molecules are allowed to change their positions and orientations, the final configuration (Fig. 4.4) at 1 K is still a $p(2\times1)$ structure. From the distrubition of the polar angle the molecules are found to be tilted by an angle of 18° and align in rows with the same azimuthal orientation of ±90°. These rows alternate their orientations and form a canted antiferroelectric structure. At a temperature of 1 K the monolayer binds to the surface with binding energy of -159 kcal/mol, which yields energy per molecule of -1.11 kcal/mol. This value is significantly less than that of a single CO molecule.

Our $p(2\times1)$ structure is similar to the low temperature structure of a monolayer of CO molecules on a NaCl(001) surface. It was found that the $p(2\times1)$ structure of the CO monolayer adsorbed on NaCl(001) surface undergoes an order-disorder transition around 35 K [93]. Such a

transition was not found in the CO/MgO system, instead, the monolayer became unstable around T = 10 K and at 11 K about 36 CO molecules left the first layer and started to form a second layer (as shown in Fig. 4.5). The 108 CO molecules remaining in the bottom layer were used as an initial structure for Monte Carlo simulations at 1 K. The resulting binding energy per molecule was -3.0 kcal/mol (-324 kcal/mol for the layer) and the molecules had a very broad distribution of tilt angles with a maximum at 25°. This layer did not show any long range ordering in terms of azimuthal orientation of the molecular axes or adsorption site occupation. The remaining 108 molecules form a layer with a coverage of (3/4) of a monolayer which has a coverage identical to that of the $c(4\times2)$ structure which will be discussed in the next section. The $p(2\times1)$ structure has not been observed experimentally and is not likely to be observed experimentally as discussed below. Previous semi-empirical calculations on the CO/MgO system by Jug and Geudtner [65] yielded a similar $p(2\times1)$ structure with a molecular tilt angle of 13°.

The $p(2\times1)$ structure is not likely to be realized experimentally. Since the lattice constant of bulk MgO is 4.20 Å, then the distance between neighbouring CO molecules (Mg-Mg distance) is 2.97 Å. This distance is smaller than the distance between CO molecules in their bulk phase (3.99 Å). For this reason the MgO surface is not expected to accommodate all molecules for a full monolayer coverage. As seen in

Table 4.1 there are considerable repulsion interactions between the CO molecules, these repulsion interactions are overcome by the attraction interactions between the molecules and the MgO surface. The competition between molecule-molecule and molecule-surface interactions force the CO molecules to adopt a high packing density structure of $p(2\times1)$ at temperatures below 10 K due to the strong attraction of the molecules to the surface. Nonetheless, a lower density structure is expected to be energetically more stable

4.3.3. CO adlayers: c(4×2) structure

From experimental investigations a $c(4\times2)$ structure was observed at low temperatures (below 40 K). Besides these experimental studies, several intensive theoretical investigations were considered in the 0 K limit to understand the origin and details of this structure. We have mentioned in section 1.4.1 that, three different models of the $c(4\times2)$ structure have been proposed [35][36][64]. The coverage of this structure was suggested to be 75% of full monolayer coverage. The proposed models consist of two or more adsorption sites for the CO molecules with each site having a different binding energy and molecular orientation.

There are many different proposed configurations at 0 K with very close adsorption energies but the experiments were performed at a finite

temperature. Hence, our simulations, which are performed at a finite temperature, give a better understanding of the stability of the c(4×2) structure. The number of adsorbed molecules is 108, for a coverage of 3/4. The simulations of each initial structure were run for at least 30 kcycle at 1 K. The cutoff radius was 13.5 Å. In Fig. 4.6 we show as an example the initial configuration similar to that proposed by Panella *et al.*[35]. Also, additional initial configurations were tested via our Monte Carlo simulations. In these initial configurations the CO molecules were either initially all pointing straight up as shown in Fig. 4.7 or all set parallel to the surface as shown in Fig. 4.8. All these initial configurations evolved to a single final configuration. This final configuration, shown in Fig. 4.9, is very close to the G-H model.

Our MC data gives us valuable knowledge of the orientation (azimuthal angle φ and polar angle θ) of the CO molecules forming the c(4×2) structure. In Fig. 4.10 we show the polar angle (θ) distributions at various temperatures (1K, 35K and 45K). At low temperature (1 K) the polar angle distribution function possesses two maxima at the values of θ equal to 0° and 31°. As the temperature increases up to 35 K the polar angle distribution still has the same two maxima ($\theta=0^\circ$ and $\theta=31^\circ$), but the distribution gradually becomes broader than at 1 K. This result is in good agreement with the experimental values of the tilt angle, $\theta=0^\circ$

and 29°, obtained using FTIR results near 35 K. Calculations of the area under these two peaks of the polar angle distribution at 35 K allow us to correlate the ratio of 1:2 between the area under the first peak ($\theta = 0^{\circ}$) and the area under the second peak ($\theta = 31^{\circ}$) with the experimental ratio of 1:2 between perpendicular and tilted molecules [36,37]. This behavior of the distribution function remains the same up to 40 K. As the temperatures increases above 40 K the maximum at 31° gradually moves towards lower values of θ and diminishes in size relative to the 0° peak. This behavior (diminishment of the 31° peak and the growth of the 0° peak) appears to be coupled to a phase transition in which some of the tilted molecules have untilted and adopted a perpendicular orientation.

Fig. 4.11 presents the azimuthal angle φ distribution at 1 K, 35 K and 45 K. At 1K the distribution of the azimuthal angle is highly uniform but additionally exhibits two maxima at $\varphi \sim \pm 90^{\circ}$. The areas under these two peaks can be correlated to that of the second peak ($\theta = 31^{\circ}$) of the polar angle distribution at 1 K to show that the preferred values of the azimuthal angle of the tilted molecules are $\varphi \sim \pm 90^{\circ}$. From these peaks we conclude that the $c(4\times2)$ structure (coverage of 3/4 of a monolayer) is highly ordered at 1 K and the tilted molecules are oriented along the symmetry axes of the surface. As the temperature grows we do not see any change in the positions of the peaks of the azimuthal

angle distribution (*i.e* at temperatures 35 K and 45 K) but they are broader indicating that the $c(4\times2)$ phase persists to at least 40 K.

The average deviations of the C atoms of the adsorbed CO molecules from the registry sites are calculated. It was found that the molecules with perpendicular orientation sit directly over top Mg^{2+} ions while the C atoms of the tilted CO molecules are displaced by approximately ±0.46 Å with respect to the Mg^{2+} ion along the y-axis.

From the above results, we can conclude that there are two kinds of oriented molecules (tilted and untilted molecules). The tilted molecules are found to form rows in which every site is occupied and the adjacent molecules in each row are tilted in opposite directions. The untilted molecules form rows where every other site is occupied so that untilted row separate nearby tilted rows. These two kinds of orientations also have different binding energies and may be thought of as two different adsorption sites. The average binding energy for the 36 perpendicular molecules is -153.72 kcal/mol and yields a binding energy of -4.27 kcal/mol for a perpendicular molecule. The average binding energy for the remaining 72 tilted molecules is -244.08 kcal/mol and thus yields a binding energy of -3.39 kcal/mol per tilted molecule. In Table 4.1 we have presented the binding energies of all these different adsorption sites. The total binding energy of the whole 3/4 layer is -

398.6 kcal/mol which yields an average binding energy per molecule of -3.69 kcal/mol.

Our MC simulations show clear evidence of the expulsion and subsequent desorption of CO molecules at 41 K. This behavior was inferred from the HAS experiments, where it was observed that the HAS diffraction spots of the $c(4\times2)$ structure, which had disappeared at 50 K, were restored upon cooling to 35 K only if the surface was exposed to additional CO gas. Direct evidence from the MC simulation is provided via the distribution function of the height z of the C atom with respect to the MgO(001) surface. At very low temperature, in particular at 1 K as shown in Fig. 4.12, the distribution has two peaks at 2.525 Å and 2.575 Å. The areas under these two peaks reveal that the first peak at 2.525 Å, corresponds to the perpendicular molecules while the second peak corresponds to the tilted molecules. The ratio of the areas under these both peaks is approximately 1:2, which is the same as that between the perpendicular and the tilted molecules. This result demonstrates that besides the difference in angular orientation, molecules show a slight difference in height z between the two adsorption sites (perpendicular and tilted sites). As the temperature increases up to 35 K, these two peaks merge into on broad single peak at 2.55 Å. As shown in Fig. 4.13, the height distribution at 45 K shows a new feature; an additional peak at ~4.5 Å that gradually grows and broadens as the temperature

increases. This additional peak clearly demonstrates that some molecules have left the substrate surface and begin to form a disordered second layer. By correlating the area under the two peaks of the height distribution z at 45 K with the final configurations at the same temperature, we observe that 12-CO molecules were desorbed and began to form a second layer leaving the bottom layer with only 96 molecules.

It is worth noting that the 96 CO molecules that remain in the bottom layer after the desorption of some CO molecules, are the same number of CO molecules required to form the $p(3\times2)$ structure proposed by Panella *et al.*[35] with the same density. In order to check whether the remaining 96 will evolve into a $p(3\times2)$ structure and to check if any further desorption will occur, the 12 molecules in the disordered second layer were removed and the simulation was subsequently run for an additional 60,000 cycles at 50K. The total binding energy of the 96 molecules after 60 kcycles is -342 kcal/mol. No further desorption took place at this temperature and from the final configuration shown in Fig. 4.14 we see that the adlayer is largely disordered, although there are small regions with either the $c(4\times2)$ structure or a $p(3\times2)$ structure. The latter structure is discussed below.

4.3.4 CO adlayers: *p*(3×2) structure

As discussed in section 1.4.1, the c(4x2) structure is transformed into a *p*(3×2) structure at temperatures between 40 and 50 K. The *p*(3×2) structure proposed by Panella *et al.* [35] contains four molecules with three different orientations per unit cell. In order to test the stability of this proposed structure we have run the Monte Carlo simulations for 60 kcycle at 1 K with an initial configuration similar to the proposed *p*(3×2) structure as can be seen in Fig. 4.15. The final configuration is shown in Fig. 4.16 with a unit cell that contains four molecules of which two molecules stand upright while the other two are tilted in opposite directions.

The distribution of the azimuthal angles (φ) at 30 K and 45 K, as shown in Fig. 4.17 has two peaks centered on $\varphi=\pm 90^{\circ}$. The distribution of the polar angles (θ) at 30 K and 45 K as shown in Fig. 4.18 exhibits two peaks at $\theta=0^{\circ}$ and 31°. It should be noted that orientations of the adsorbed molecules in the *p*(3×2) structure are the same as that of the *c*(4×2) structure.

The areas under the two peaks of the polar angle distribution are the same, which indicates that on average the number of perpendicular molecules is equal to that of the tilted molecules. However, the local

density of the tilted molecules is found to be higher than that of the perpendicular molecules and forms lines across the width of the *p*(3×2) unit cell with every adsorption site occupied.

Our *p*(3×2) structure possesses a single type of tilted site and a higher degree of symmetry than the *p*(3×2) structure proposed by Panella *et al.* [35], which has three kinds of tilted sites. The azimuthal and polar angle distributions show that there are only two kinds of oriented molecules (tilted and perpendicular), which may be thought of as two different adsorption sites with different binding energies. The average binding energy for a perpendicular molecule is -4.25 kcal/mol. The average binding energy for a tilted one is -3.40 kcal/mol. These values of the binding energy are close to those of the *c*(4×2) phase. Table 4.1 contains the binding energies of all these different adsorption sites. The total binding energy of a 2/3 layer with 96 molecules is -367.6 kcal/mol, which is weaker than that of the *c*(4×2) structure, and is due to the lower average density of molecules in the *p*(3×2) phase. The average binding energy per CO molecule of the *p*(3×2) structure is found to have a value of -3.829 kcal/mol at 1 K. Because of the higher percentage of perpendicular molecules in the *p*(3×2) structure than that of the *c*(4×2), the average binding energy per molecule of the *p*(3×2) phase is stronger than the *c*(4×2) phase.

It is worth noting that when MC simulations were run at 45 K for the remaining 96 molecules in the first layer of the c(4x2) structure (due to the expulsion of molecules from the *c*(4×2) phase as discussed in section 4.3.3), the resulting total binding energy of the remaining layer is weaker than that of the *p*(3×2) phase. In other words, the ordered *p*(3×2) structure is more stable. This *p*(3×2) structure at 45 K is shown in Fig. 4.19.

Finite temperature simulations of the *p*(3×2) structure have shown that this structure is thermally stable up to a temperature 50 K (see Fig. 4.19 and Fig. 4.20). Above 50 K some of the CO molecules were expelled from the layer and the level of disorder within the bottom layer significantly increased (see Fig. 4.20). As can be seen in Fig. 4.21, the distribution function P(z) of the height (z) of a C atom above the surface at 55 K, and the magnified region around 4.5 Å, show that six CO molecules were expelled from the first layer after 80 kcycle of MC steps. The remaining 90 molecules have a coverage of 62.5 % which is the same coverage needed to form a *c*(8×2) structure. This important result is in a good agreement with the LEED experiment [35] where the *p*(3×2) structure undergoes a phase transition into a lower density sequence of (n×2) structures with "n" an integer increasing with temperature. Even though the *p*(3×2) structure has a smaller binding energy per unit area

than the $c(4\times2)$ structure, as shown in Table 4.1, the $p(3\times2)$ phase can survive to temperatures higher than those which the $c(4\times2)$ phase can.

As we have seen in section 4.3.3, the analysis of the polar angle distribution for $c(4\times2)$ structure at 45 K indicates that some of the tilted molecules adopt a perpendicular orientation. Also by comparing the geometry of the $c(4\times2)$ and $p(3\times2)$ structures we found that the number of stripes of tilted molecules is lower in the $p(3\times2)$ phase than those in the $c(4\times2)$ phase whereas the number of perpendicular sites in $p(3\times2)$ is more than that of the $c(4\times2)$ structure. This increase in the occupation of perpendicular sites as the temperature is increased suggests that under the right conditions an adlayer will sequentially expel and convert tilted molecules to perpendicular ones in order to increase the distance between the remaining rows of tilted molecules. This would result in the following sequence of transformations:

$$c(4\times2) \rightarrow p(3\times2) \rightarrow c(8\times2) \rightarrow p(5\times2) \rightarrow c(12\times2) \rightarrow \ldots\ldots \rightarrow c(2\times2)\ .$$

The above sequence of transformations might be the set of $(n\times2)$ structures observed by Panella *et al.*[35]. In this case it arises from the coupling of molecular positions and orientations as suggested in Ref. 35. In order to shed more light on this sequence of transformations we have run MC simulations for the $c(8\times2)$ and $c(2\times2)$ structures.

4.3.5 CO adlayers: c(8×2) structure

It is important to perform MC simulations in order to study the stability of the *c*(8×2) structure which was suggested to be part of the sequence of transformations mentioned in the end of the previous section 4.3.4. It is worth noting that this structure was not observed definitively by experiments, but the LEED experiments [35] suggested that such a structure would exist as part of the sequence of (*n*×2) transition that were observed.

In order to perform these simulations and satisfy the boundary conditions this structure needs a larger surface area than that used for the *c*(4×2) and *p*(3×2) structures. Thus, an initial configuration consisting of 160 molecules over top of a 16×16 patch of MgO(001) surface was used. This initial structure has a surface coverage of 5/8 of a monolayer.

The final configuration obtained from the MC simulations at 1 K is shown in Fig. 4.22. The unit cell of this structure contains ten CO molecules with five different orientations (polar and azimuthal). This can be also seen in Fig. 4.23, where the polar angle distribution (θ) at 1 K exhibits three maxima: the first at $\theta=0^{\circ}$, the second at $\theta=7^{\circ}$ and the third at $\theta=31^{\circ}$. So that the unit cell consists of two untilted molecule,

four molecules with a tilt angle of $\theta=7^{\circ}$ and four molecules with a tilt angle of $\theta=31^{\circ}$. Note, however, that the molecules with a tilt of 7° have an orientation that is closer to the untilted molecules ($\theta=0°$) than the molecules tilted by 31°.

This structure is found to have a total binding energy of -622.5 kcal/mol, and yields a binding energy of -3.89 kcal/mol per molecule. The thermal stability of this structure is examined via the MC method. We found that this structure is stable up to 45 K. The final configuration at 50 K after 60 kcycles shown in Fig. 4.24, indicate that, some islands of this structure survive until 50 K and that a small portion of a unknown new pattern arises as well.

4.3.6 CO adlayers: $c(2\times2)$ structure

The initial configuration for our Monte Carlo simulations of the $c(2\times2)$ consists of 72 molecules where only half of the Mg sites are occupied by CO molecules placed in a checkerboard pattern. We started our simulations at 1 K with all molecules perpendicular to the surface and occupying every other Mg^{+2} site. Although the molecules are allowed to change their positions and orientations during the simulations the final structure stayed almost the same as the initial configuration as shown in Fig. 4.25. From the simulations at 1 K the resulting binding

energy per molecule is -4.13 kcal/mol where the binding energy of the layer of c(2x2) structure is -297.2 kcal/mol (see Table 4.1). The value of the binding energy per molecule for the *c*(2×2) is slightly more than the surface binding energy (-3.88 kcal/mol) of an isolated perpendicular molecule and also greater than that of the binding energy per molecule in case of *c*(4×2) and *p*(3×2) structures. The difference between this binding energy and the binding energy of the isolated molecule is accounted for by the net attraction of -0.25 kcal/mol between the molecules. Although this structure has higher (weaker) binding energy per unit area than that of the *c*(4×2) and *p*(3×2) phases, it was found to be stable over a wider temperature range (1 K to 100 K).

4.3.7 Stability of the *c*(4×2) and *p*(3×2) phases

Since the *c*(4×2) and *p*(3×2) phases have different numbers of molecules over top the same surface area and the number of tilted and untilited molecules is different in these two phases, it is not appropriate to study their relative stability in terms of their binding energy per molecule. Instead we could use their total binding energies for the whole layers. By looking to the total binding energies of these two structures at 1 K as in Table 4.1 we can see that at 1 K the *c*(4×2) has total binding energy lower by 31 kcal/mol than that of the *p*(3×2) phase. This indicates that the c(4×2) phase is more stable than the *p*(3×2) phase.

However the relative stability between the two phases becomes difficult to compare because the number of adsorbed molecules is not the same. The appropriate quantity to examine is therefore the Gibbs free energy. As discussed in the previous sections, experiments and our simulations show that the *c*(4×2) phase becomes unstable at 40 K and transforms either into a disordered (1×1) phase or the *p*(3×2) phase depending on the conditions of the experiments *i.e;* pressure of the gas above the surface. The appropriate method to study and the relative stability beween these two phases is the Monte Carlo simulations using the grand canonical ensemble. We have not performed such a calculation but instead have attempted to understand the origin of the pressure and temperature dependent instability through the use of a relatively simple theory.

We start by constructing a difference function from the Gibbs free energies of the two phases. In particular, we form $\Delta G = G_a - G_b$ where G_a is the Gibbs free energy of the *c*(4×2) phase and G_b is that of the *p*(3×2) phase. If ΔG is negative then the *c*(4×2) phase is stable, whereas if ΔG is positive then the *p*(3×2) phase is stable. The difference in Gibbs free energies may be expressed in terms of other macroscopic variables as follows,

$$\Delta G = G_a - G_b = - A' (\tilde{\gamma}_a - \tilde{\gamma}_b) + \mu'(N_a - N_b) \qquad (4.1)$$

where A′ is the surface area covered by the film, μ′ is the chemical potential of the film which is in equilibrium with the gas resevoir above the surface, $\tilde{\gamma}_j$ is the surface tension and N_j is the number of CO molecules in phase *j* covering area A′. Once again the subscripts "a" and "b" refer to the *c*(4×2) phase and *p*(3×2) phase respectively. In order to closely mimic our simulations and simplify the calculations the two different phases are taken to have the same number of molecules, *i.e.* the number of molecules found in the *c*(4×2) phase. This creates an excess of particles for a *p*(3×2) monolayer and leads to a structure with two layers: the bottom layer has the *p*(3×2) structure discussed in Section 4.3.4 with the excess molecules residing in a second layer above the bottom layer. The difference in Gibbs free energy therefore depends only on the difference in surface tensions of the two phases. An algebraic expression of ΔG as a function of gas pressure P and temperature T can be obtained if the pressure and temperature dependence of the surface tensions are known. Such an expression should yield the correct temperature (T = 40 K) at which the *c*(4×2) phase becomes unstable. Furthermore it should contain information on the pressure dependence of the stabilities.

The surface tension of a film can be expressed in terms of the grand partition function Ξ as follows

$$\tilde{\gamma} = \tilde{\gamma}^{0} - N_0 k_B T[ln(\Xi)]_{P'=0}^{P'=P} \tag{4.2}$$

where $\tilde{\gamma}^0$ is the surface tension of the clean surface. The grand canonical partition function for our two phases can be expressed generally as a model with three adsorption sites: two sites in the first layer and one site in the second layer. The c(4×2) phase of course has no molecules in the second layer and hence is a special case of the two layer model. We further require that the occupancy of the various sites always be equal to the ratios found in their respective "monolayer" structures. Using the methods of statistical mechanics applied to adsorption [150], the grand canonical partition function may be expressed as follows,

$$\Xi = 1 + \left[\frac{n_1}{N_0} exp((\mu' + \varepsilon_1)\beta) + \frac{n_2}{N_0} exp((\mu' + \varepsilon_2)\beta)\right] \times \left[1 + \frac{n_3}{N_0} exp((\mu' + \varepsilon_3)\beta)\right] \tag{4.3}$$

where n_i is a number of CO molecules in site i with a binding energy of ε_i (i=1,23), $\frac{1}{k_B T} = \beta$, N_0 is the total number of adsorbed molecules. Note that the convention used in the formula above is to express the binding energies as positive numbers. The surface tension can therefore be expressed as,

$$\tilde{\gamma} = \tilde{\gamma}^{o} - k_B T \ln\left\{1 + \left[\frac{n_1}{NP_1^*} + \frac{n_2}{NP_2^*}\right]P + \frac{n_3}{N}\left[\frac{n_1}{NP_1^*} + \frac{n_2}{NP_2^*}\right]\frac{P^2}{P_3^*}\right\} \tag{4.4}$$

with the half coverage pressures P_i^* defined as,

$$P_i^* = (k_B T)^{7/2}\left(\frac{m}{2\pi\hbar^2}\right)^{3/2}\left(\frac{2I}{\hbar^2}\right)exp\left(\frac{-\varepsilon_i}{k_B T}\right) \tag{4.5}$$

where m is the mass of the molecule (m =4.65×10^{-26} kg), I the moment of inertia (I =14.4×10^{-47} kg•m^2•molecule^{-1}) [151] and $\hbar = \frac{h}{2\pi}$ where h is the planck's constant. Note that the expression for the chemical potential of an ideal gas has been used, *i.e.*,

$$exp(\mu'\beta) = \frac{P}{(k_B T)^{7/2}\left(\frac{m}{2\pi\hbar^2}\right)^{3/2}\left(\frac{2I}{\hbar^2}\right)} \tag{4.6}$$

Finally, using equations (4.1) and (4.4) the difference in Gibbs free energy between the phases is,

$$\Delta G = -Nk_B T \ln\left\{\frac{1 + \left[\frac{n_{1a}}{NP_{1a}^*} + \frac{n_{2a}}{NP_{2a}^*}\right]}{1 + \left[\frac{n_{1b}}{NP_{1b}^*} + \frac{n_{2b}}{NP_{2b}^*}\right]P + \frac{n_{3b}}{N}\left[\frac{n_{1b}}{NP_{1b}^*} + \frac{n_{2b}}{NP_{2b}^*}\right]\frac{P^2}{P_{3b}^*}}\right\} \tag{4.7}$$

This formula is illustrated in Fig. 4.26 where the difference in Gibbs free energy, ΔG, is plotted as a function of temperature for several different values of the pressure. The values of the binding energies needed for the evaluation of the P^* used in the formula are found in

Table 4.1 and the value used for ε_3 is -1.24 kcal/mol. All of the curves have negative values for ΔG at temperatures below 40 K and are coincident showing that ΔG is almost independent of pressure below this temperature. The negative values of ΔG indicate that the *c*(4×2) phase has the lower free energy and hence is the stable phase up to 40 K. This is in agreement with the experimental findings as well as our simulations. Above 40 K the values of the free energy depend on the pressure as well as the temperature. At a pressure of 10^{-7} mbar and temperatures above 40 K the free energy takes on positive values indicating that the *p*(3×2) phase is stable. The free energy eventually rises to a maximum of 0.045 kcal/mol near 48 K. The model therefore predicts that a phase transformation from the *c*(4×2) phase to the *p*(3×2) phase should occur at 40 K. Such a transformation was observed in the LEED work [35] done at 10^{-7} mbar.

At pressures below 10^{-7} mbar the maximum of ΔG shifts to lower temperatures and diminishes in value. At very low pressures and temperatures above 40 K, the value of ΔG becomes negligibly small implying that the *p*(3×2) phase is at best marginally stable with respect to the *c*(4×2) phase. Hence the *c*(4×2) phase might not undergo a transformation to the *p*(3×2) phase before becoming disordered. This kind of behaviour has been observed in the HAS and PIRS experiments

done at 10^{-9} mbar where the *c*(4×2) phase disorders at 45 K without converting to the *p*(3×2) phase. However, at this pressure Eq. 4.7 yields a curve with a maximum of 0.025 kcal/mol occurring at 44 K indicating that the *p*(3×2) phase would be stable above 40 K. This discrepancy with the experimental findings might be due to the crudeness of the model or possibly the experimental process not providing sufficient time for the transformation to occur, *i.e.* the *c*(4×2) phase might be metastable. Despite this deficiency, the model predicts a transformation temperature in agreement with the LEED results and qualitatively suggests that at low enough pressures the transformation to the *p*(3×2) phase would be suppressed in accord with the PIRS and HAS work.

In the above calculations the lateral interactions between molecules have been included. If these interactions are omitted the transformation temperature shifts to near 50 K and becomes pressure dependent. It therefore seems necessary to include molecule-molecule interactions to achieve good agreement with experiment.

4.3.8. Realization of the theory of devil's staircase

The stable and highly ordered commensurate structures discussed in the previous sections are thought to be part of a sequence of transformations that interconvert these (n×2) structures and thus

provide an example of the devil's staircase phenomenon, which was discussed in chapter 1. Such a phenomenon is due to the coupling of changes in positions and orientations of the adsorbed molecules. The manner of this transformation is discussed below.

Through the use of MC simulations, it was shown that the $c(4\times2)$ structure becomes unstable above 41 K while the $p(3\times2)$ structure become unstable beyond 50 K. Both of these structures become unstable due to the desorption of some CO molecules from the first layer to form a second one. Also some molecules convert their orientation states from tilted to untilted. These two features may be viewed as evidence in support of the LEED observation of a sequence of transformations giving rise to a series of $(n\times2)$ phases. Our simulations indicate that in the CO/MgO system the number of tilted and untilted rows is changing in each succeeding transformation, while the number of tilted rows between untilted rows is increased in each succeeding stable structure. It was found that the c(2×2) structure with 1/2 coverage consists of only untilted molecules, while the monolayer was found to adopt a $p(2\times1)$ structure formed entirely from rows of tilted molecules. Between these two limiting structures the sequence proceeds as follows. The c(4×2) structure has one untilted row between tilted rows; the $p(3\times2)$ structure has two untilted rows between tilted rows; the c(8×2) has three untilted rows between tilted rows, *etc.* This idea has allowed us to write

the coverage of any succeeding structure as a function of untilted rows between tilted rows;

$$\Theta_n = \frac{1 \cdot 1 + n \cdot 0.5}{1+n} = \frac{n+2}{2n+2} \tag{4.8}$$

where Θ_n is the coverage of a structure with n untilted rows between the nearby tilted rows (n=0,1,2,3,...). Thus when n=0 the coverage equals one which corresponds to monolayer coverage; when n=1 the coverage equals 3/4 which corresponds to the *c*(4×2) structure, when n=2 the coverage equal 2/3 which corresponds to the *p*(3×2) structure, when n=3 the coverage equal 5/8 which corresponded to *c*(8×2) *etc*... We propose that a sequence of transitions through a set of (n×2)-type structures with ever decreasing density is possible under suitable conditions of temperature and pressure. This sequence of transitions is an example of devil's staircase phenomenon.

4.3.9 Discussion and conclusions

Through Metropolis Monte Carlo simulations we have performed a computational study on the stabilities and structures of different phases of CO molecules physisorbed on an MgO(001) surface. Some of these phases have been observed experimentally and were also the subject of intensive theoretical studies in the limit of 0 K temperature. There were

some discrepancies in the experimentally observed structures at high temperatures (around 45 K): LEED experiment showed that the c(4×2) phase undergoes a phase transition into *p*(3×2) structure and then at 51 K undergoes a sequence of (n×2) phases, while the HAS experiments had found that c(4×2) structure transforms directly into a lower density disordered phase accompanied by the desorption of some CO molecules. Attempts, through energy minimization at 0 K, to resolve these discrepancies have failed. The main cause of this failure is that the experiments were performed at finite temperature whereas the theoretical studies were performed in the 0 K limit. By including for the first time the thermal effects on the stabilities of the different observed phases, we have resolved some of the discrepancies in the results of these experiments. Besides, this valuable achievement we have proven that our model can reproduce most of the experimentally known data. In addition, we have shown that the phase transitions in the CO/MgO(001) system is a possible realization of a devil's staircase. A summary of the various structures is given below.

A single CO molecule was found to adsorb on top of Mg^{2+} ion with a C atom down and binding energy of -3.88 kcal/mol. This result is in a good agreement with the most recent experimental values of the binding energy of CO molecules on MgO(001) surface[68][79].

A monolayer, where every site of Mg^{2+} is occupied by one CO molecule, was found to adopt a $p(2\times1)$ structure at 1 K which is very similar to that observed in CO/NaCl system. This structure could not survive as the temperature was increased to 5 K, beyond which some CO molecules desorbed from the layer, the density of the remaining molecules is the same as that of the $c(4\times2)$ structure.

Our simulations confirm for the first time that the c(4×2) structure, with a symmetry similar to that of the G-H model, is the most stable structure below 40 K. In agreement with the experiments, this structure contains three molecules per primitive unit cell (six per centered cell): two tilted CO molecules in opposite direction ($\theta=31^{\circ}$) separated by one perpendicular molecule. These two kinds of orientations could be considered as two adsorption sites: one (perpendicular) is localized on an Mg^{2+} ion, while the other one (tilted) is displaced from the Mg^{2+} ion by 0.46 Å in the direction of the tilt.

A further increase of the temperature shows that the $c(4\times2)$ structure is thermally stable up to 40 K after which the structure becomes unstable. This instability, accompanied by desorption of some molecules and the conversion of tilted molecules to untilted ones, causes the surface density (coverage) to be lowered to that required for the $p(3\times2)$ structure. It should be pointed out that the remaining molecules

in the first disordered layer do not explicitly evolve into a uniform $p(3\times2)$ structure in the time allotted for the simulation but they do adopt similar features in terms of coverage and numbers of tilted and perpendicular molecules. Energetic considerations suggest that the $p(3\times2)$ structure will emerge out of the disordered structure. If conditions are such that the disordered structure persists then thermal effects will cause the vacancies in the adsorption sites to behave like a lattice gas. This feature coupled with dynamical effects governing the librations of the CO molecules [151] may cause the layer to appear to have the (1×1) structure observed in the HAS and PIRS experiments.

The $p(3\times2)$ phase is found to be stable up to 50 K. the unit cell of this structure contains four molecules with a 1:1 ratio of tilted (31°) and untilted molecules. Two rows of untilted molecules separate nearby tilted rows. It is worth nothing that this phase is thermally stable between 40 K and 50 K whereas the $c(4\times2)$ phase is not stable in this range of temperatures. This feature can be viewed as evidence in support of the LEED observation of the $p(3\times2)$ structure in this range of temperatures. Beyond 50 K this structure becomes unstable due to the desorption of some CO molecules from the first layer to form a second one. Also, some molecules convert their states from tilted to untilted states. These two features may be viewed as evidence in support of the

LEED observations of a sequence of transformations giving rise to a series of (n×2) phases as discussed previously.

Besides MC simulations, a study of the relative stabilities of the c(4×2) and the p(3×2) structures, through the use of a microscopic model for the surface tension, was conducted. In particular the difference in Gibbs free energies of the two phases was calculated for a variety of pressures over the temperature range of interest ~30–60 K. It was found that below 40 K the c(4×2) structure was indeed more stable than the p(3×2) structure, but above this temperature the reverse was true. This finding is consistent with the MC simulations where the c(4×2) structure became unstable at 40 K while the p(3×2) structure remained stable up to 50 K. The relative stability between these two phases was found to be a function of pressure. At very low pressures the difference in Gibb's free energies between the two phases became so small that the likelihood of the c(4×2) phase transforming into the p(3×2) phase above 40 K was deemed negligible. Instead the c(4×2) phase is thought to simply expel molecules and become disordered. This combination of findings from simulations and calculations reconciles the seemingly contradictory experimental results, namely, that above 40 K and at pressures near 10^{-7} mbar the c(4×2) phase transforms to the p(3×2) phase in agreement with the LEED work [33][35] while at lower pressures the c(4×2) phase will

disorder and appear as a (1×1) phase in agreement with the results of HAS [36] and PIRS [37]. It would be useful if LEED work could be done in conjunction with HAS and PIRS to confirm this explanation, especially in the temperature range of 40–60 K where the phase transformations and devil's staircase phenomenon occur. Additional theoretical investigations using grand canonical Monte Carlo and molecular dynamics methods might also shed more light on this system.

TABLE 4.1: Geometries ($Z_{C\text{-}Mg}$ (Å) the height of C atom above Mg^{2+} ion , and the tilt angle θ of the molecular axis with respect to the surface normal), binding energy $E_{molecule}$ (kcal/mol) per molecule, total binding energy E_{total} (kcal/mol) for tilted CO∠ molecules and untilted $CO_{\perp}$ molecules and E_{layer} (kcal/mol) average binding energy of all CO molecules adsorbed on MgO(100) surface.

structure	1 CO	144 CO	108 CO		96 CO		72 CO
Coverage		*p*(2×1)	*c*(4×2)		*p*(3×2)		*c*(2×2)
Sites	$CO_{\perp}$	1.0 CO∠	0.75 $CO_{\perp}$	CO∠	0.66 $CO_{\perp}$	CO∠	0.50 $CO_{\perp}$
CO molecules	1	144	36	72	48	48	72
$Z_{C\text{-}Mg}$ (Å)	2.58	2.588	2.525	2.575	2.525	2.575	2.525
θ	0	17	0	31	0	31	0
$E_{molecule}$	-3.88	-1.1	-4.27	-3.39	-4.25	-3.4	-4.13
E_{total}	-3.88	-158	-154	-244	-204	-163	-297
E_{layer}	-3.88	-158	-398.6		-367.6		-297
Total E/molecule	3.88	-1.1	-3.69		-3.83		4.13

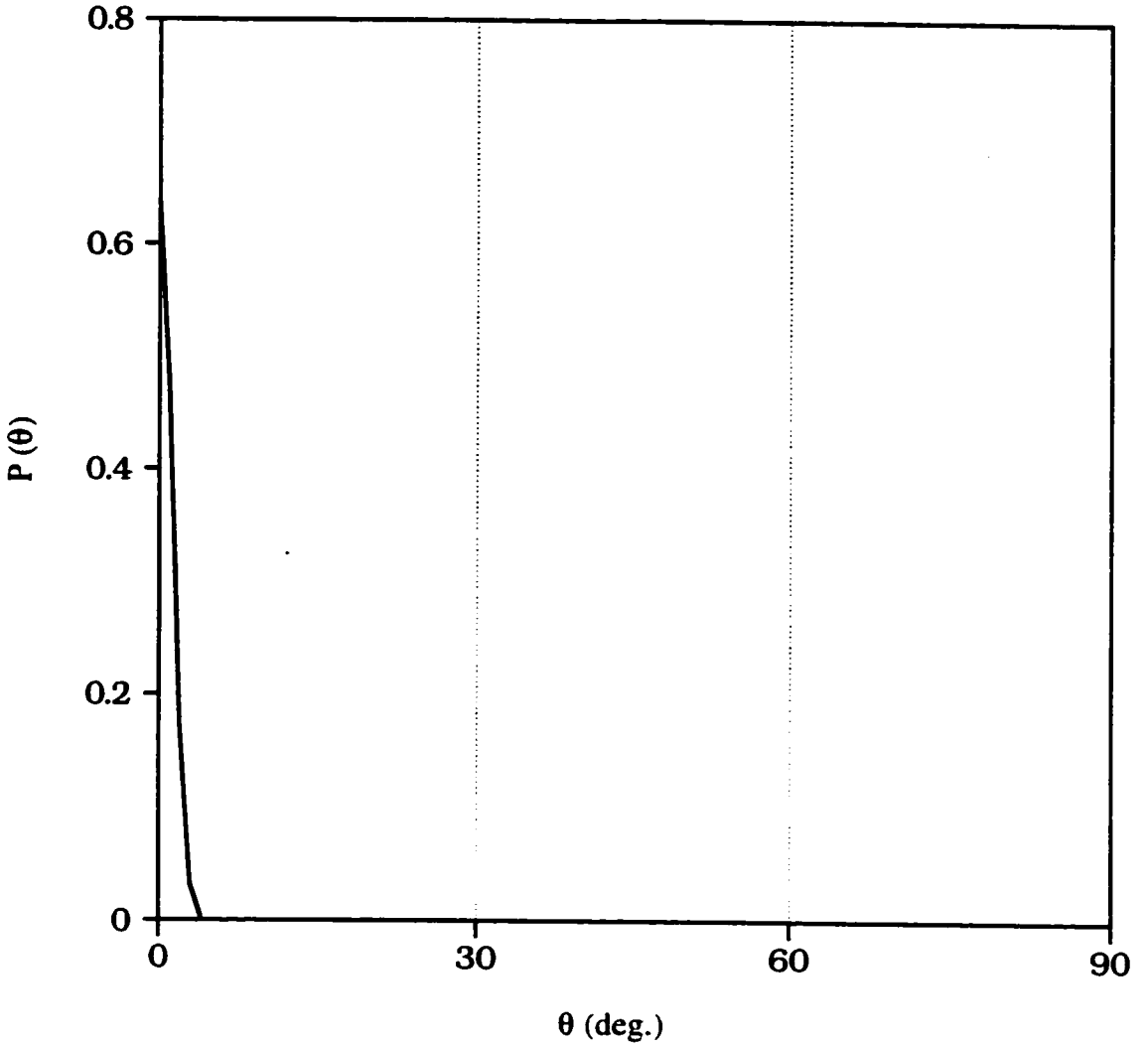

Figure 4.2. Polar angle (θ) distribution for one CO molecule adsorbed on MgO(001) surface at 1 K. Note that the distribution has a peak centered on θ=0 (deg.). CO molecule stand perpendicular to the surface. The data are obtained from 50 kcycle of MC steps after equilibration.

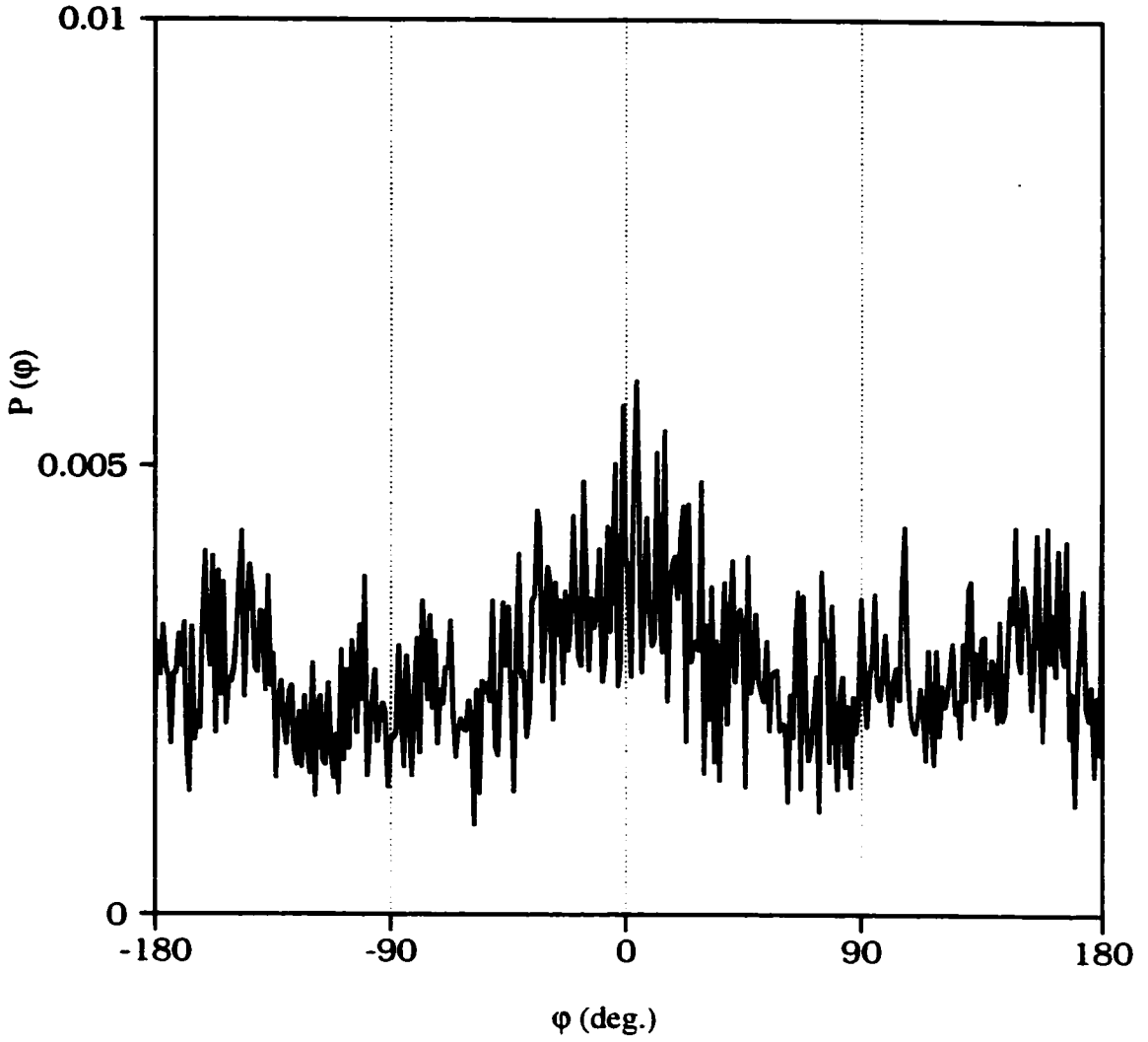

Figure 4.3. Azimuthal angle (φ) distribution for one CO molecule adsorbed on MgO(001) surface at 1 K. Note that CO molecule does not prefer any azimuthal orientation. The data are obtained from 50 kcycle of MC steps after equilibration.

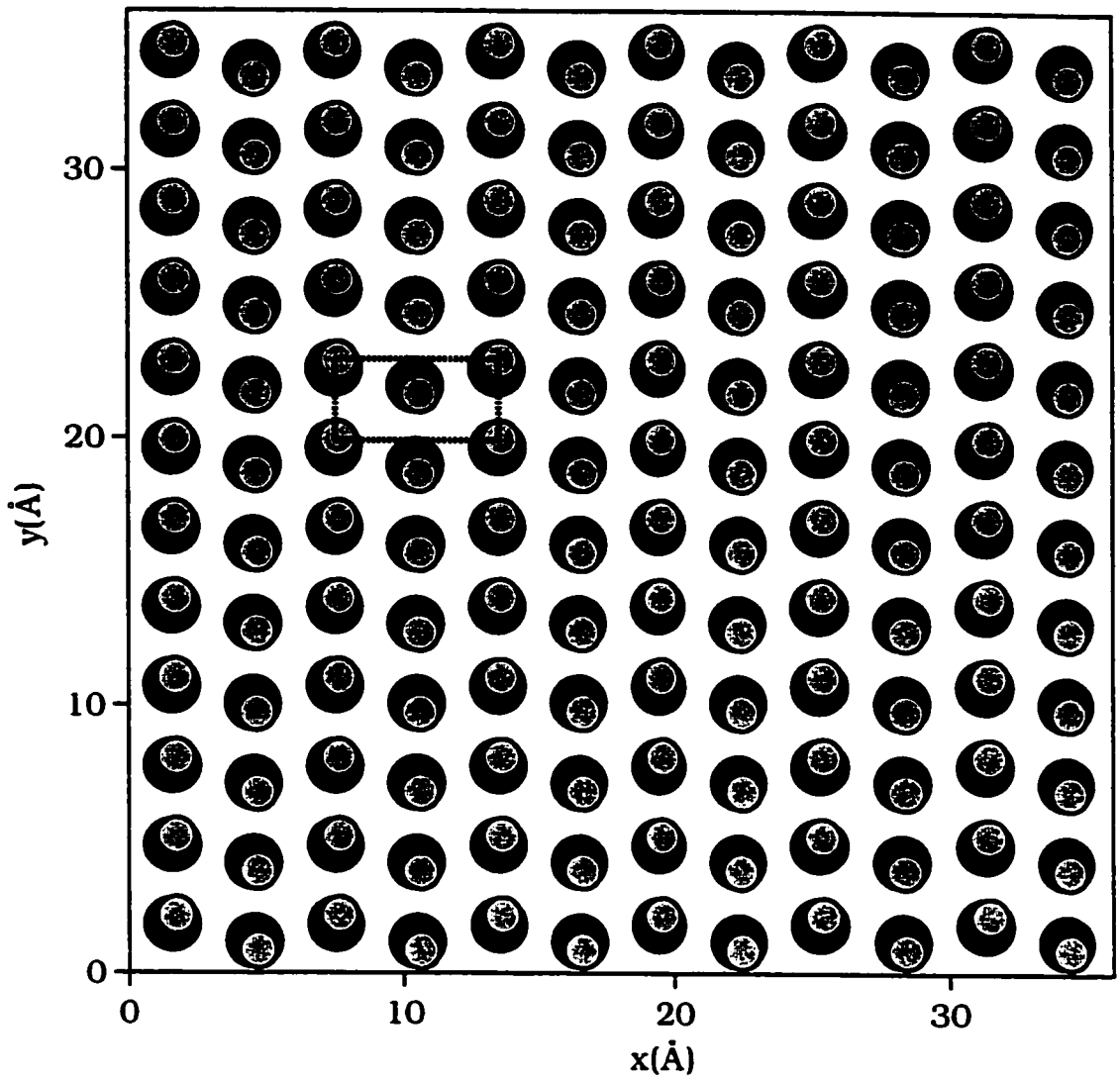

Figure 4.4. An overview of a typical monolayer of *p*(2x1) configuration of 144 CO molecules physisorbed on MgO(001) surface at 1 K . The C atoms closest to the surface are shown as black and the O atoms as gray. The *p*(2x1) unit cell is shown by square with dot lines.

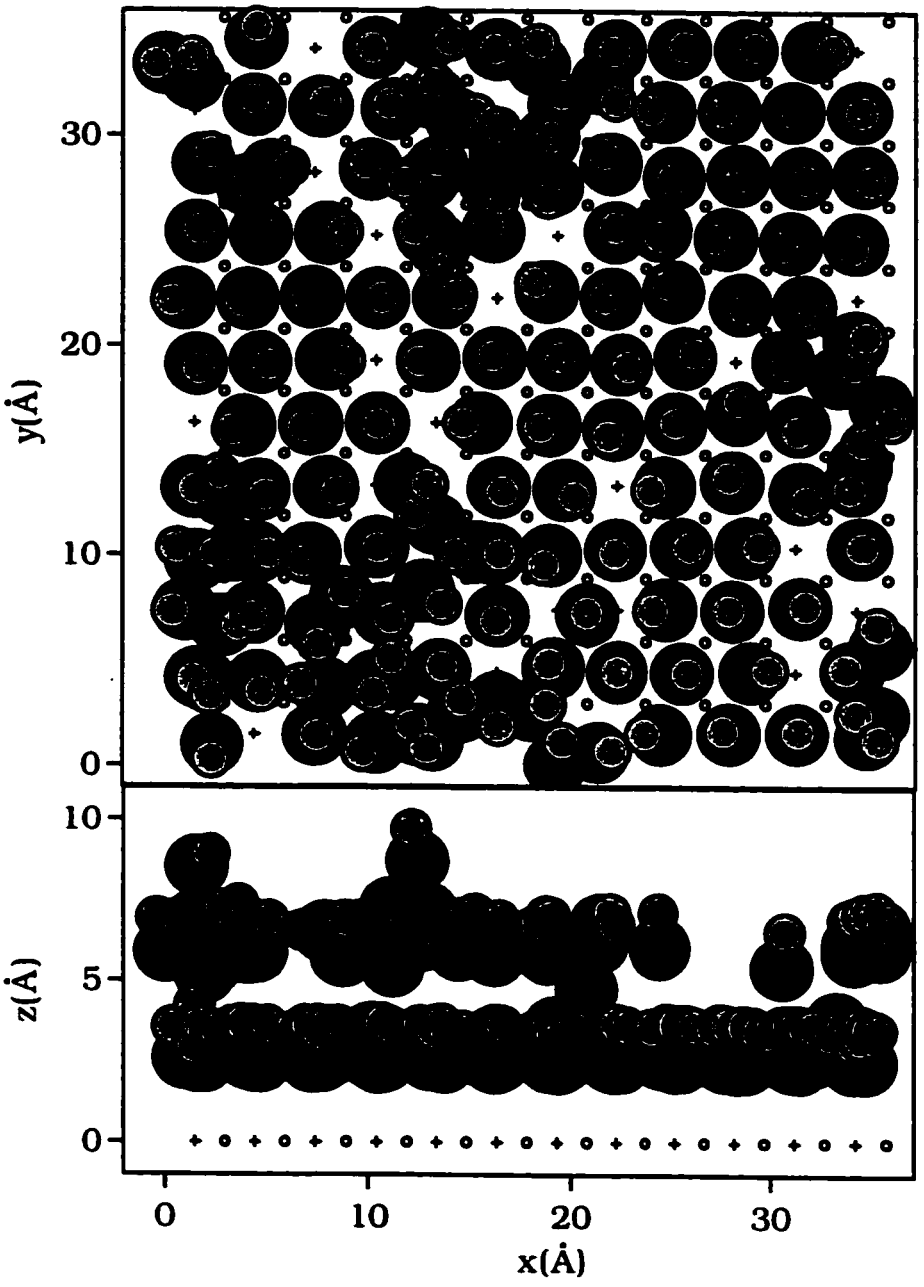

Figure 4.5. An overview of final configuration of 144 CO molecules at 11 K (top panel) where the *p*(2x1) structure become unstable and 36 molecules desorbed from the first layer to form a second layer. The bottom panel is a sideview of the top panel. Mg^{2+} ions presented by + sign while O^{2-} ions presented by a small circle.

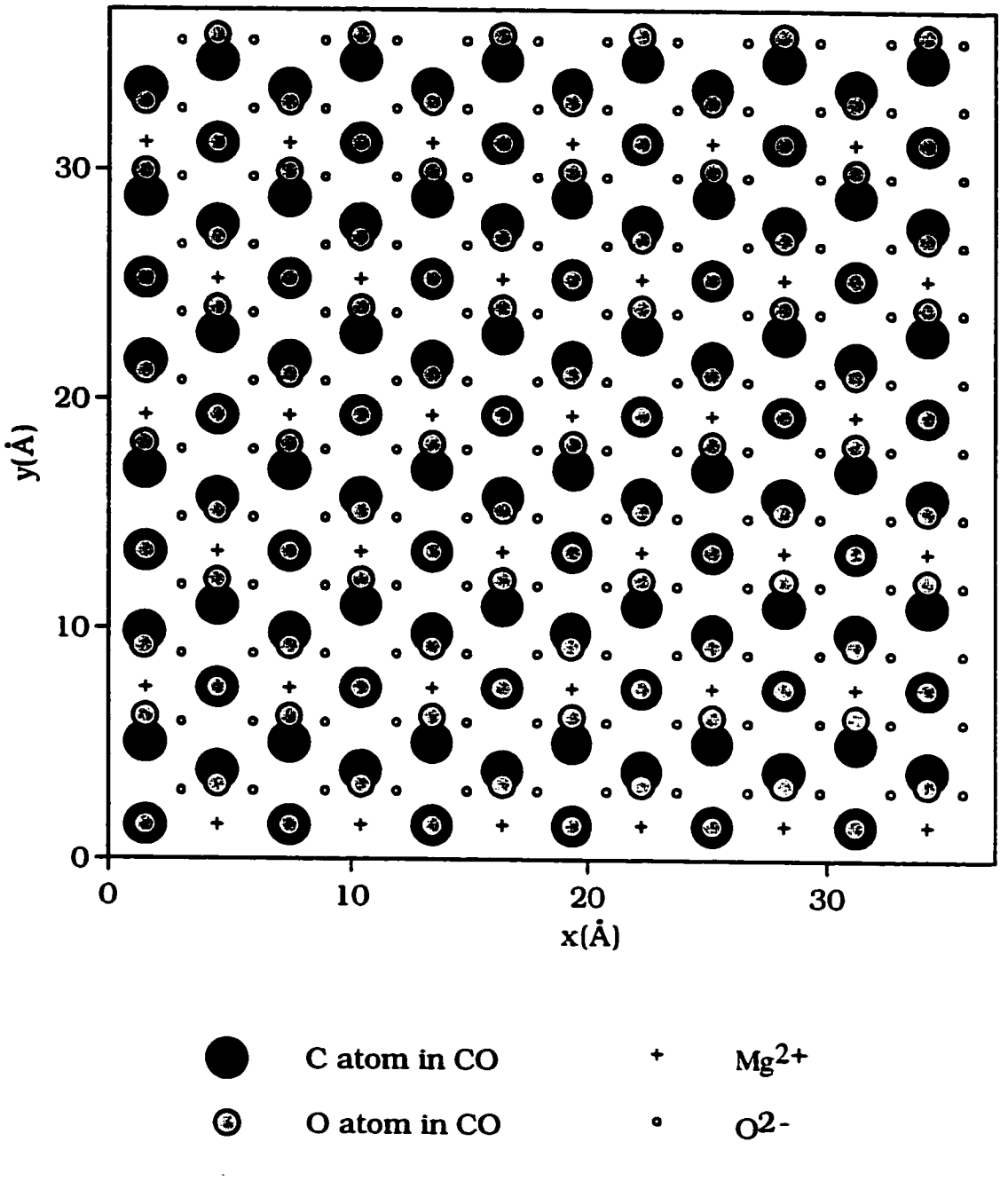

Figure 4.6. Initial configuration of the (4x2) structure similar to that proposed by Panella *et al.*[35]

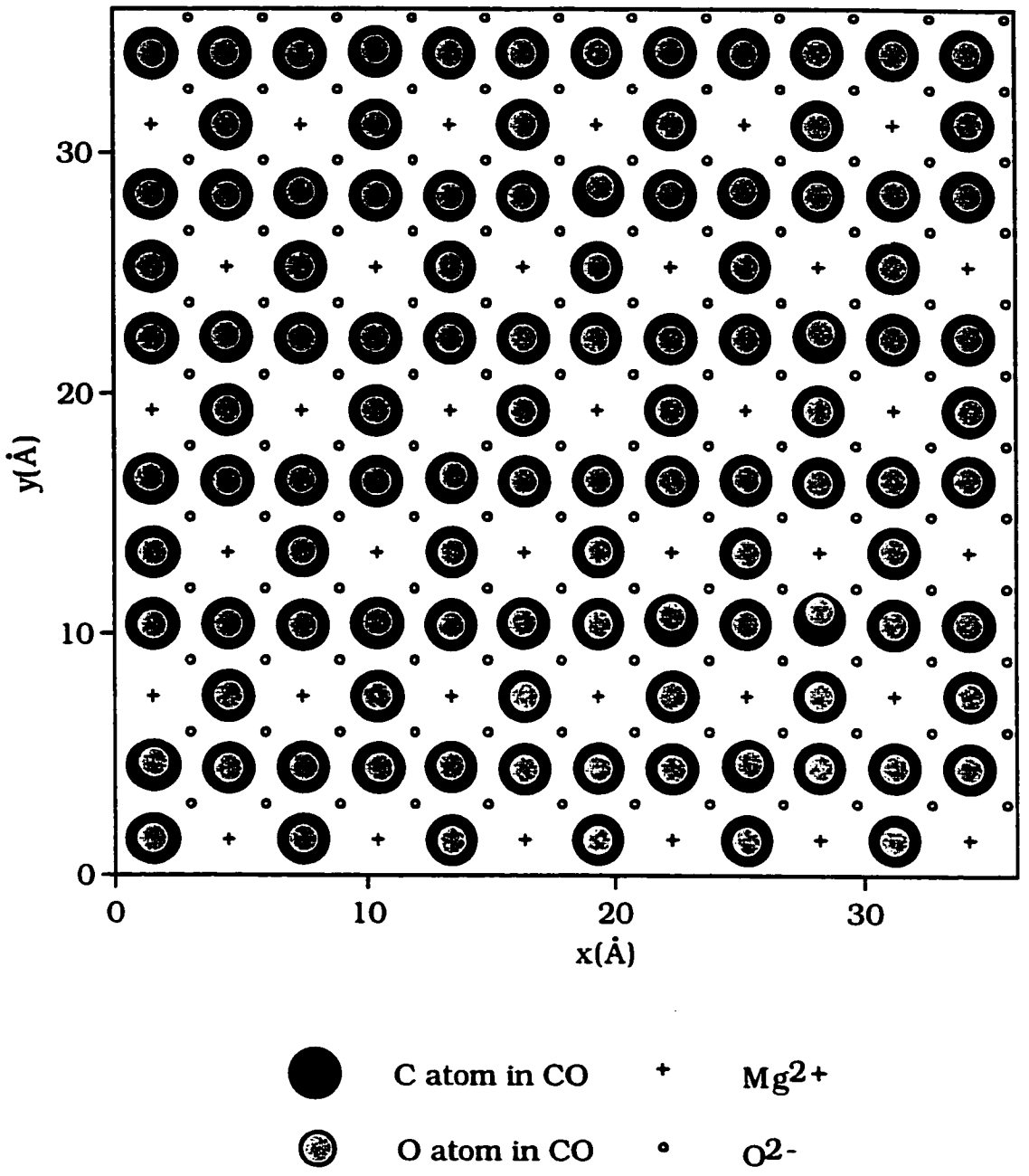

Figure 4.7. Initial configuration of straight up structure of the (4x2) structure of CO molecules on MgO(001) surface.

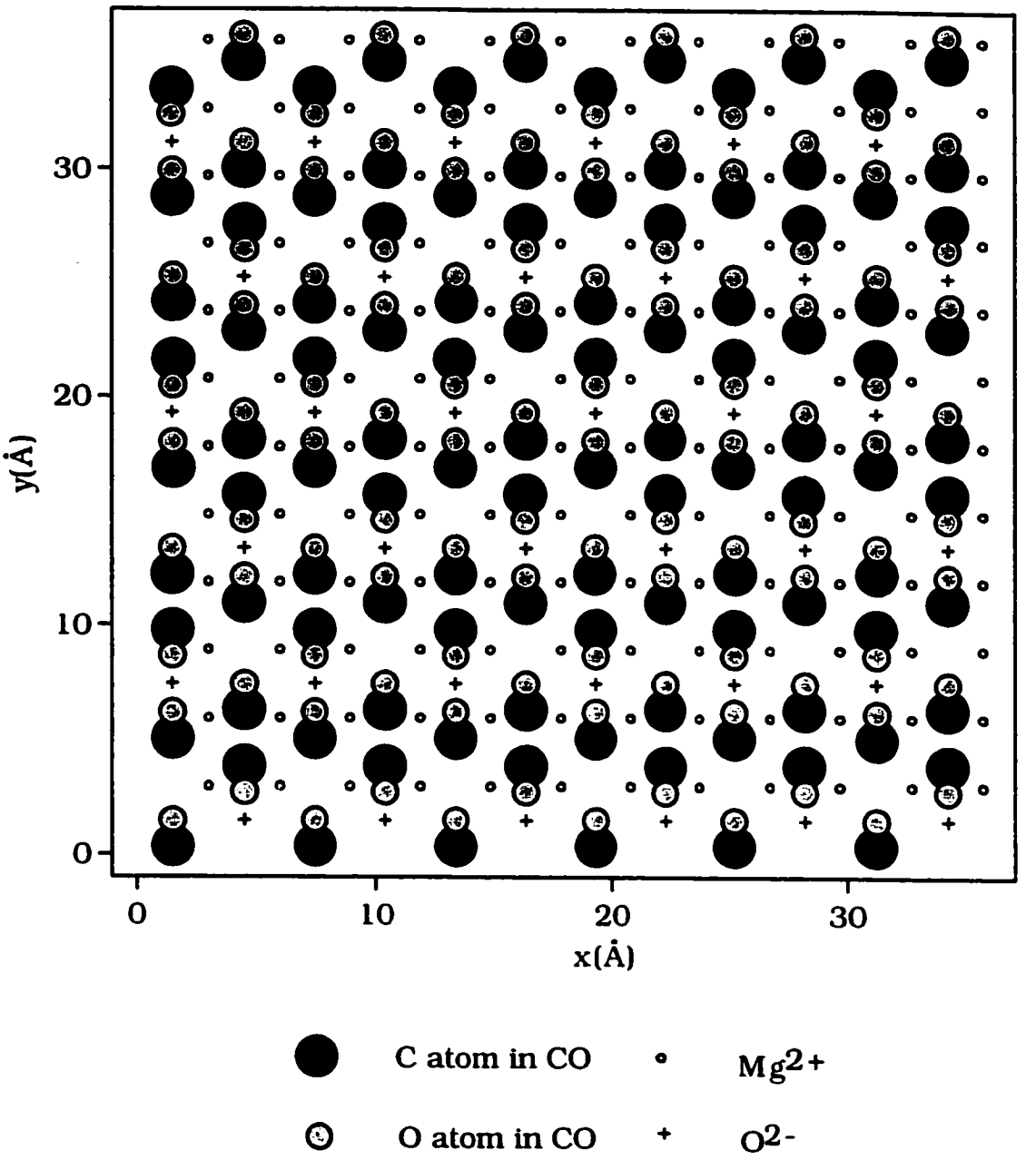

Figure 4.8. Initial configuration of the (4x2) structure. All the CO molecules are paralell to the surface.

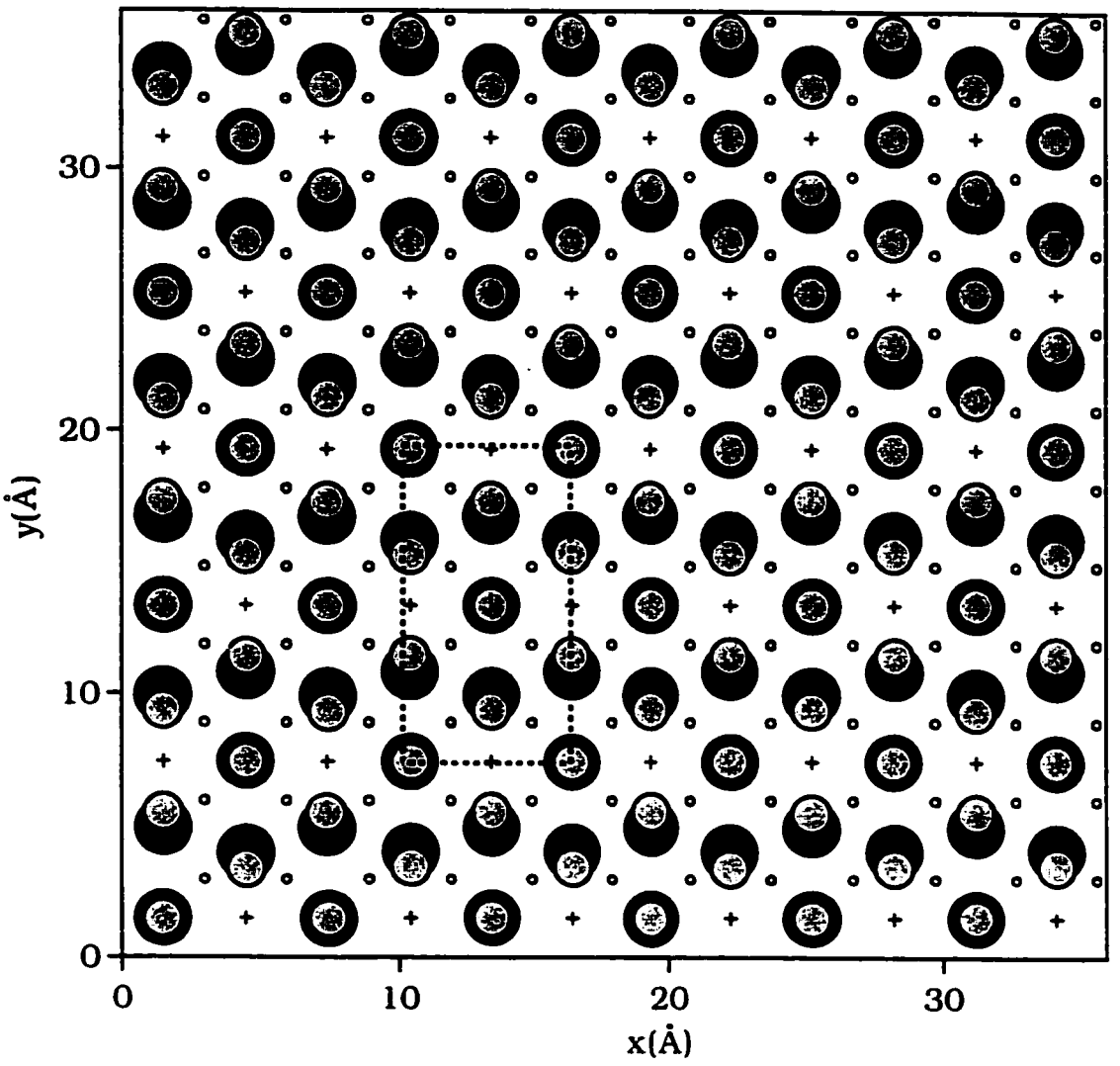

Figure 4.9. A top view of the final configuration where the MgO(001) surface covered with 108 CO molecules at 1 K. The carbon atoms are shown as black and the oxygen atoms as gray. The (+) symbol represents a Mg^{2+} ion and (∘) symbol represents a O^{2-} ion. Note that the origin is centered on a O^{2-}. The unit cell of *c*(4x2) structure is shown (dot lines)

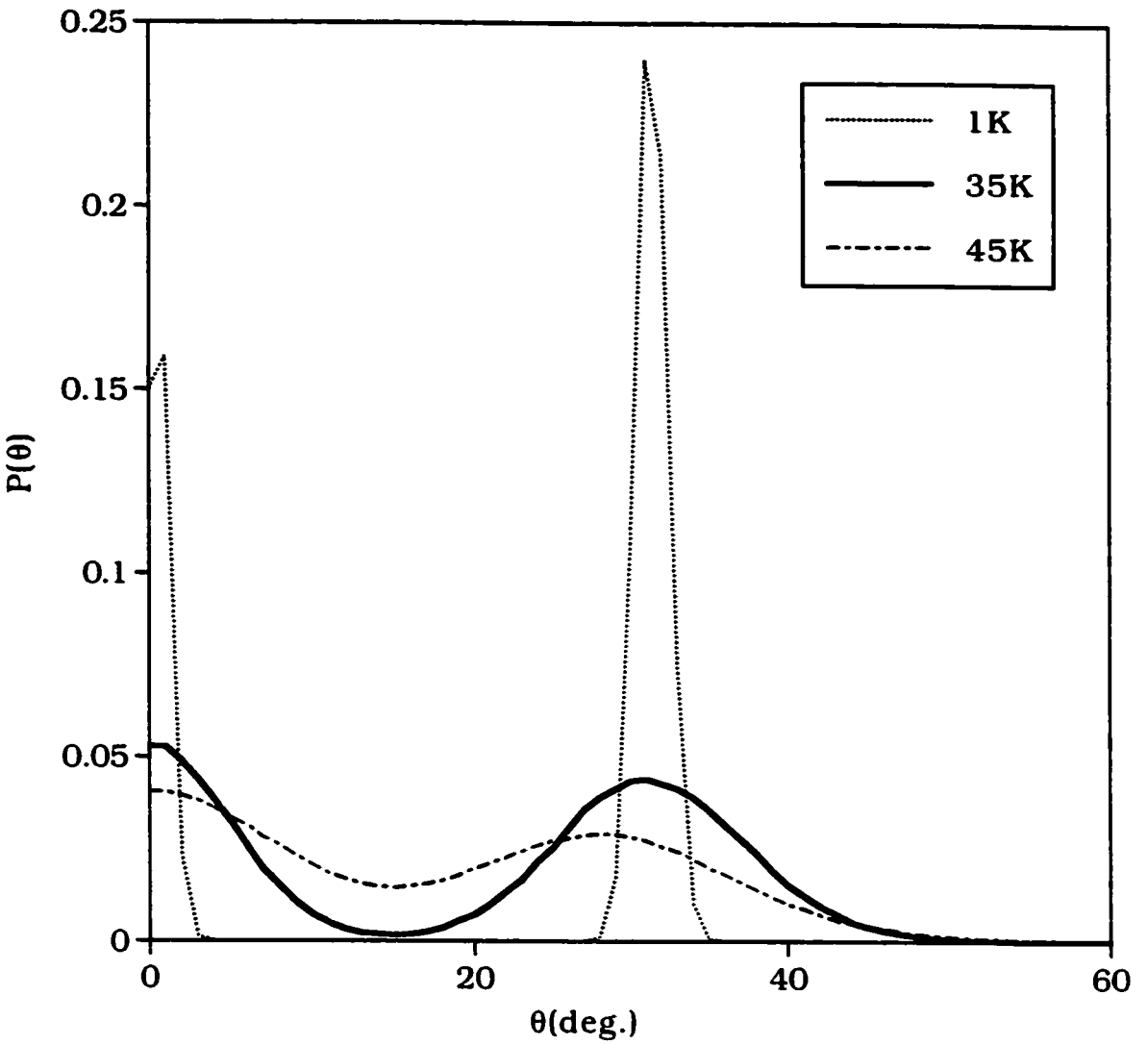

Figure 4.10. The polar (tilt) angle (θ) distribution is plotted for temperatures T=1, 35, 45 K. At 1 K the distribution is symmetric an centered on the θ=0°, 31°. As the temperature increases this peak decreases in height and broadens in width. The peak centered on θ=31° at 1K shifts to θ=28° at 40 K.

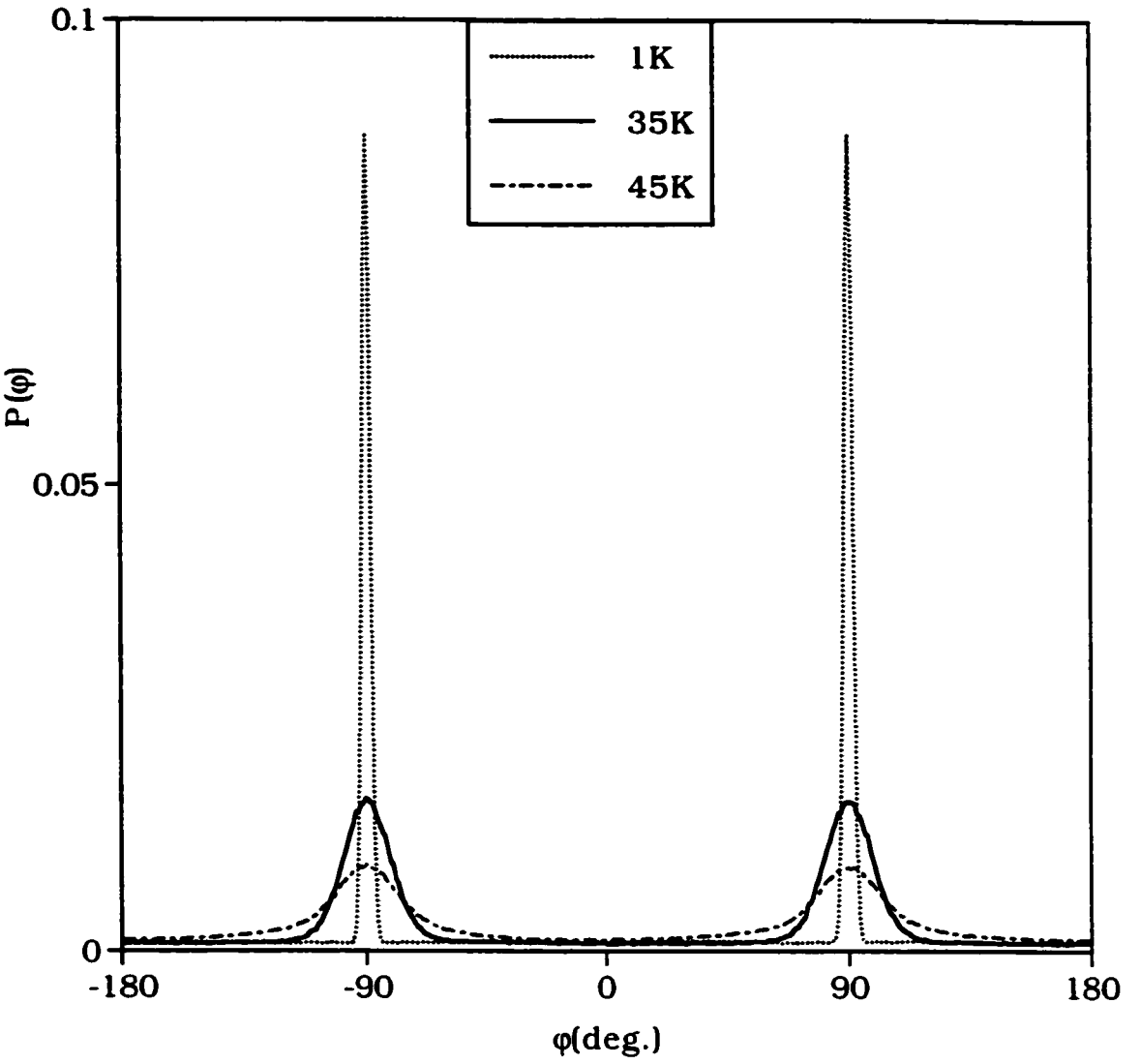

Figure 4.11. The azimuthal angle (φ) distribution of the c(4x2) phase for temperatures T=1, 35, 45 K. Note that the peaks are symmetric and centered on the φ=±90° directions. As temperature increases the peaks heights decrease and the widths broaden.

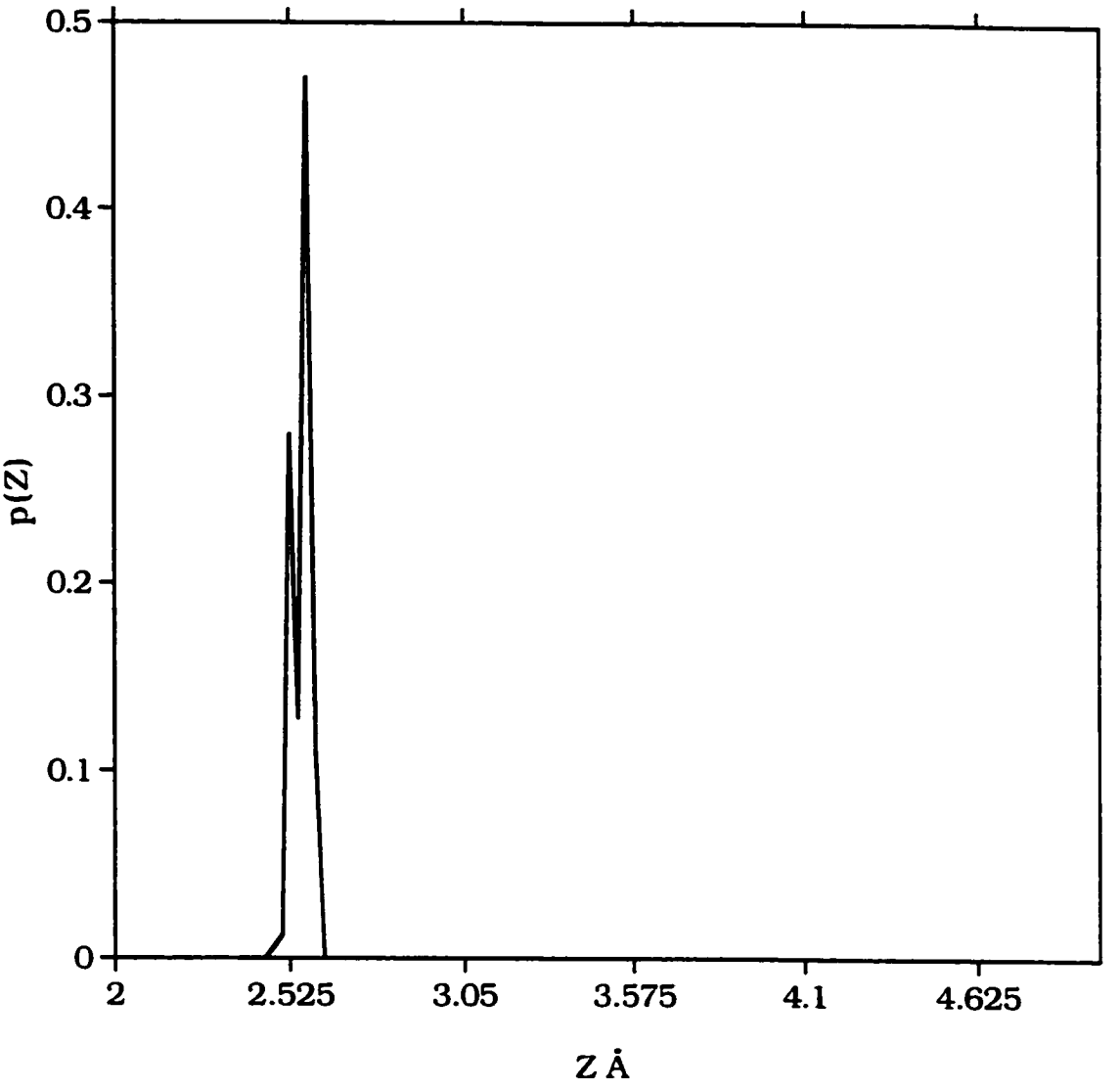

Figure 4.12. The average height of a C atom above the MgO(001) surface Z_C distribution) is plotted for T=1 K. At T=1 K the peaks are centered on the Z_C=2.525 Å for perpendicular CO molecules and 2.575 Å for tilted CO molecules.

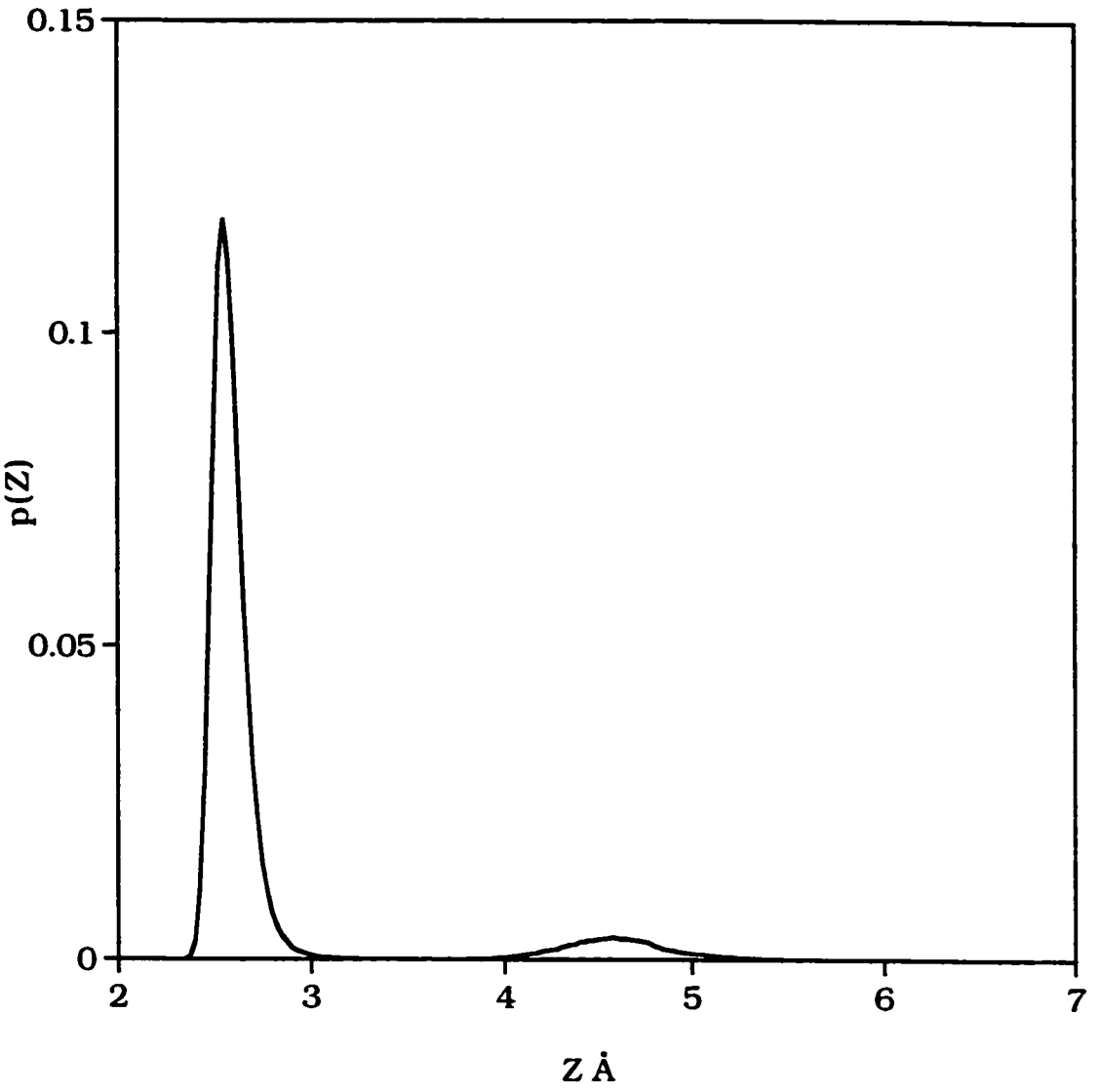

Figure 4.13. The average height of a C atom above the MgO(001) surface Z_C distribution) is plotted for T=45 K. At T=45 K the peaks observed at 1 K merge into single peak centered on Z_C=2.525 Å. An additional peak at 4.5 Å is shown. This indicates that some molecules start to desorb from the first layer to the second layer.

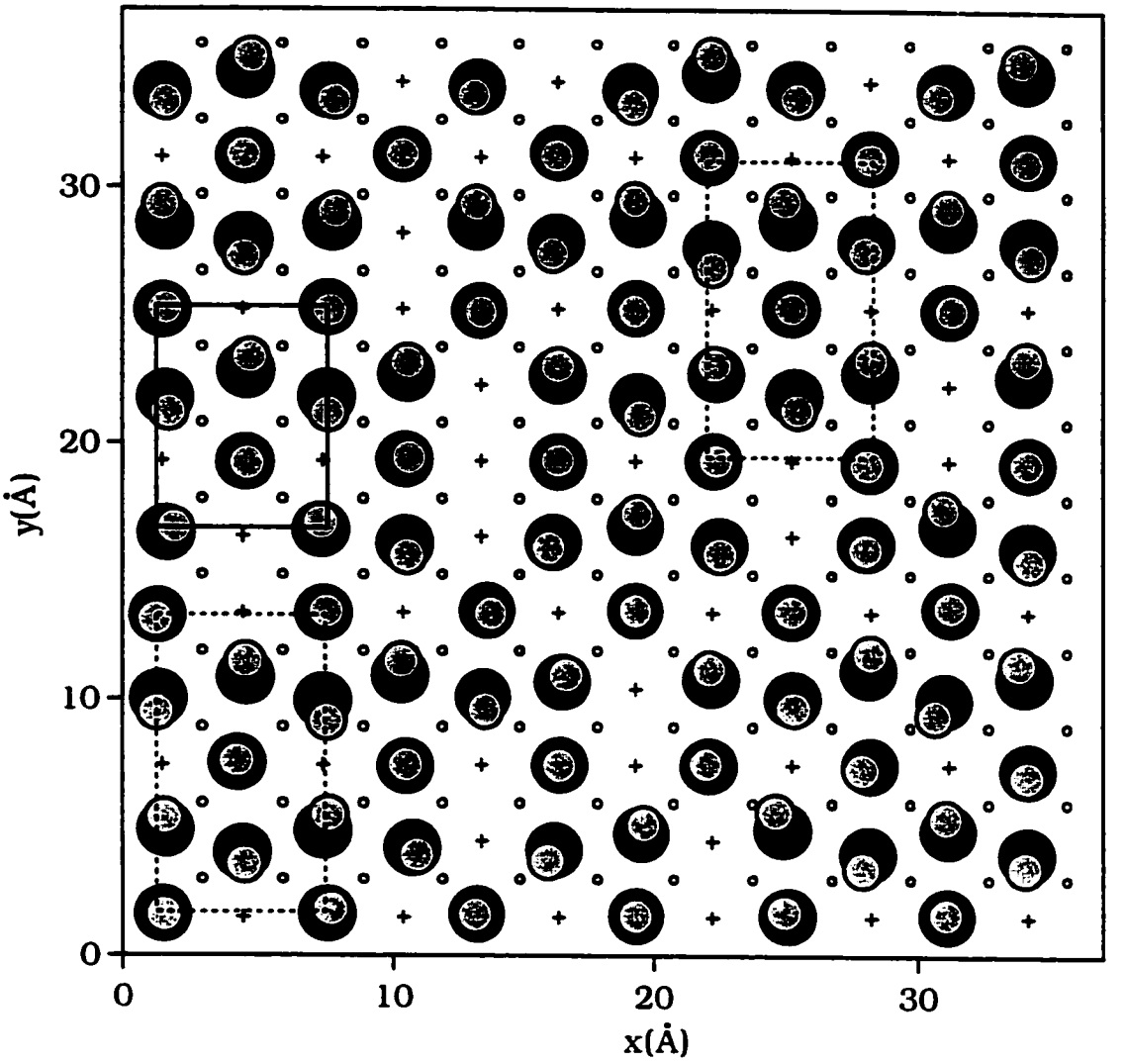

Figure 4.14. A top view of the final configuration of the remaining 96 CO molecules in the first layer from the c(4x2) structure at 45 K. 12 CO molecules in the second layer were removed . the carbon atoms are shown as black and the oxygen atoms as gray. the (+) symbol represents a Mg^{2+} ion and (°) symbol represents a O^{2-} ion. It can be seen that the adlayer is largely disordered. There are a small regions with either *c*(4x2) (dot lines) or *p*(3x2) (solid lines) structures.

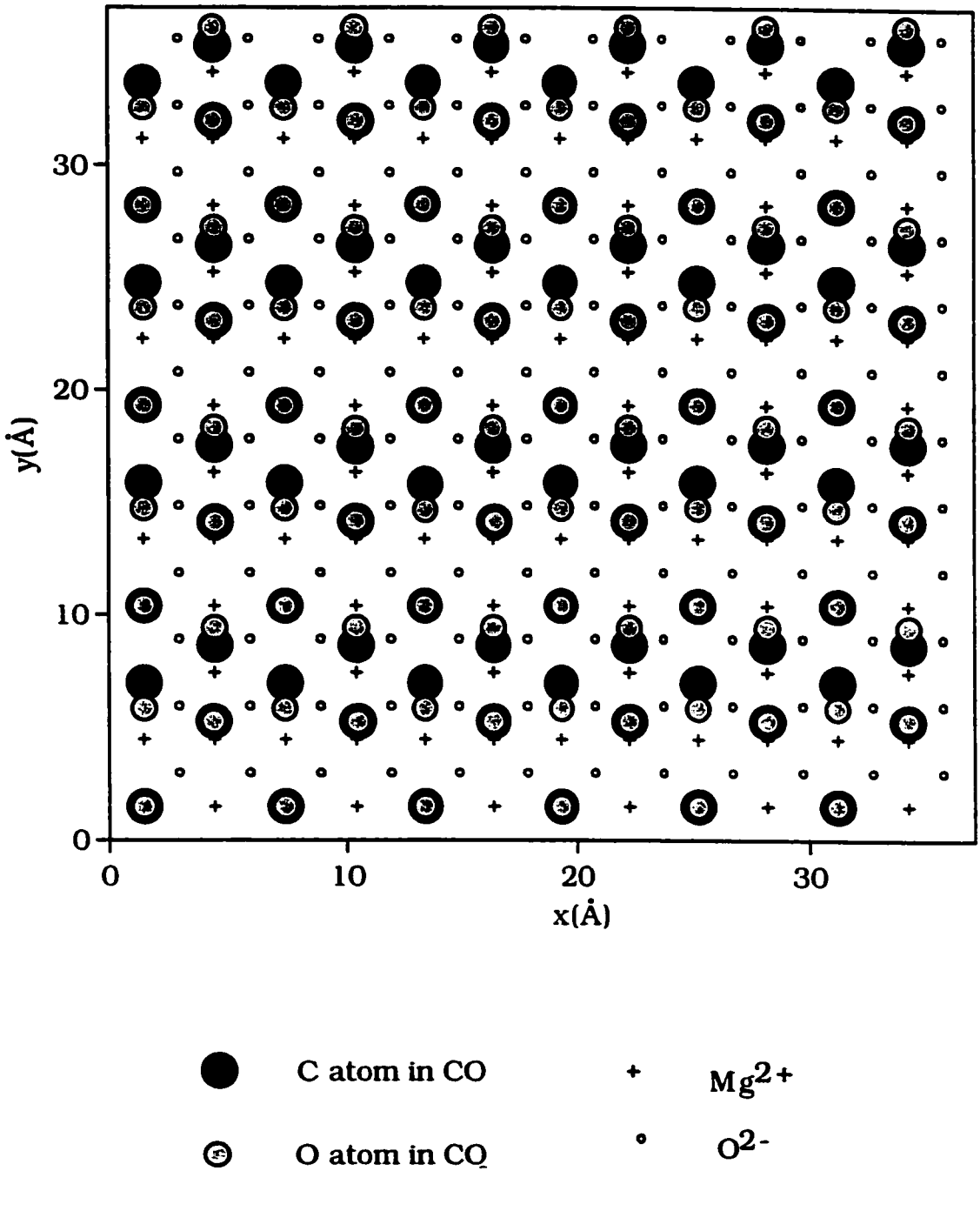

Figure 4.15. Initial configuration of the *p*(3x2) structure similar to that proposed by Panella *et al.* [35].

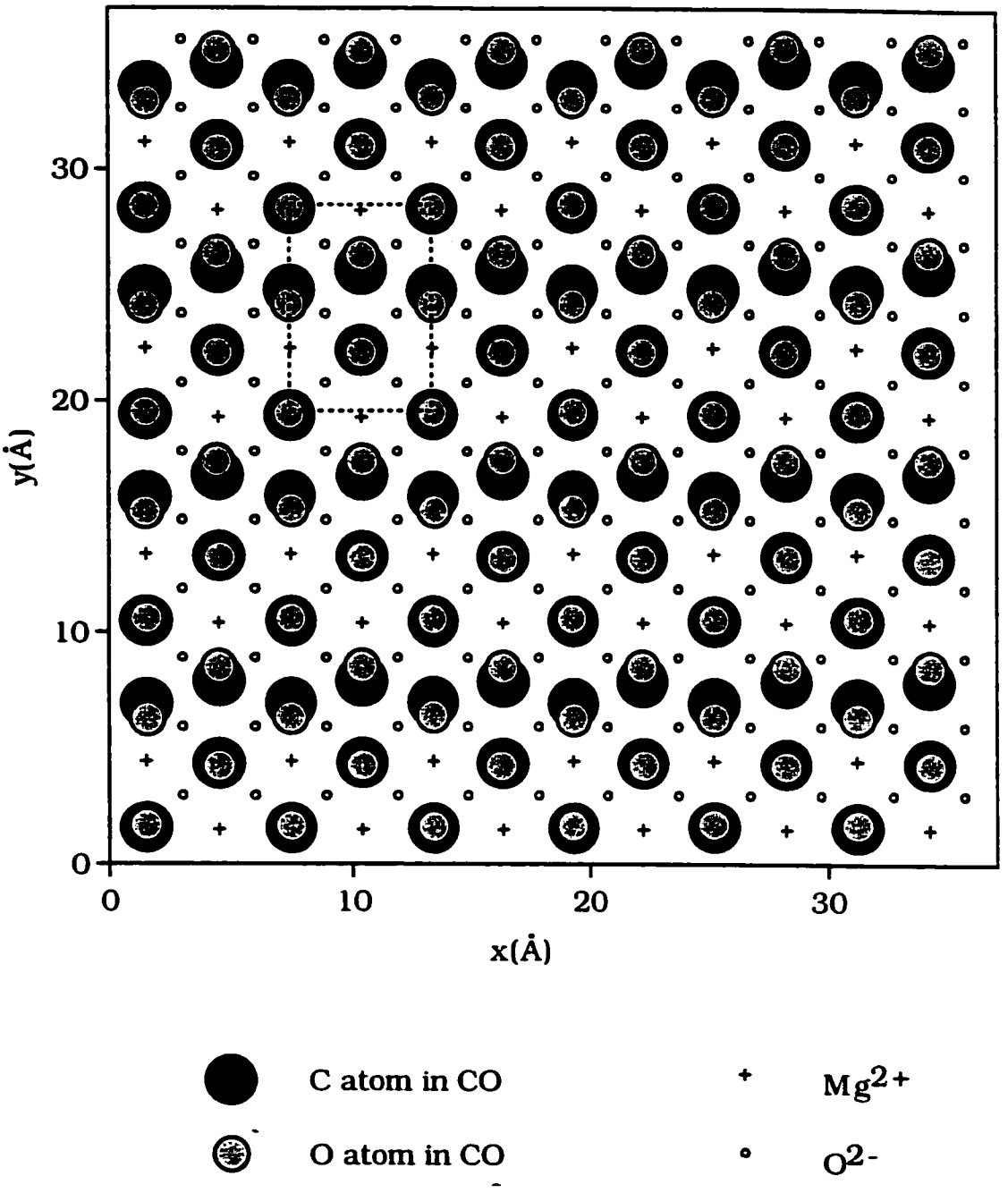

Figure 4.16. A top view of the MgO(001) surface covered with 96 CO molecules at 1 K. The origin is centered on a oxygen ion. The resulting *p*(3x2) unit cell is shown (dot line).

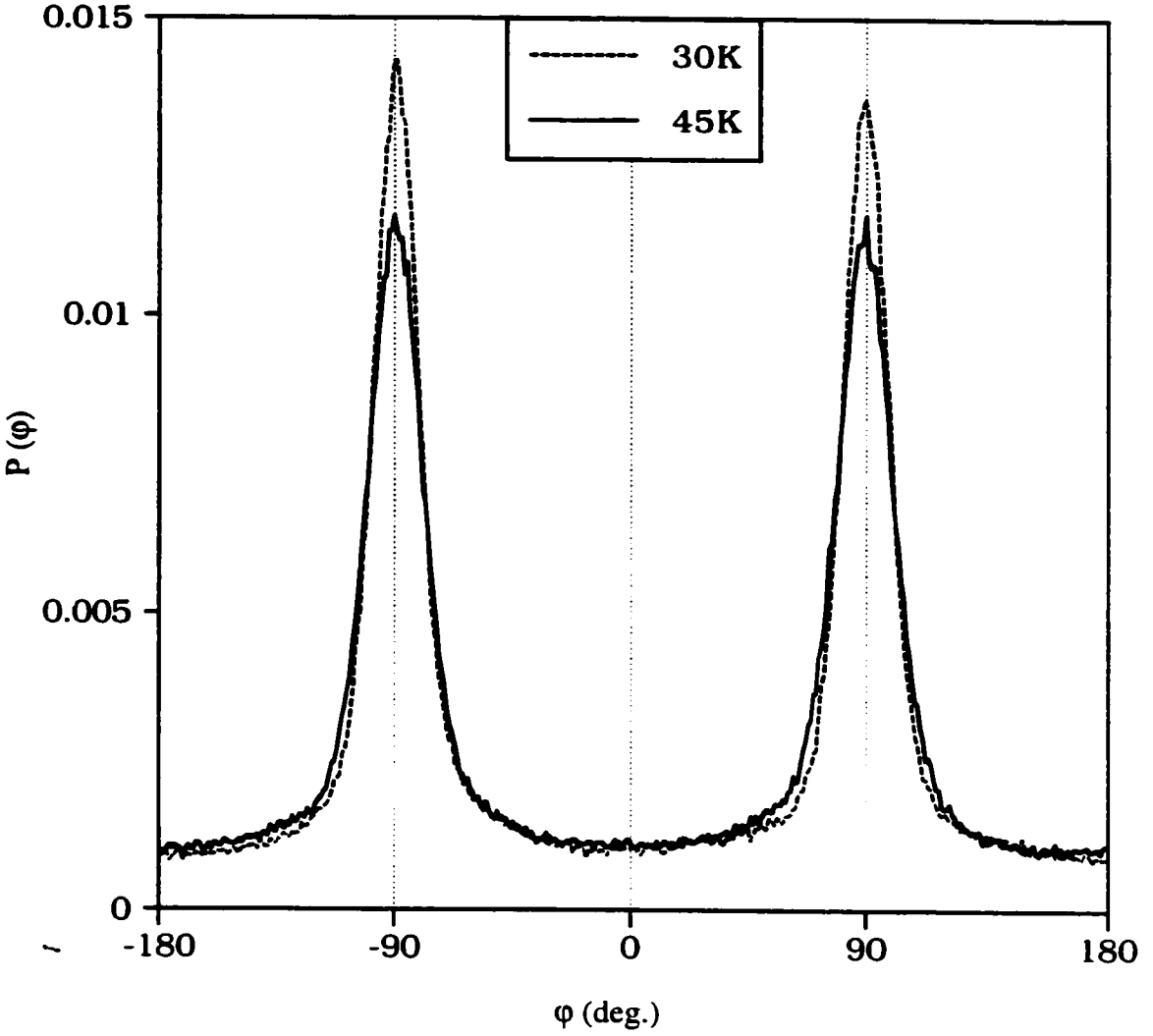

Figure 4.17. The azimuthal angle (φ) distribution of the *p*(3x2) phase for temperatures 30 K an 45 K. The peaks are symmetric and centered on φ=±90°. Note that the behaviour of the distribution is similar to that of the *c*(4x2) phase.

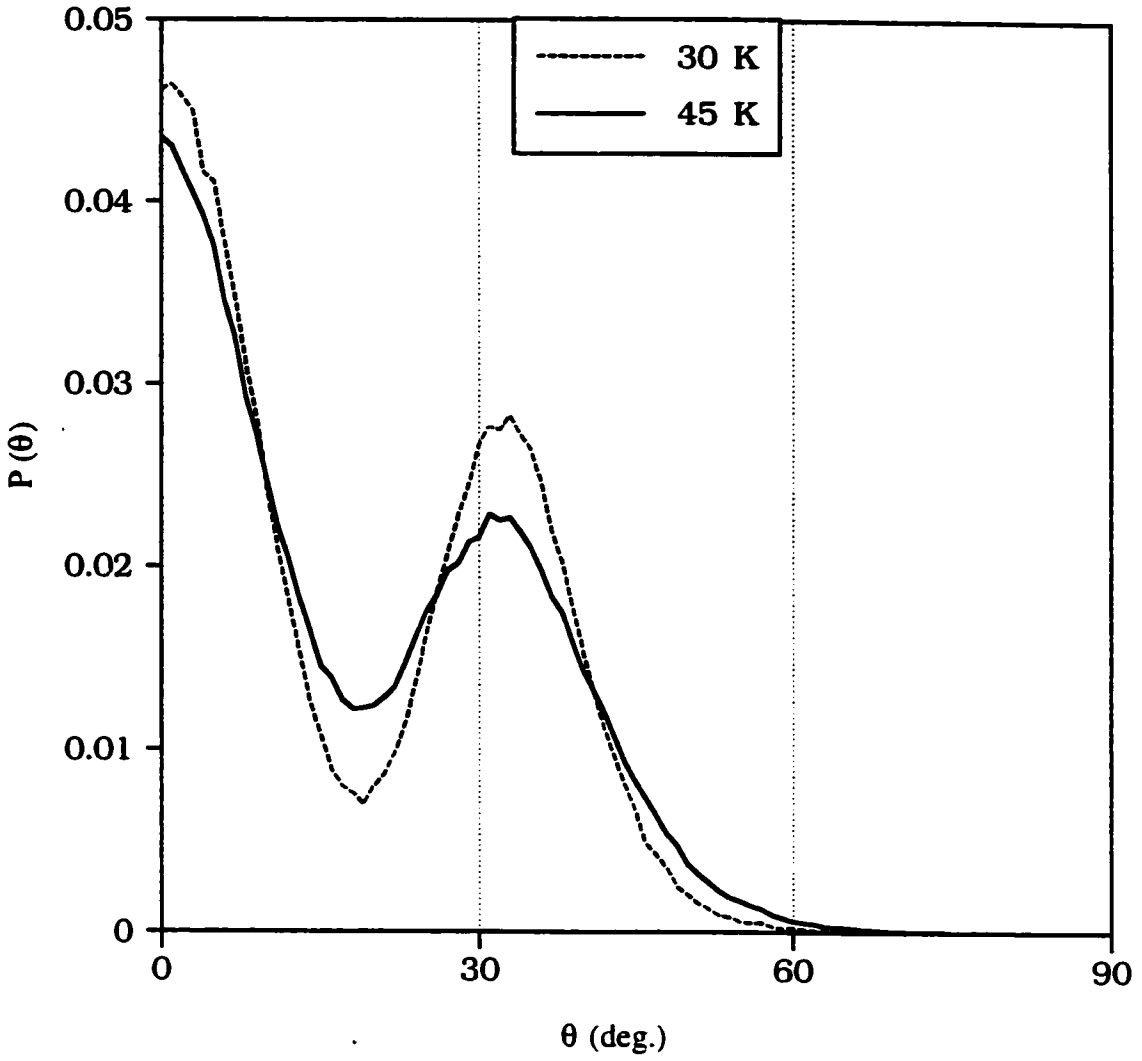

Figure 4.18. The polar angle distribution function P(θ) for the *p*(3x2) phase of CO/MgO(001) system at different temperatures.

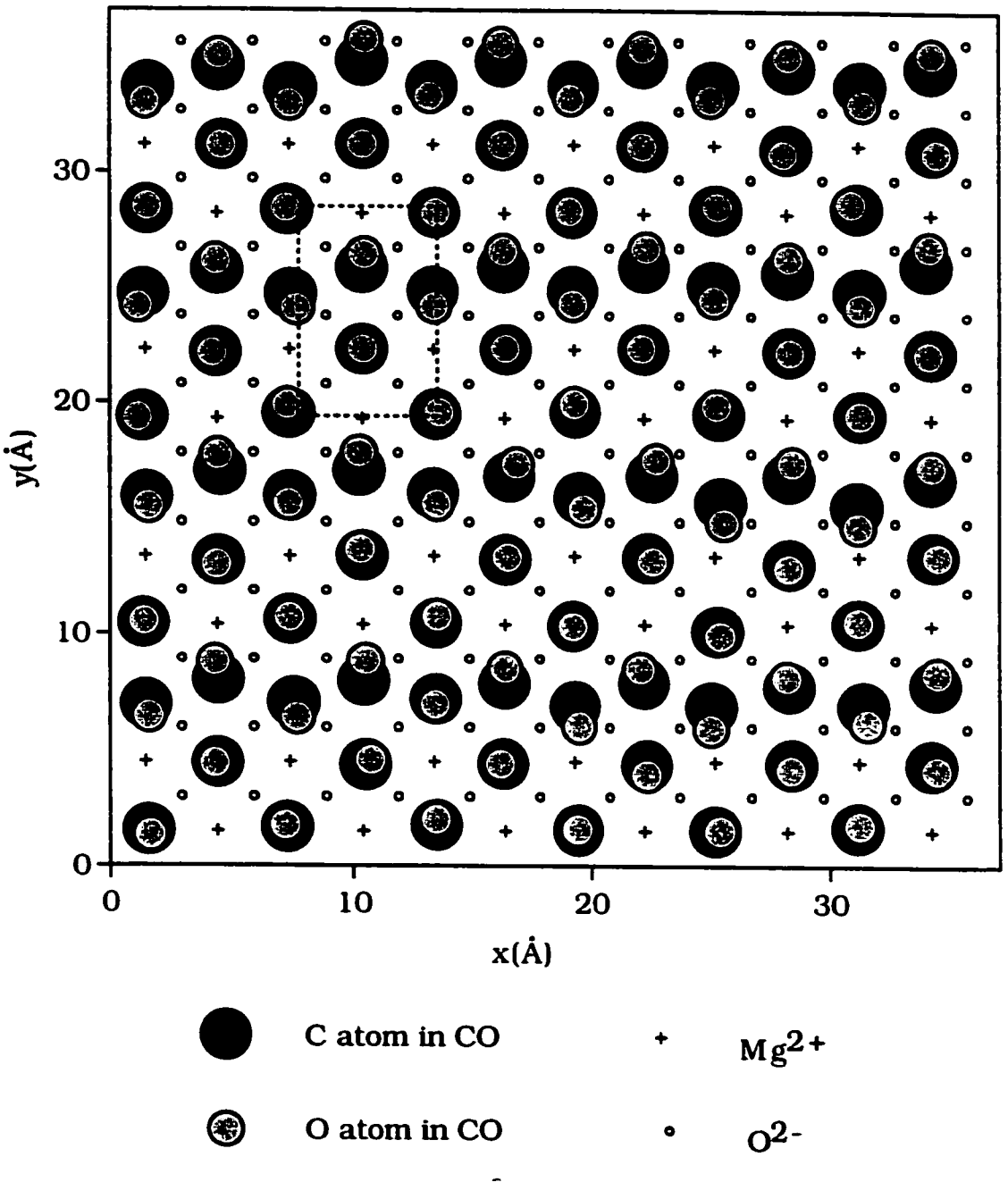

Figure 4.19. Final configuration of *p*(3x2) phase of CO/MgO(001) system at 45 K. This shows that this phase is thermally stable and well ordered at 45 K.

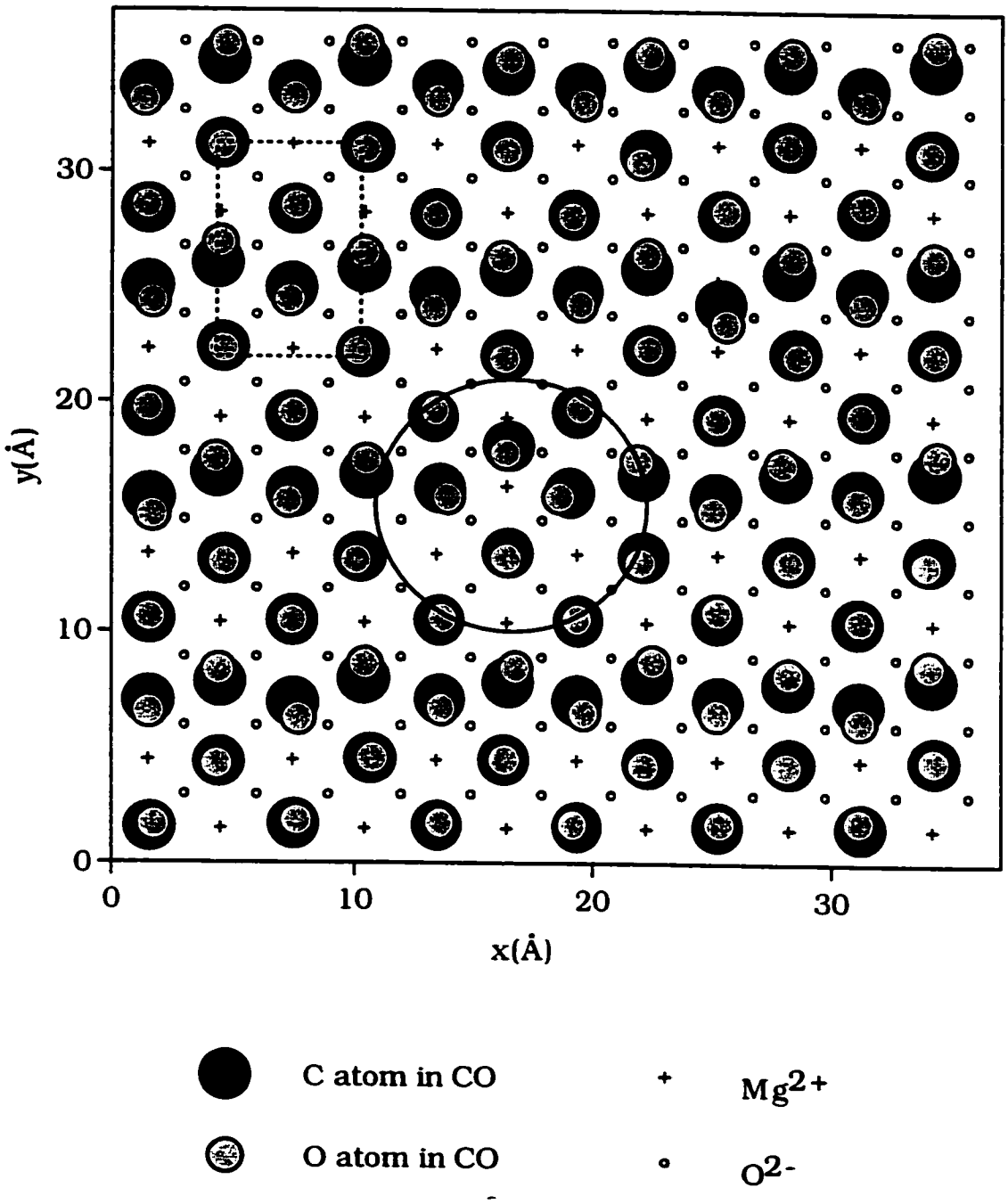

Figure 4.20. Final configuration of *p*(3x2) phase of CO on MgO(001) surface at 50 K. Although small defects (the big circle) in the layer start to appear at this temperature, the *p*(3x2) structure is still largely ordered.

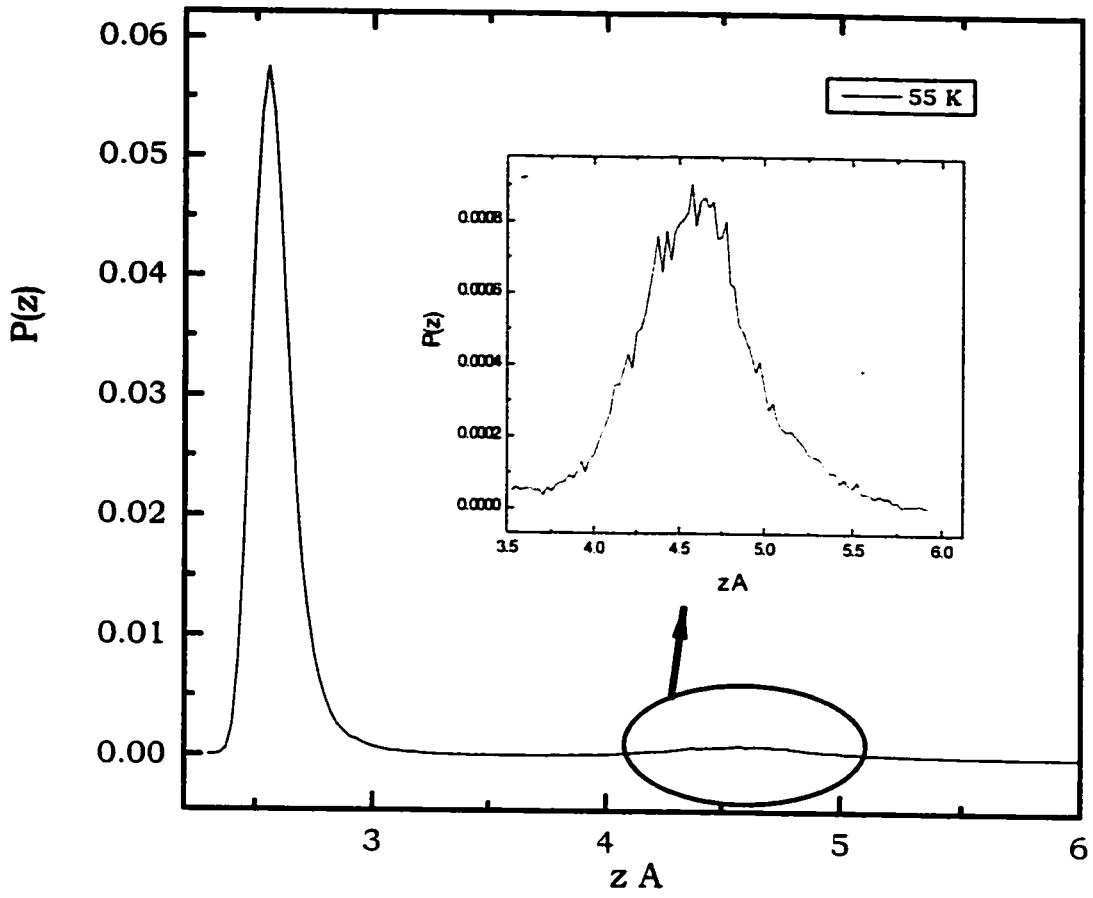

Figure 4.21. The average height of a C atom above the MgO(001) surface Zc distribution) for $p(3\times2)$ structure is plotted for T=55 K. At T=55 K the peaks observed at 1 K merge into single peak centered on Zc=2.525 Å. An additional peak at 4.5 Å is shown. This indicates that some molecules start to desorb from the first layer to the second Layer.

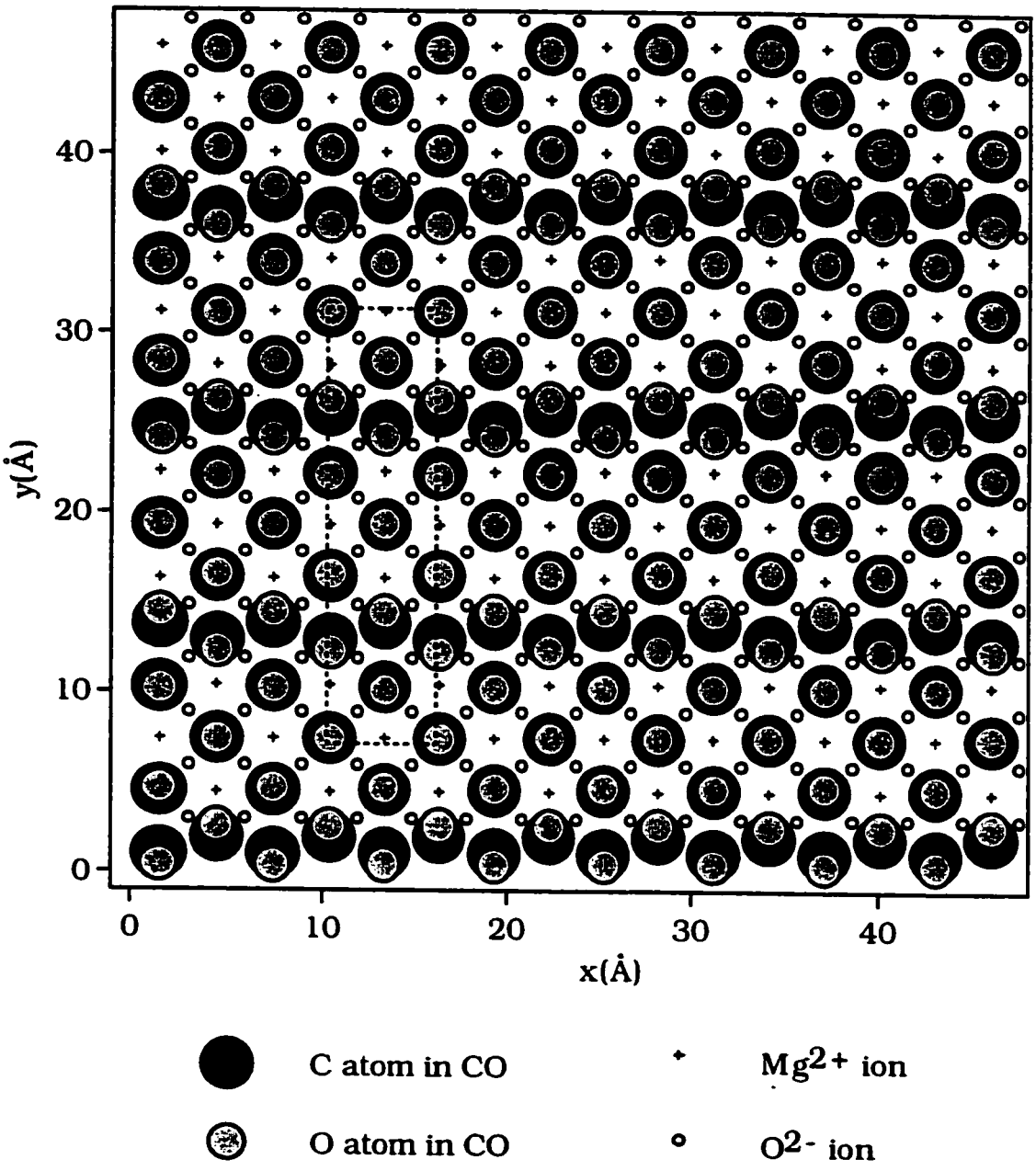

Figure 4.22. A top view of the MgO(001) surface covered with 160 CO molecules at 1 K. The origin is centered on a oxygen ion. The resulting *c*(8x2) unit cell is shown (dot lines).

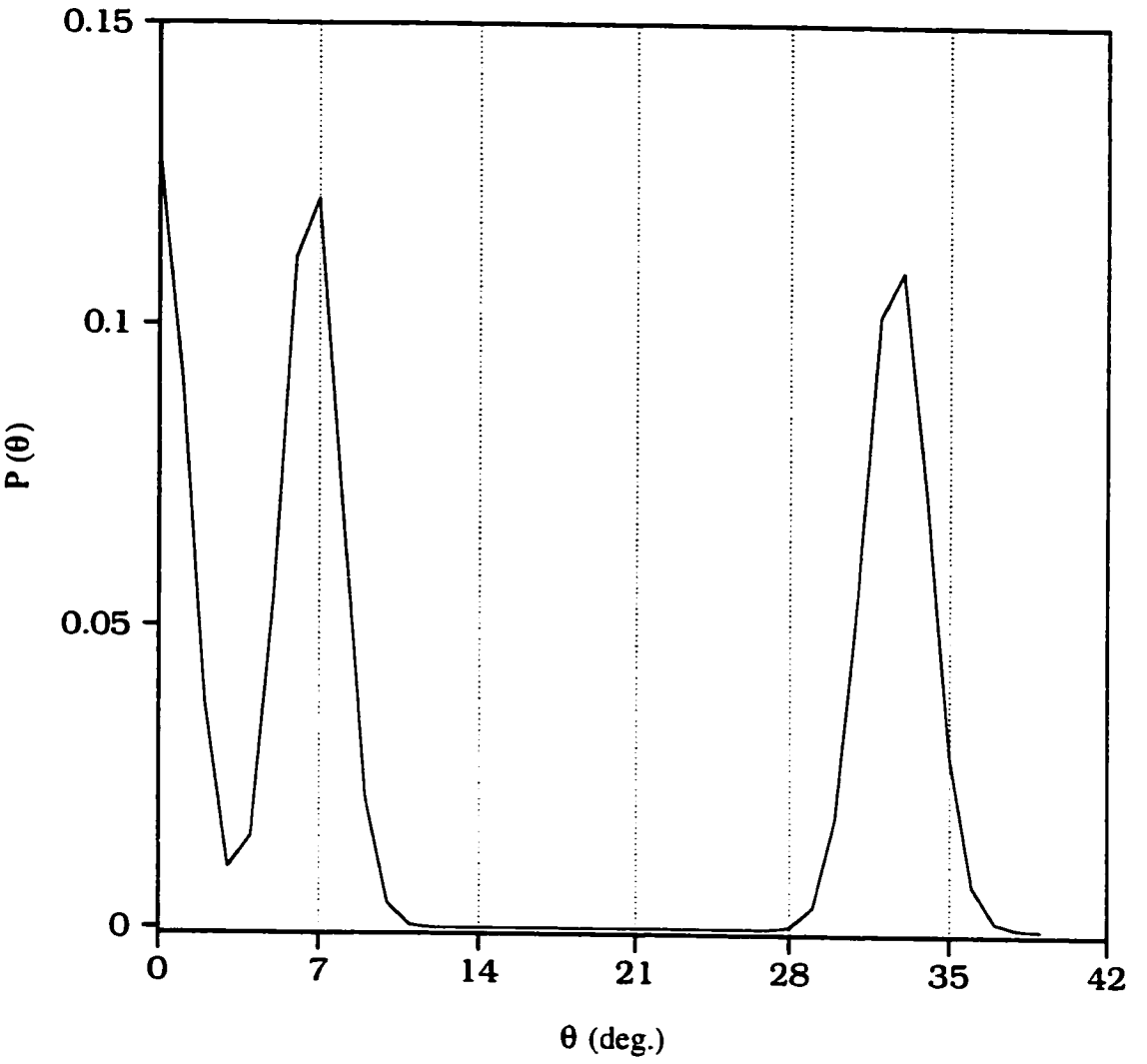

Figure 4.23. Polar angle (θ) distribution for *c*(8x2) phase at 1 K. The distribution exhibits three maxima at θ=0°, θ=7° and θ=31°.

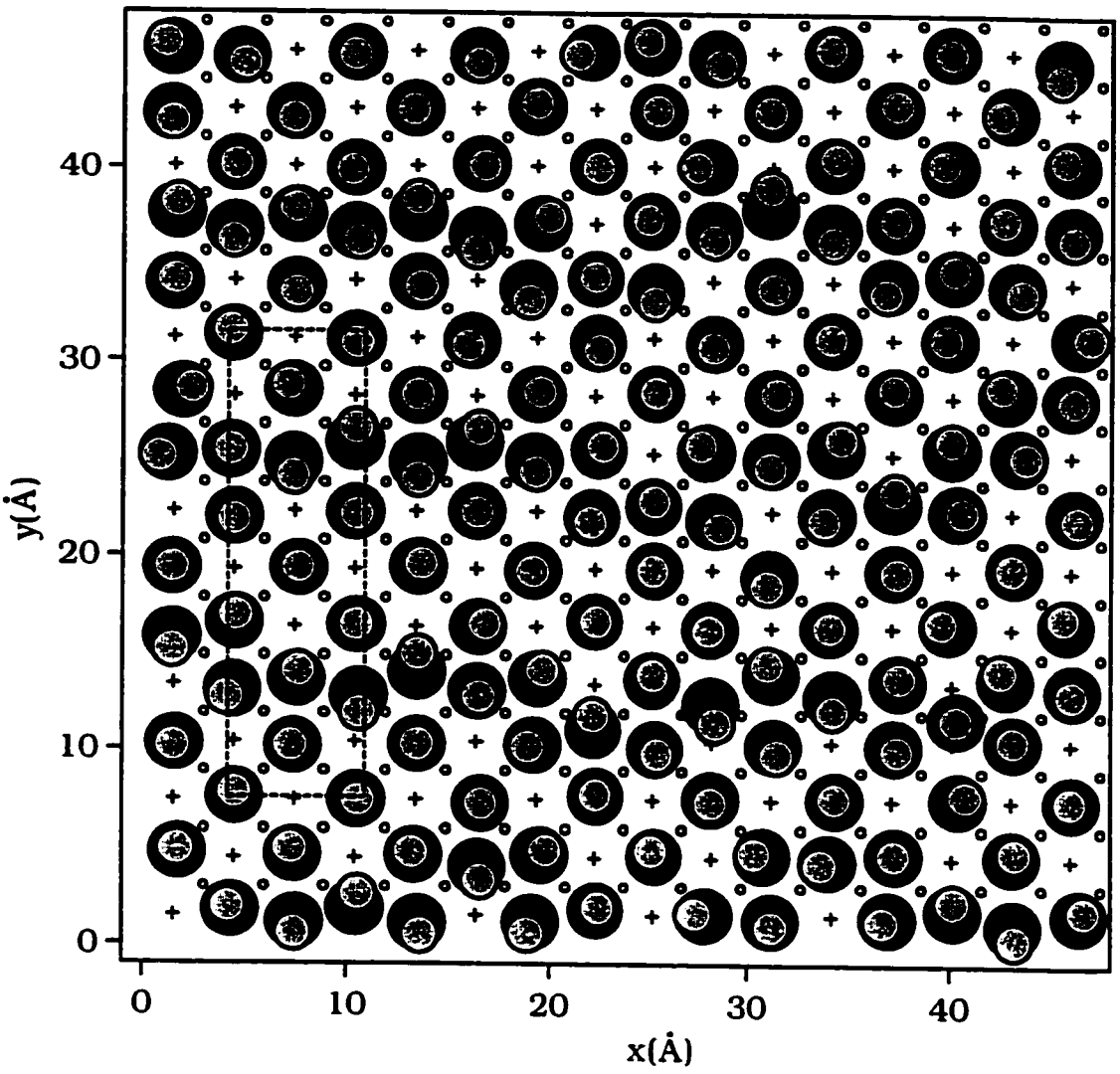

Figure 4.24. Final configuration of the *c*(8x2) structure at 50 K after 80 kcycle. The structure is largely disordered but portions of *c*(8x2) is still existing. The unit cell is shown (dot lines)

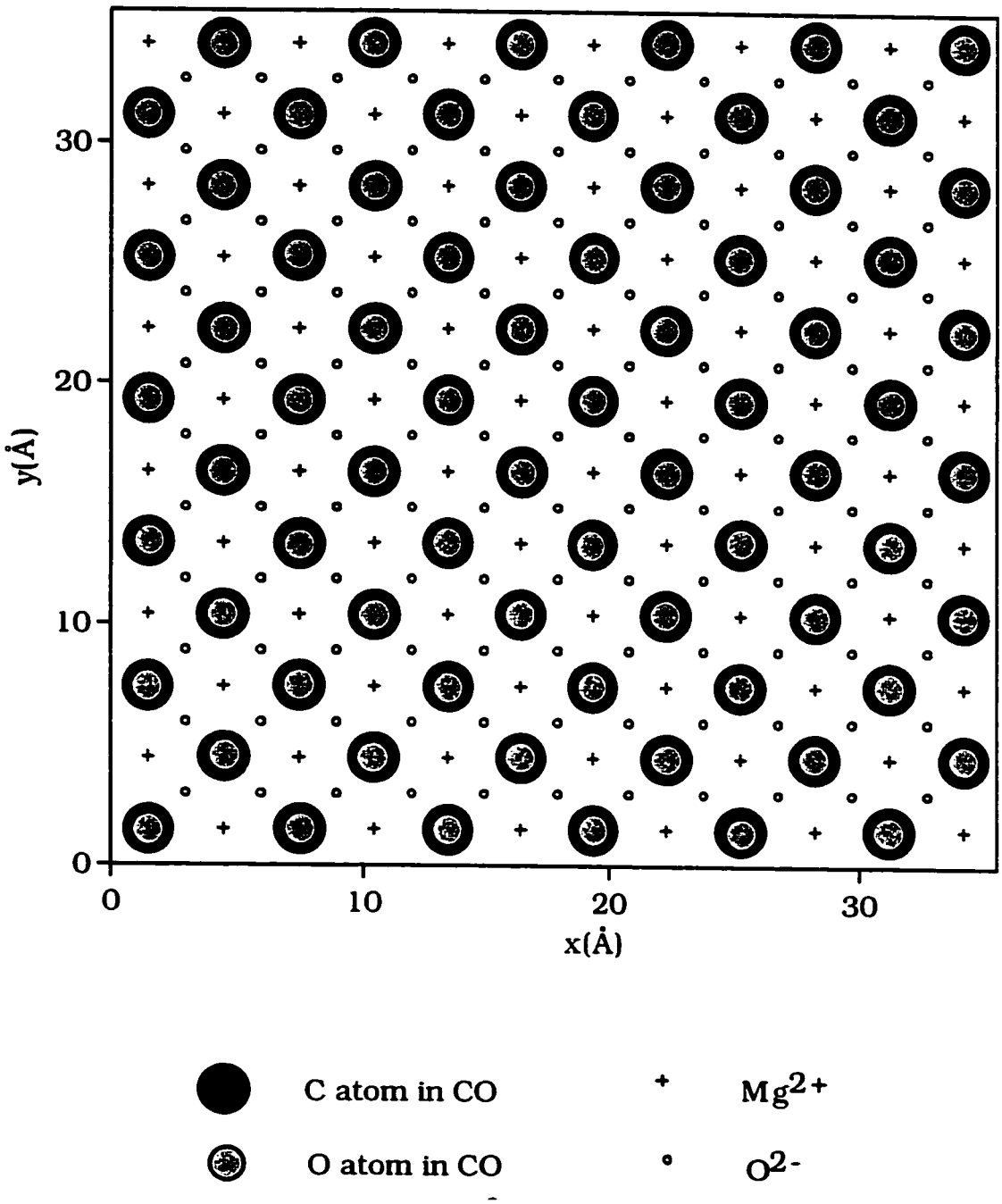

Figure 4.25. Final configuration of c(2x2) structure of CO/MgO (001) at 1 K.

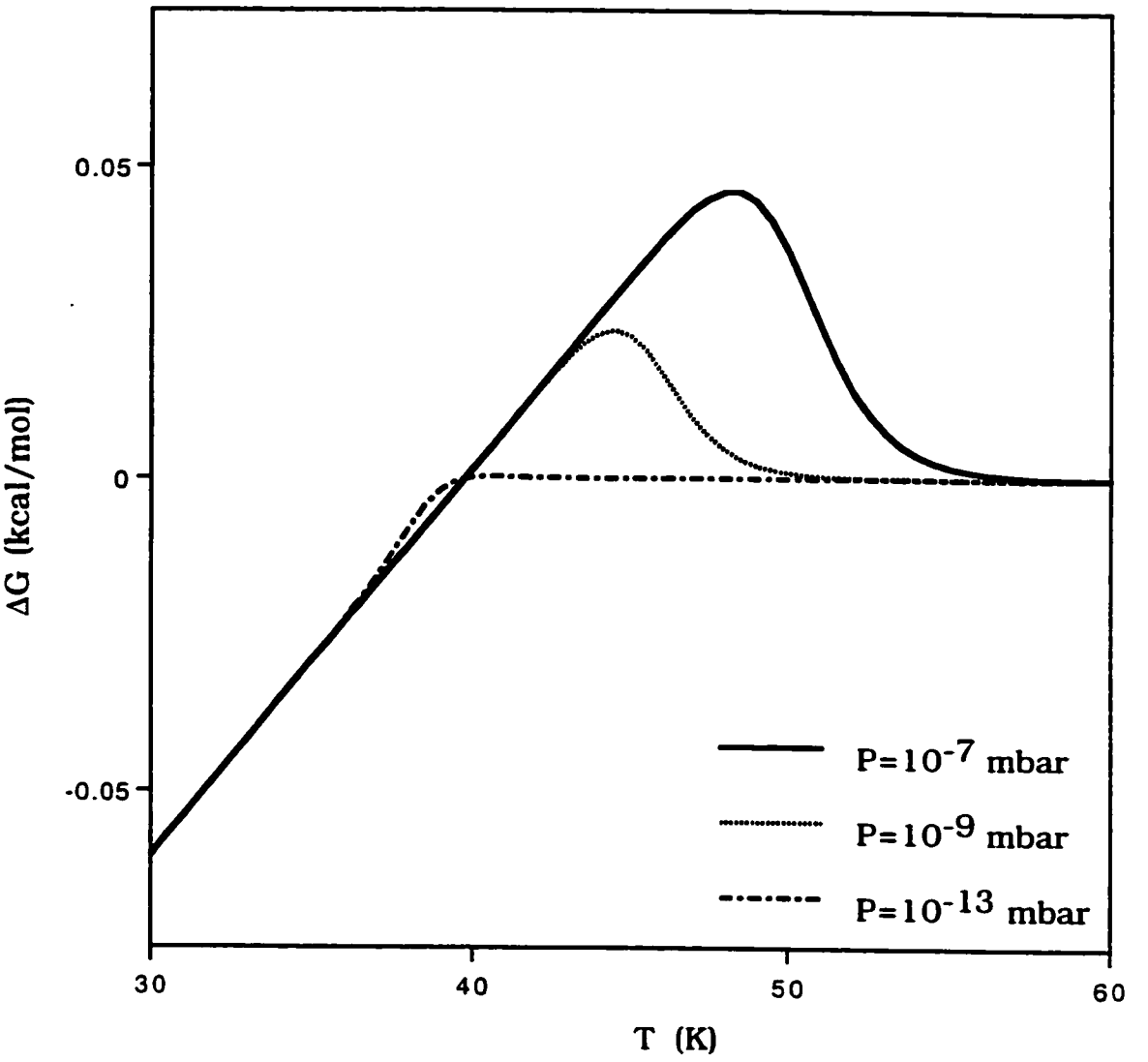

Figue 4.26. The Gibbs free energy difference (ΔG) (ΔG =Gibbs energy of *c*(4×2) structure – Gibbs energy of c(3×2) structure) as a function of temperature for pressures $P = 10^{-5}$, 10^{-8} and 10^{-10} mbar. We see that ΔG is always less than or equal 0 for pressures equal or lower than 10^{-8} mbar and T less than 40 K, This indicates that the *c*(4×2) is more stable than the *p*(3×2). At sufficiently high pressure and temperatures above 40K ΔGis greater than zero which means that the *p*(3×2) phase is indeed more stable than the *c*(4×2) phase.

5. Nitrogen (N_2) physisorbed on MgO(001)

In this chapter our focus will be on studying the structures and stabilities of another type of adsorbate, namely nitrogen (N_2), physisorbed on MgO(001). Hence the surface substrate remains the same as in chapter 4 while the adsorbate is different. Nitrogen is a nonpolar molecule with shorter ranged interactions than that of CO molecules (quadrupolar *vs.* dipolar interactions). The diatomic molecules N_2 and CO have almost the same bulk properties; their mass, crystal size and structure are similar. The main differences between them are that the quadrupole moment of CO is larger by a factor of 1.3 than that of N_2, and the CO molecule possesses a permanent dipole moment. The similarity of the CO and N_2 molecules in terms of their physical interactions suggests that the translation and orientational ordering of both molecules on the MgO(001) surface should be similar, and as a result it was thought that the CO molecules could serve as a model for N_2 molecules. But according to the available experimental data the nitrogen molecules seem to adopt ordered structures on MgO(001) that differ from those of the CO molecules [81] and [34]. The experimentally observed structures of N_2 have been presented previously in section 1.4.2.

In order to clarify experimental results on this system and to test the possibility of applying to the N_2/MgO(001) system the model proposed for describing the devil's staircase in CO/MgO system, we have

performed for the first time Monte Carlo simulations to study the structures and thermal stabilities of layers of nitrogen molecules on the MgO(001) surface.

5.1 Potentials and simulation method.

The methods, potentials and coordinate system is similar to that of CO/MgO(001) system, as can be seen in the previous chapters. As a reminder, the potential consists of two parts: molecule-molecule interaction and molecule-surface interactions. Tang-Toennies and Buckinghan atom-atom/ion potentials with summation over a two body interactions is applied to describe the repulsion and dispersion terms of molecule-molecule and molecule-surface interactions. The electrostatic interactions are mediated by point dipoles $\vec{\mu}$ that are distributed on the atomic sites in such a way that the known multipole moments of the molecule can be reproduced. The parameters governing the potentials are chosen so as to reproduce various experimental molecular properties of N_2 and the heat of adsorption of N_2 adsorbed on MgO(001). Potential parameters are given in chapter 2 (see Tables 2.1-2.7). The coordinate system is as that of CO/MgO(001) described in chapters 3 and 4 (see Fig. 3.2). In our MC simulations the surface ions are not allowed to move. The adsorbed molecules are considered to be rigid (fixed bond length) but

are allowed translations in all directions (lateral and perpendicular) as well as rotations.

5.2 Simulation Results

5.2.1 Single N_2 molecule adsorbed on the MgO(001)

By studying the adsorption of a single nitrogen molecule on the MgO(001) surface through the use of the steepest decent method and Monte Carlo simulations, we can examine the suitability of the molecule-surface interaction parameters presented in chapter 2. By comparing our results for a single molecule with the available experimental and theoretical data for low coverage, we were able to fine-tune these parameters. Results from the steepest decent method at 0 K show that the N_2 molecule adsorbed perpendicular to the surface over top an Mg^{2+} site with a binding energy of -2.78 kcal/mol and a height of the closest atom to the surface (N-Mg^{2+} distance) of 2.45 Å. This binding energy matches the experimental value of -2.85 kcal/mol at 1 K [32][34][38]. In terms of geometry, this result matches the result for the CO/MgO system presented in chapter 4 and also the experimental and simulation work of CO/NaCl, but it seems different from the results found by Laklifi *et al.* [1] where they found that an N_2 molecule lies parallel to the surface along the Mg-Mg channels. This discrepancy with Laklifi *et al.* [1] might be due to their use of on effective charge of only 1 q/e for the Mg ion in their work instead of +2 q/e.

Through the use of Monte Carlo simulations we test the orientation of a single nitrogen molecule at finite temperatures (1-60 K). We have run the Monte Carlo simulation for 50 kcycle with an initial configuration of one N_2 molecule lying flat over top of a 13×13 patch of the MgO(001) surface. The simulations show a uniform distribution in the azimuthal angle and a Gaussian-like distribution for the polar angle around $\theta=0^{\circ}$. Thus the N_2 molecule is adsorbed perpendicular with respect to the surface on top of a Mg^{2+} ion with a binding energy of -2.91 kcal/mol. The height ($N\text{-}Mg^{2+}$ distance) of the closest atom of N_2 molecule to the surface is found to have a value of 2.32 Å. As the temperature is increased the N_2 molecule does not show any preferred azimuthal orientation or any tilt angle. This result is similar to that found in the CO/MgO(001) and CO/NaCl(001) systems.

5.2.2 N_2 adlayers: $\left(\sqrt{13}\times\sqrt{13}\right)R33.7^{\circ}$ structure

In this section we present for the first time the results of Monte Carlo simulations of the $\left(\sqrt{13}\times\sqrt{13}\right)R33.7^{\circ}$ structure. Thermal stabilities, orientations and the geometry of this structure are studied.

In order to satisfy the periodic boundary conditions a 13×13 patch of MgO surface was used, so that the number of available adsorption

sites (Mg^{2+}ion) is 169. The coverage, as proposed by Trabelsi *et al.* [34] is 69.8 % of a monolayer, this means that the number of adsorbed nitrogen molecules should be 117 molecules. The Monte Carlo simulations were therefore started with an initial configuration of 117 N_2 molecules that were given a perpendicular orientation and positions similar to those proposed by Trabelsi *et al.* [34] (there were no definite positions or orientations given in Ref. [34]). The simulations were run for 50 kcycle at 1 K and with a cutoff radius of 18.5 Å. The final configuration contains portions of a $\left(\sqrt{13}\times\sqrt{13}\right)$ structure. Also, by monitoring the binding energy of each MC cycle we noted that the system had not yet reached the equilibrium state, this implies that it will evolve into the $\left(\sqrt{13}\times\sqrt{13}\right)$ structure. The Monte Carlo simulation was started again with an initial $\left(\sqrt{13}\times\sqrt{13}\right)$ configuration arranged in the same fashion that the molecules liked to adopt in the previous run, and run for 50 kcycles. The final configuration at 1 K, shown in Fig. 5.1, is indeed a highly ordered commensurate phase with $\left(\sqrt{13}\times\sqrt{13}\right)$ symmetry.

Satisfied that this phase is stable at 1 K we examined the thermal stabilities of this phase via Monte Carlo simulations at temperatures 13 K and higher. The reason we started with 13 K is that the two experiments mentioned above were performed around 13 K. The initial configuration for these runs where taken from the final configuration at

1K (see Fig. 5.1). The final structure at 13 K after 50 kcycle was the same as the initial one (see Fig. 5.2). The cell of this phase contains nine molecules with either horizontal or perpendicular molecules. The number of molecules in the cell is in agreement with the experimental data [34][38].

The tilt angle distribution at 13 K has a Gaussian-like distribution with two peaks at 0° and 85° (Fig. 5.3.). This implies that there are two kinds of adsorption sites (horizontal and perpendicular sites). The azimuthal angle distribution shown in Fig. 5.4 shows that the nitrogen molecules adopt an azimuthal angle (φ) of $\pm 180^\circ$ or 0°. These two sites also have different heights above the surface. As shown in Fig. 5.5, the distribution of the height (z) of the closest atom of N_2 to the surface at 13 K shows two peaks at 2.35 Å and 3.35 Å. These two adsorption sites of the nitrogen molecules are localized near the cation sites. The perpendicular molecules adsorb over top the Mg^{2+} ion, whereas the horizontal molecules are displaced by 0.6 Å in the direction of the tilt (x direction in our case). These results differ from that proposed by Trabelsi *et al.* [34] where they assume that the molecules have only one adsorption site with a tilt angle common to all ($\theta=30^\circ$) and with a single azimuthal angle $\varphi=30^\circ$ where their φ is defined along a crystallographic

axis Mg-O-Mg. In our nomenclature this would be $\varphi=15^{\circ}$ (all molecules pointing in the same direction).

The total binding energy of the layer at 1 K is found to have a value of -335.26 kcal/mol, which yields a binding energy of -2.87 kcal/mol per molecule and –0.23 kcal/mol/Å^2 per unit area. This is in agreement with the experimental value of -2.85 kcal/mol for a monolayer [34]. This structure has features in common with the $c(4\times2)$ structure in the CO/MgO system; both of them contains rows of tilted molecules separated by untilted ones.

By testing the thermal stability of this phase at higher temperature we find that the $\left(\sqrt{13}\times\sqrt{13}\right)$ structure is stable up to around 20 K. The polar angle (tilt angle) distribution at temperatures 16 K and 20 K show the same peaks as in the case of 13 K, but they get progressively broader (see Fig. 5.3). Also by looking to the final configurations at 25 K as shown in Fig. 5.6 we see that the $\left(\sqrt{13}\times\sqrt{13}\right)$ phase has lost its long range order and adopts a new less dense phase since some molecules have started to desorb from this layer to form a second layer. The evidence for the desorption of these molecules is shown in Fig. 5.5 where at 25 K new peaks appear in the z-distribution at around 4.3 Å and 5.4 Å. From the area under these new peaks at 25 K we have found that on average eight nitrogen molecules desorbed from the first layer to form a

second layer and hence leaving the surface layer with a density of 0.64 of the monolayer. This density is the same as the density required for the $(\sqrt{25}\times\sqrt{25})R36.9^{\circ}$ phase observed by HAS experiments and which will be discussed in the next section. Also in Fig. 5.6 we see some evidence that the number of untilted columns between tilted ones has increased, this increase is essential in the transformation from the $(\sqrt{13}\times\sqrt{13})$ phase into the $(\sqrt{25}\times\sqrt{25})R36.9^{\circ}$ phase. This density remains constant up to 30 K (see to the area under the peaks in Fig. 5.5. At 35 K the number of nitrogen molecules that desorbed from the first layer is 14 molecules. This indicates a phase transition to a new phase with a coverage of 61 % which is less dense than that required for the $(\sqrt{25}\times\sqrt{25})R36.9^{\circ}$ phase. From the z-distribution at 35 K in Fig. 5.5 it is clear that the phase occurring at 35 K is different from that at 30 K in terms of density. This can be viewed as support for the HAS experiment at 36 K, where it was shown that the $(\sqrt{13}\times\sqrt{13})R33.7^{\circ}$ structure is not stable, and a structural phase transition to a lower density phases occurs. They found that the structure at 36 K has a lower density than that of $(\sqrt{25}\times\sqrt{25})R36.9^{\circ}$.

5.2.3 N_2 adlayers: $(\sqrt{25}\times\sqrt{25})R36.9^{\circ}$ structure

The HAS experiments [38] show that at a coverage below that of the $(\sqrt{13}\times\sqrt{13})$ structure the nitrogen molecules adopt the

$(\sqrt{25}\times\sqrt{25})R36.9^{\circ}$ structure at 12 K. Also it is suggested that the $(\sqrt{13}\times\sqrt{13})$ structure undergoes a structural phase transition at higher temperatures. In order to obtain a structure that would give details of this phase we performed MC simulations. We have used the results discussed in section 5.2.2, to generate the initial structure for a $(\sqrt{25}\times\sqrt{25})R36.9^{\circ}$ structure. The initial configuration contains 400 molecules over top a 25x25 patch of surface. The final configuration obtained from MC after 50 kcycle at 1 K is shown in Fig. 5.7. This structure, with a coverage of 0.64 of a monolayer, is indeed a $(\sqrt{25}\times\sqrt{25})$ phase.

This structure also has two types of adsorption sites; perpendicular and horizontal (θ=85°) with the horizontal molecules having an azimuthal angle of 0° and 180° (this picture is similar to that of the $(\sqrt{13}\times\sqrt{13})$ structure). Locations of these sites appear in the same locations of that the $(\sqrt{13}\times\sqrt{13})$ structure (near the Mg^{2+} adsorption sites).

The horizontal (tilted) molecules occupy every site along a column with neighbouring molecules possessing alternating azimuthal orientations. These columns consist of seven molecules before a kink

occurs and shifts the columns over one lattice spacing. At the kink there are two molecules one tilted and one untilted.

The total binding energy of the $(\sqrt{25}\times\sqrt{25})$ phase at 1 K has the value of –1160 kcal/mol, which yields a binding energy of -2.90 kcal/mol per molecule and a binding energy of 0.21 kcal/mole per unit area. This is reasonably close to that of Traeger *et al.* [38]

The thermal stabilities of this structure were tested via the use of MC simulations. It was found that this structure is thermally stable below 27 K, above which some molecules desorbed and the orientations of other molecules converted from tilted to untilted states. This is in agreement with the HAS results which suggest the appearance of a structure with a lower density than the $(\sqrt{25}\times\sqrt{25})$ structure at 36 K. Even though this structure has a smaller binding energy per unit area than that of $(\sqrt{13}\times\sqrt{13})$ structures, the $(\sqrt{25}\times\sqrt{25})$ structure survives to higher temperatures than the $(\sqrt{13}\times\sqrt{13})$ structure.

5.2.4 N_2 adlayers: (n×2) structure

The structures and stabilities of (*n*×2)-type structures were also examined. This sequence of structures was observed by the LEED experiments but with a poor degree of ordering. HAS experiments exclude any possibilities of the occurrence of *c*(4×2) structure but it did suggest the presence of an incommensurate phase with coverage less

than the coverage of the $\left(\sqrt{13}\times\sqrt{13}\right)$ and greater than that of the $\left(\sqrt{25}\times\sqrt{25}\right)$ phase. In order to shed some light on these issues we ran the Monte Carlo simulation for several (n×2) structures *i.e.* c(4×2), p(3×2), c(8×2) and (2×2).

5.2.4.1 N_2 adlayers: c(4×2) structure

This structure was tested via MC simulation at 1 K. The initial structure is similar to that obtained for CO/MgO(001). The c(4×2) phase was not stable at 1 K where many molecules desorbed to form a second layer. So in agreement with the HAS experiments and the neutron diffraction experiments this structure is excluded.

5.2.4.2 N_2 adlayers: p(3×2) structure

The p(3×2) structure similar to that discussed in chapter 4 (Fig. 4.17) for CO/MgO system was tested and was found to be unstable. It is worth noting, however that large portions of the molecules stay on the surface adopting this structure up to 25 K where the structure becomes mostly disordered. We should note that the stability of this structure could be viewed as a support to the results of LEED experiments.

5.2.4.3 N_2 adlayers: c(8×2) structure

The initial configuration is similar to that discussed in chapter 4 (see Fig. 4.22). The MC was used to simulate this structure at 1 K, 10 K,

20 K and 25 K. Each run consist of at least 50 kcycle after equilibration with a cutoff radius of 18.5 Å. It was found that this structure is stable at 1 K. The final configuration, as seen in Fig. 5.9, contains rows of horizontal molecules separated by rows of perpendicular molecules. The tilt angle distribution (not shown) has peaks at $\theta=0^{\circ}$ and 85°. This differs from the results obtained for CO/MgO(001) where the tilt angle was found to be $\theta=0^{\circ}$ and 31°. This structure has a coverage lower than that of the $\left(\sqrt{25}\times\sqrt{25}\right)$ phase. The total binding energy at 1 K was found to be -465.57 kcal/mol this yields a binding energy of -2.91 kcal/mol per molecule and -0.206 kcal/mol per unit area.

Thermal stabilities of this structure are tested and was found to be stable up to 15 K. This finding also supports the LEED experiment where some (n×2) structures where observed for a submonolayer coverage. Beyond 20 K the structure shows small portions of defects in the long range order. At 25 K small islands of the c(8×2) phase still exist but most of the layer undergoes a phase transition into a new structure. The symmetry of this new structure was not clear.

5.2.4.4 N_2 adlayers: c(2×2) structure

The initial configuration for our Monte Carlo simulations consists of 72 molecules where only half of Mg sites are occupied by N_2 molecules

placed in a checkerboard pattern. We started our simulations at 1 K with all molecules perpendicular to the surface and occupy every other Mg^{+2} site (see Fig. 4.25). Although the molecules are allowed to change their positions and orientations during the simulations the final structure stayed almost the same as the initial configuration. From the simulations at 1 K the resulting binding energy per molecule is -2.95 kcal/mol where the binding energy of the layer of $c(2\times2)$ structure is -213 kcal/mol. The value of the binding energy per molecule for the $c(2\times2)$ is slightly more than the surface binding energy (-2.91 kcal/mol) of an isolated perpendicular molecule and also greater than that of the binding energy per molecule in case of $\left(\sqrt{13}\times\sqrt{13}\right)$ and $\left(\sqrt{25}\times\sqrt{25}\right)$ structures. The difference between this binding energy and the binding energy of the isolated molecule is accounted for by the net attraction of -0.25 kcal/mol between the molecules. Although this structure has a higher (weaker) binding energy per a unit area than that of $\left(\sqrt{13}\times\sqrt{13}\right)$and $\left(\sqrt{25}\times\sqrt{25}\right)$ phases, it was found to be stable over the temperature range of 1 K to 60 K.

5.3 Discussion and conclusions

We have performed Monte Carlo simulations to test and study the possible structures and phase transitions in the N_2/MgO(001) system. This work is the first computational study on this system. As we have

discussed in the introduction, this system has also been the subject of a variety of experimental studies *i.e.* helium atom scattering, low energy electron diffraction and neutron diffraction techniques. We have shown that our model for the N_2/MgO system is able to reproduce most of the available experimental data regarding this system. Furthermore we predict a sequence of phase transitions similar to that observed for CO/MgO(001). We have illustrated this sequence as another example of the devil's staircase in molecular systems.

In agreement with experiments, our simulations confirm the observation of the $\left(\sqrt{13}\times\sqrt{13}\right)$ structure with nine molecules in its cell and a coverage of 70 %. In agreement with HAS experiment, this structure has two adsorption sites (perpendicular and horizontal) and was found to be thermally stable below 20 K. Beyond 20 K the layer becomes disordered and is accompanied by the desorption of some molecules from the layer to form a second layer. This can be viewed as a support to the HAS experiments where a transformation to a lower density phase was suggested.

Although HAS experiments observed a $\left(\sqrt{25}\times\sqrt{25}\right)$ structure at 12 K and at coverages lower than that of the $\left(\sqrt{13}\times\sqrt{13}\right)$ structure, no orientation or detailed structure were proposed for this phase. To gain

knowledge of the orientations of the adsorbed nitrogen molecules in this phase, polarization infrared spectroscopy (PIRS) experiments and simulations need to be performed. Our simulations show that the $(\sqrt{25}\times\sqrt{25})$ phase is stable up to 25 K. This phase, with a coverage of 64%, has two adsorption sites (perpendicular and horizontal sites), similar to that of the $(\sqrt{13}\times\sqrt{13})$ phase. Even though this structure has a smaller binding energy (-0.21 kcal/mole per unit area) compared wit that of the $(\sqrt{13}\times\sqrt{13})$ phase (-0.23 kcal/mol per unit area), the $(\sqrt{25}\times\sqrt{25})$ phase is thermally stable to temperatures higher than that of the $(\sqrt{13}\times\sqrt{13})$ phase. This implies that a phase transition of the $(\sqrt{13}\times\sqrt{13})$ structure to the $(\sqrt{25}\times\sqrt{25})$ phase is possible around 18 K. There is no direct experimental evidence for this possible phase transition as of yet, although Traeger *et al.* [38] in their HAS experiment reach the $(\sqrt{13}\times\sqrt{13})$ structure from the $(\sqrt{25}\times\sqrt{25})$ only after a further adsorption of N_2 molecules.

In principle, a $(\sqrt{41}\times\sqrt{41})$ structure is possible but it was not seen experimentally. It could be part of sequence of transitions similar to that proposed for CO/MgO(001.). The proposed sequence of transformations in N_2/MgO(001) system has the form,

$$(\sqrt{13}\times\sqrt{13}) \text{ -> } (\sqrt{25}\times\sqrt{25}) \text{ -> } (\sqrt{41}\times\sqrt{41}) \text{ ...c(2x2)}$$

This sequence of transformations might be another example of devil's staircase phenomena.

This sequence of transformations can be understood in terms of the number of tilted columns and untilted columns similar to the CO/MgO(001) system. Previous results show that the horizontal (tilted) molecules occupy every site along a column with neighbouring molecules possessing alternating azimuthal orientations. These columns consist of four molecules in the case of the $\left(\sqrt{13}\times\sqrt{13}\right)$ phase, and seven molecules in the case of the $\left(\sqrt{25}\times\sqrt{25}\right)$ phase, before a kink occurs and shifts the columns over one lattice spacing. At the kink there are two molecules, one tilted and one untilted in the case of the $\left(\sqrt{25}\times\sqrt{25}\right)$ structure and both of them untilted in case of the $\left(\sqrt{13}\times\sqrt{13}\right)$ phase. In the case of the $\left(\sqrt{13}\times\sqrt{13}\right)$ phase there are two untilted columns separating the two nearby tilted columns, whereas in case of the $\left(\sqrt{25}\times\sqrt{25}\right)$ phase there are three untilted columns between nearby tilted columns and for $\left(\sqrt{41}\times\sqrt{41}\right)$ there are four untilted columns between nearby tilted columns, etc. For c(2×2) all the molecules are untilted. The number of molecules per cell is $(n+1)^2$ and the area per unit cell is $(n+1)^2+n^2$ so that the coverage may written as

$$\Theta_n = \frac{n^2+2n+1}{2n^2+2n+1} = \frac{(n+1)^2}{(n+1)^2+n^2} \qquad (5.1)$$

where Θ_n is the coverage of a structure with n untilted rows between the nearby tilted rows (n=2,3,...). In Table 5.1 we show the coverage as function of n and the corresponding structure. We propose that a sequence of transitions through a set of $\left(\sqrt{2n^2+2n+1}\times\sqrt{2n^2+2n+1}\right.$ structures with ever decreasing density is possible under suitable conditions of temperature and pressure. This sequence of transitions is an example of devil's staircase phenomenon.

Table 5.1 The coverage Θ_n (n is number of untilted rows between the nearby tilted rows (n=2,3,...) as function of n and the corresponding structure.

n	Coverage	Structure
2	$\frac{9}{13}=0.692$	$\left(\sqrt{13}\times\sqrt{13}\right)R33.7^\circ$
3	$\frac{16}{25}=0.64$	$\left(\sqrt{25}\times\sqrt{25}\right)R36.9^\circ$
4	$\frac{25}{41}=0.61$	$\left(\sqrt{41}\times\sqrt{41}\right)R38.7^\circ$
∞	$\frac{1}{2}=0.5$	$c(2\times2)$

No evidence was observed for the existence of $c(4\times2)$ or $p(3\times2)$ structures. These structures were not stable, even at very low temperatures (1 K). We should note that some short range elements of a $p(3\times2)$ structure remained, even at higher temperatures above (25 K). This lends support to the LEED experiments [30] that detected (n×2)

structures. In addition to this agreement we found that $c(8x2)$ structure with density of (62 %) is stable to temperatures of 25 K. At 25 K we ran the MC simulations for the $c(8\times2)$ structure for 150 kcycle. The final configuration was disordered.

It is interesting to note that despite the similarity of the CO and N_2 molecules in terms of the their physical interactions, their transitional and orientational ordering on MgO(001) surface are different. These differences might be due to the fact that the nitrogen has a smaller binding energy with MgO(001) surface than that of the CO, which allows the N_2 molecules to maximize their molecule-molecule interactions by adopting either the flat or the perpendicular orientation. The flat orientation of N_2 molecules decreases the available space in the unit cell and leads to structures with a lower density.

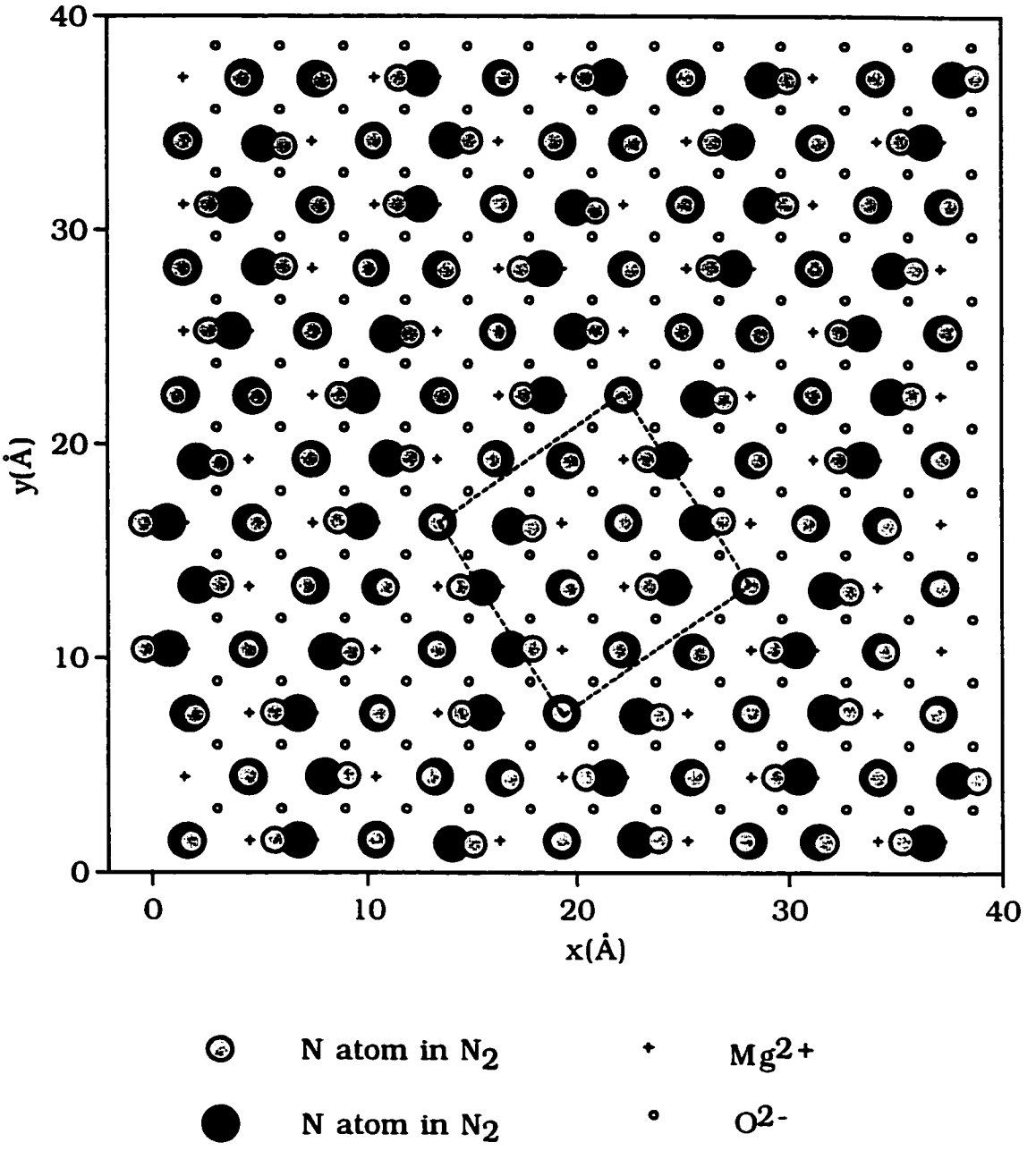

Figure 5.1. An overview of the final configuration of 117 nitrogen molecules adsorbed overtop a 13×13 patch of the MgO(001) surface at 1K. This layer forms the $\left(\sqrt{13}\times\sqrt{13}\right)$ structure. The nitrogen atoms closest to the surface are shown as black and the upper nitrogen atom as gray. The unit cell is shown (dot lines).

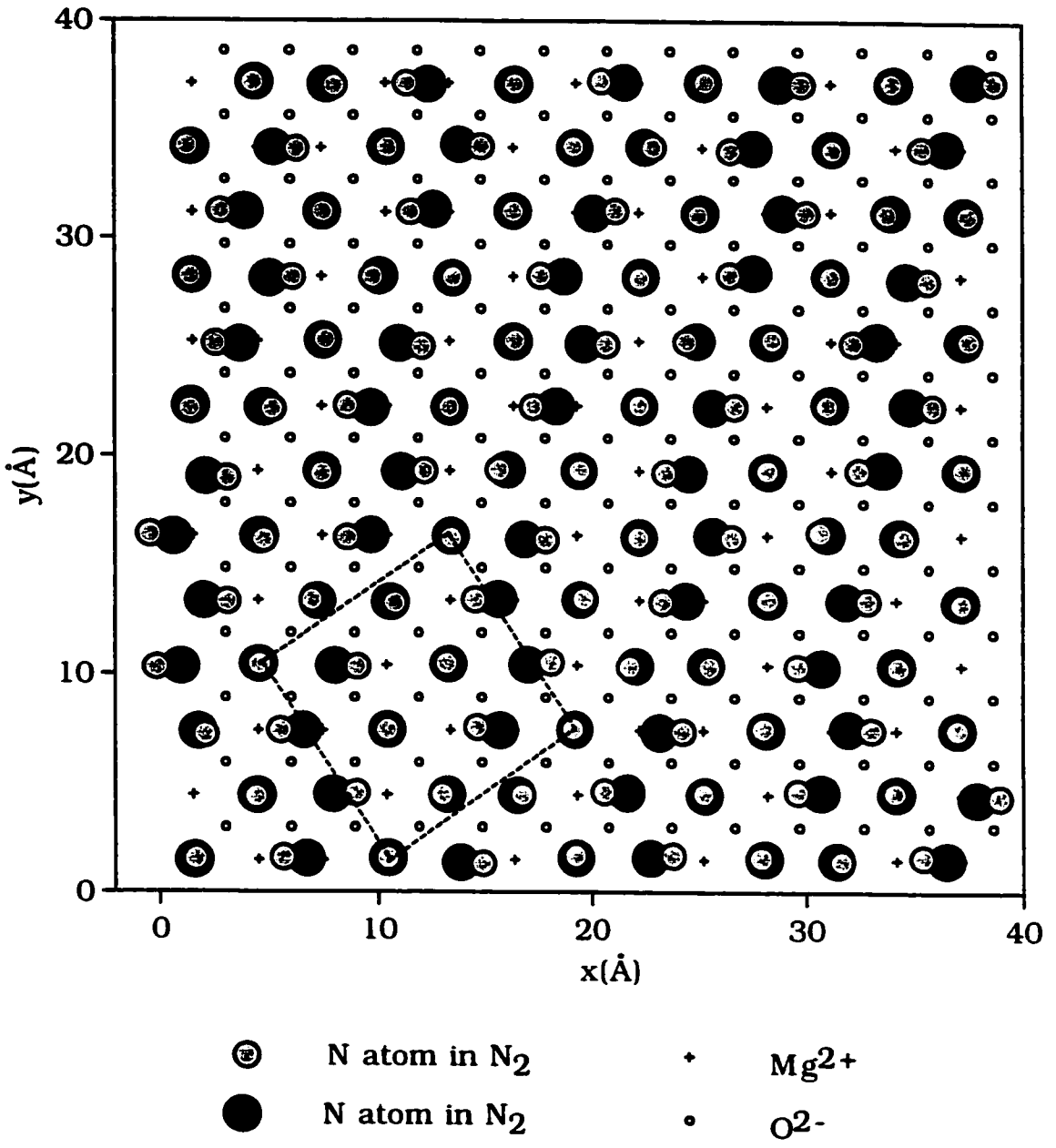

Figure 5.2. An overview of the final configuration of 117 nitrogen molecules adsorbed overtop a 13×13 patch of the MgO(001) surface at 13K. This layer forms the $\left(\sqrt{13}\times\sqrt{13}\right)$ structure. The nitrogen atoms closest to the surface are shown as black and the upper nitrogen atom as gray. The unit cell is shown (dot lines).

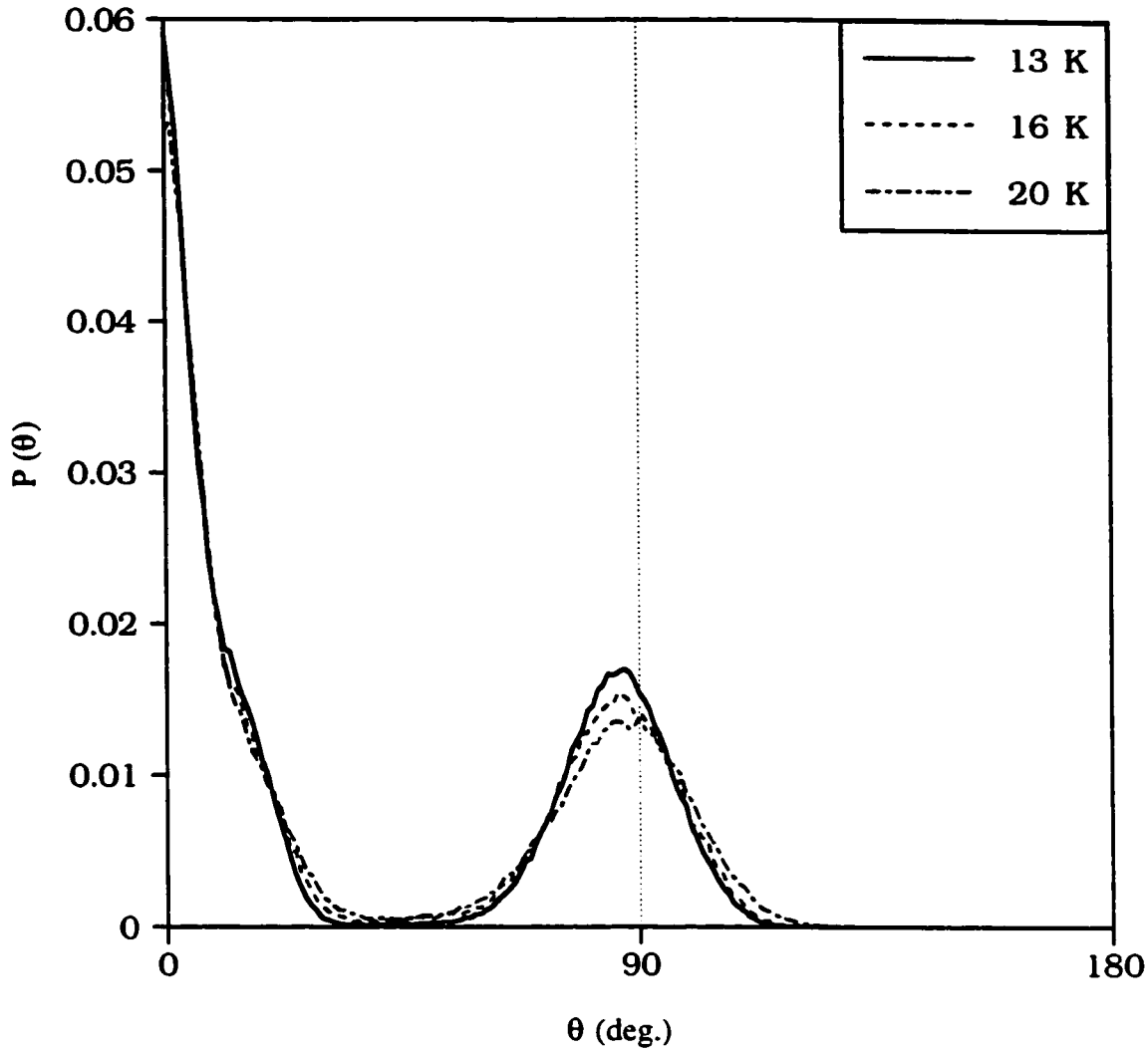

Figure 5.3. The polar (tilt) angle (θ) distribution for $\left(\sqrt{13}\times\sqrt{13}\right)$ structure is plotted for T=13 K, 16 K and 20 K. The distribution is symmetric and centered on the θ~0°, 85°.

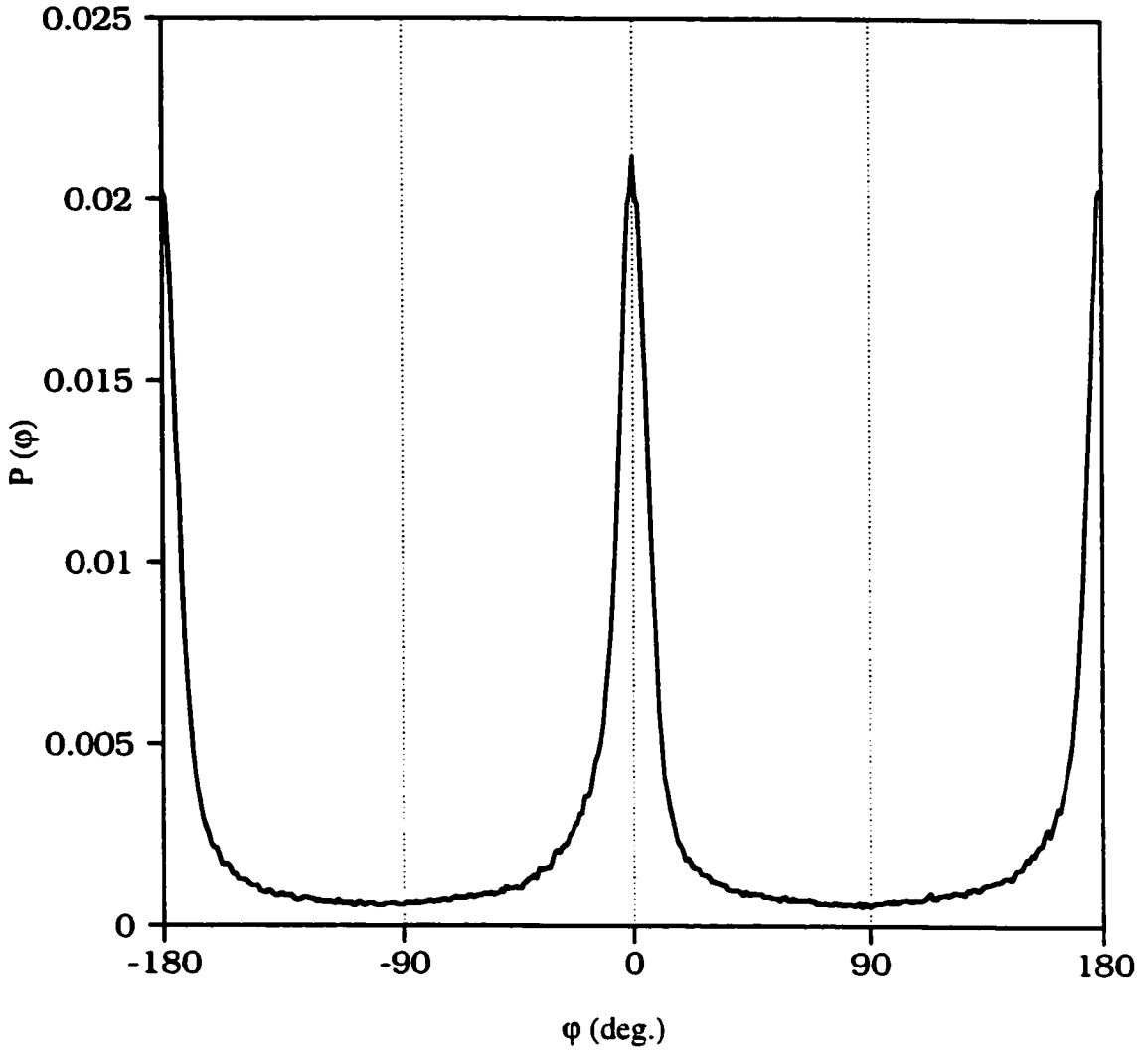

Figure 5.4. The azimuthal angle (φ) distribution of the $\left(\sqrt{13}\times\sqrt{13}\right)$ phase is plotted for T= 13 K. Note that the peaks are symmetric and centered on the φ~±180°, 0° directions.

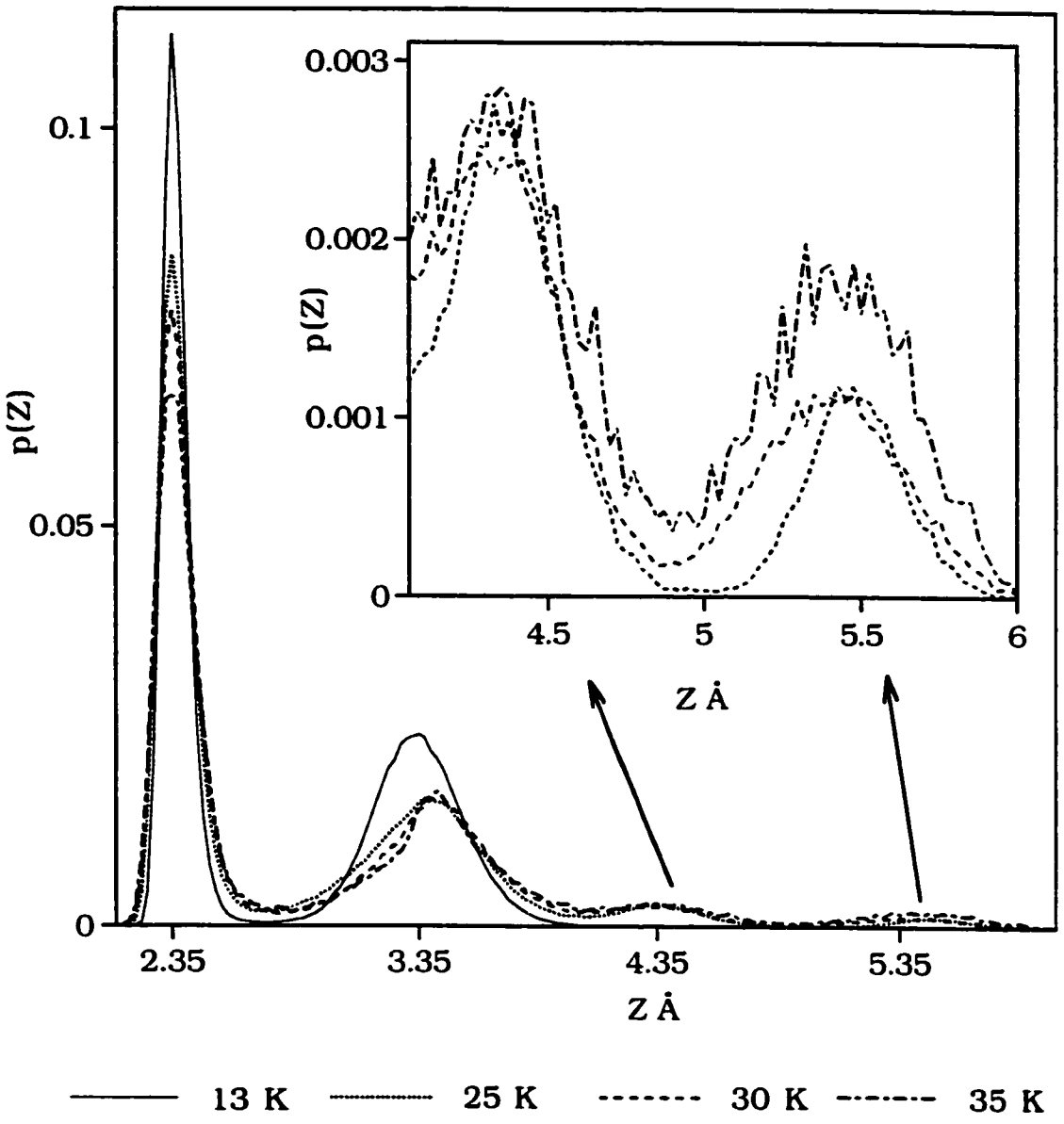

Figure 5.5. The average height of a the closest nitrogen atom above the MgO(100) surface (z distribution) for the $\left(\sqrt{13}\times\sqrt{13}\right)$ phase is plotted for T=13, 25, 30, 35 K. At T=13K the peaks are centered on the z_c =2.35 Å (for perpendicular nitrogen molecules) and 3.35 Å (for tilted nitrogen molecules). As temperature increases the peak heights decrease and widths broaden until above 25K the molecules start to leave the surface (desorb) and the distribution acquires new two peaks, z_c ~ 4.3 and 5.4 Å. The area under these new peaks indicates that the number of desorbed molecules is about 8 nitrogen molecules at 25 and 30 K, while at 35 K the number of desorbed molecules becomes 14 N_2 molecules.

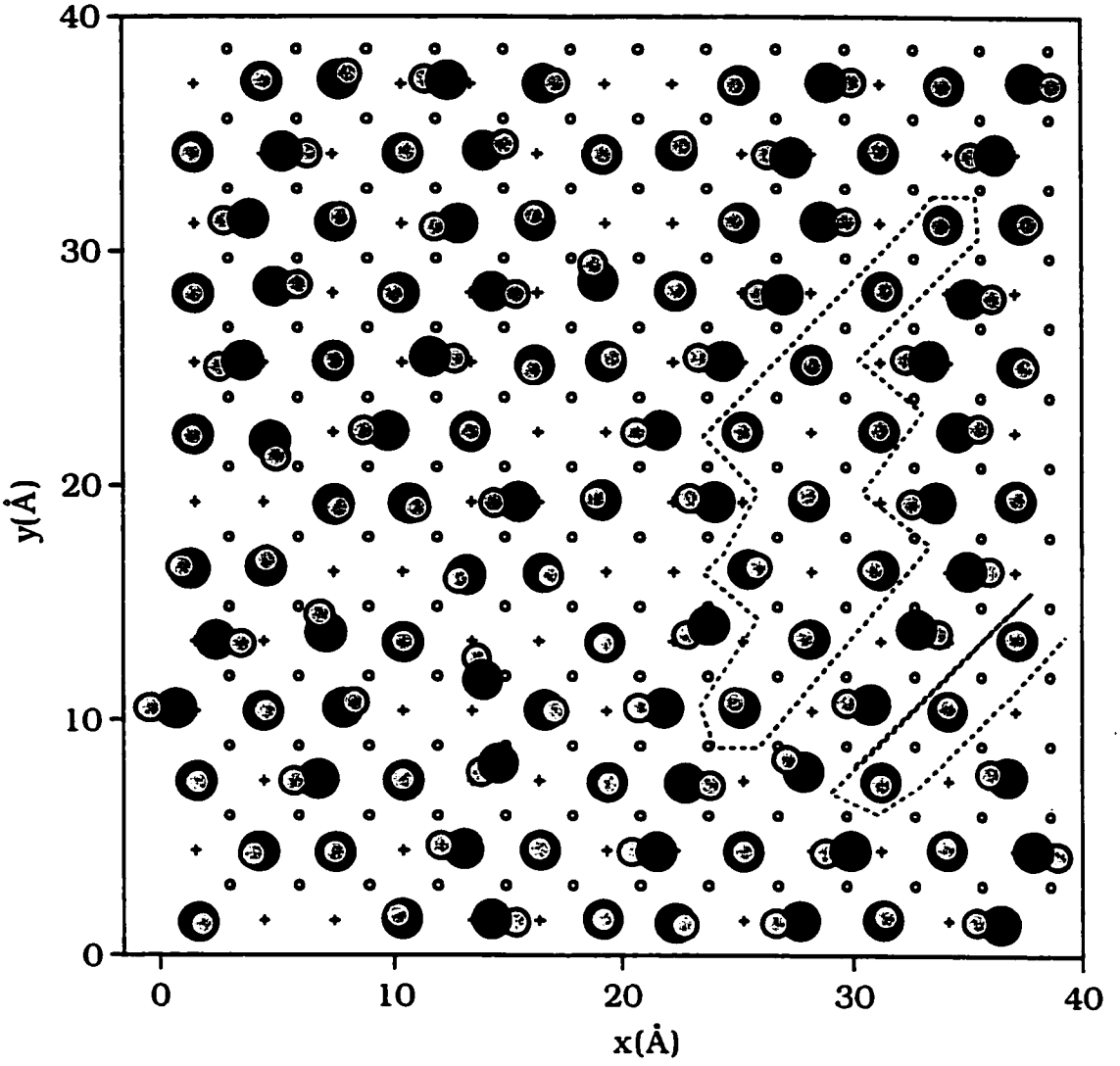

Figure 5.6. A top view of the final configuration of the remaining 109 nitrogen molecules in the first layer from the $\left(\sqrt{13}\times\sqrt{13}\right)$ structure at 25K is shown. Eight nitrogen molecules desorbed from the first layer to the second layer and were removed. The nitrogen atoms are shown as black and gray (to make it easier to see the molecules). The (+) symbol represents a Mg^{2+} ion and (o) symbol represents a O^{2-} ion. It can be seen that the adlayer is largely disordered. There are evidences that the number of untilted columns between tilted ones has increased compared with the $\left(\sqrt{13}\times\sqrt{13}\right)$phase at lower temperatures (dot lines).

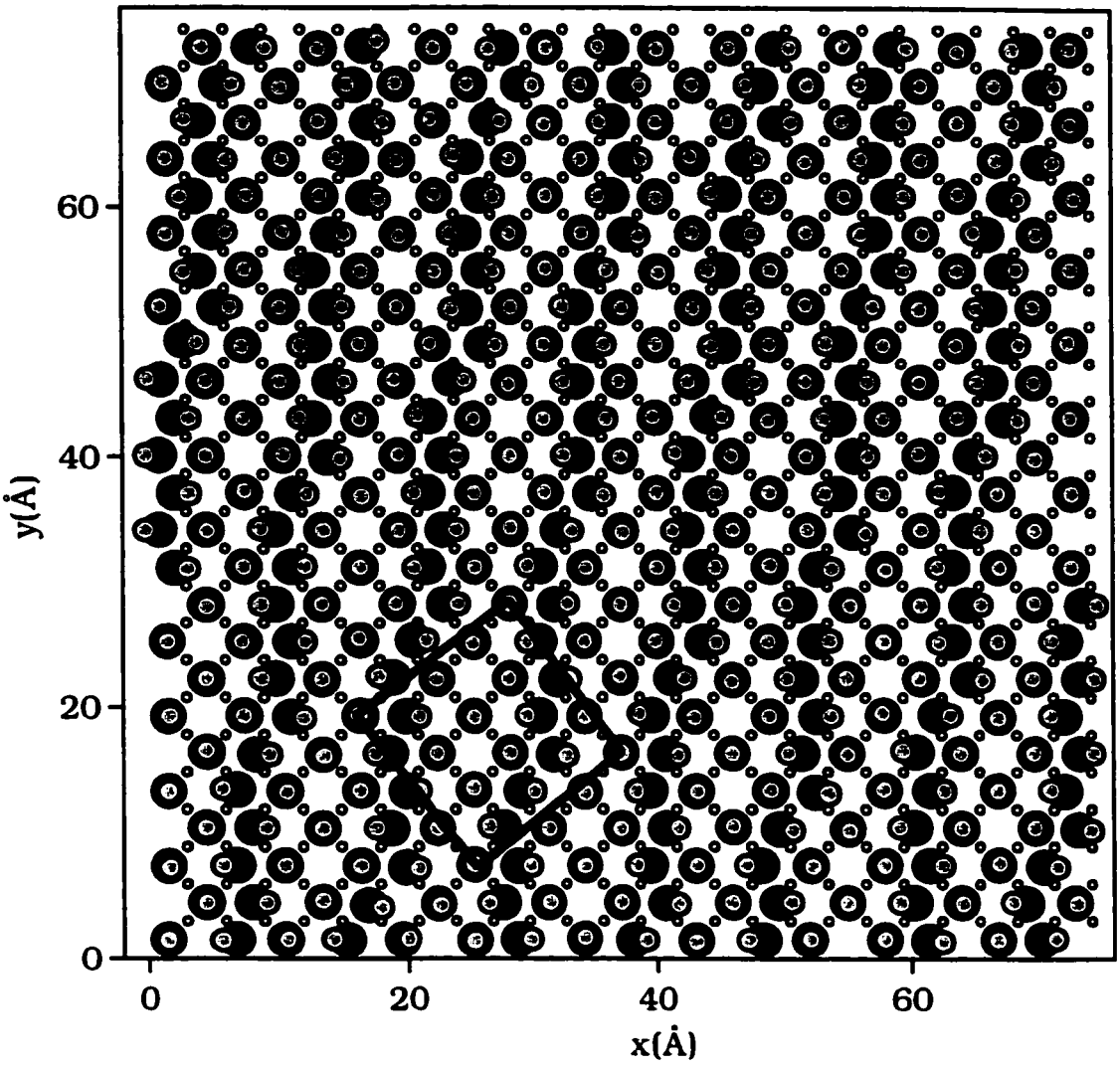

Figure 5.7. A top view of the MgO(100) surface covered with 400 N_2 molecules at 1 K. The nitrogen atoms closest to the surface are shown as black and the other atoms as gray. The (+) symbol represents a Mg^{2+} ion and (◦) symbol represents a O^{2-} ion. Note that the origin is centered on a O^{2-} ion. The resulting $\left(\sqrt{25}\times\sqrt{25}\right)$ unit cell is shown (lines).

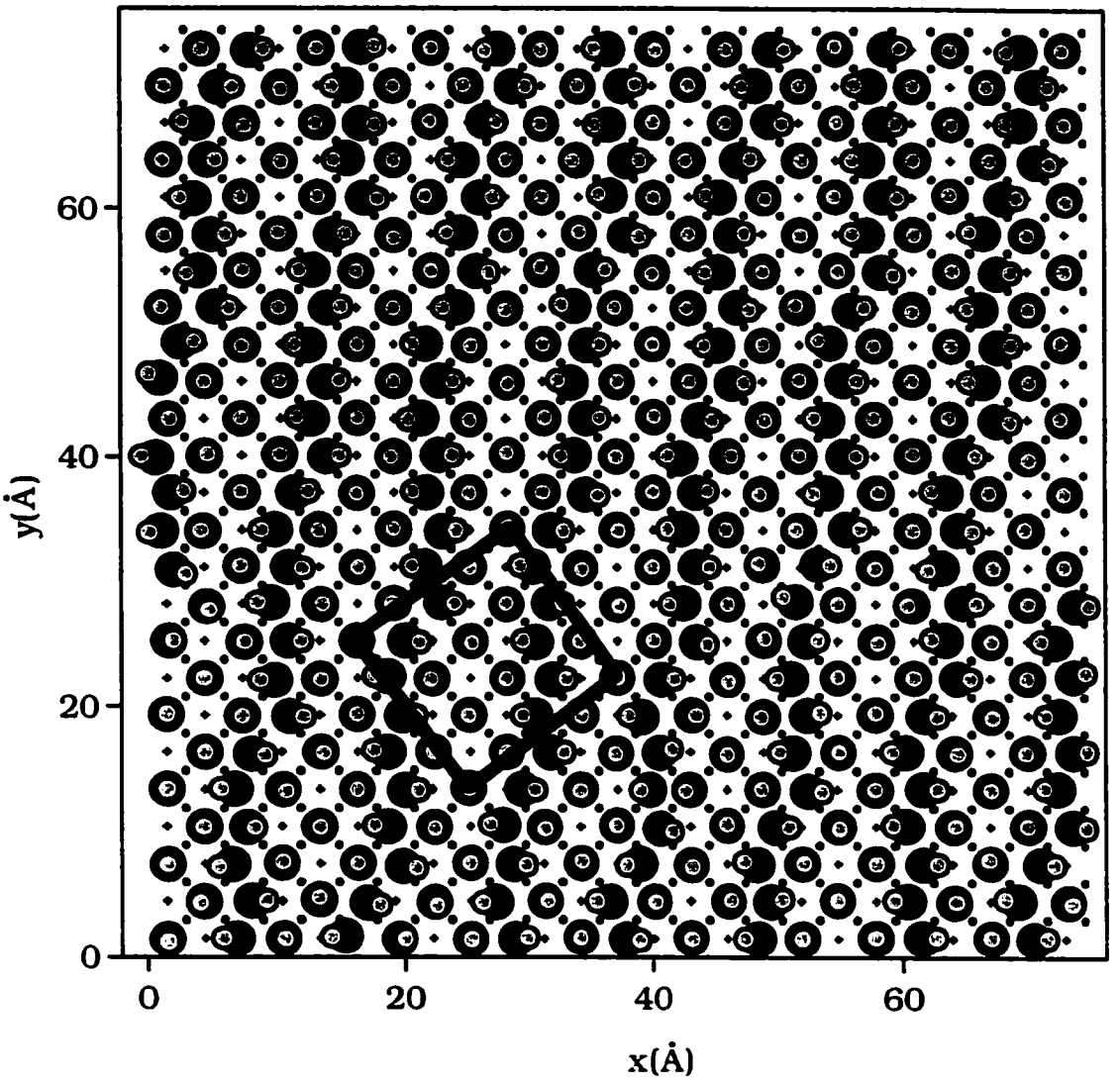

Figure 5.8. A top view of the MgO(100) surface covered with 400 N_2 molecules at 13 K. The nitrogen atoms closest to the surface are shown as black and the other atoms as gray. The (+) symbol represents a Mg^{2+} ion and (◦) symbol represents a O^{2-} ion. Note that the origin is centered on a O^{2-} ion. The resulting $\left(\sqrt{25}\times\sqrt{25}\right)$ unit cell is shown (lines).

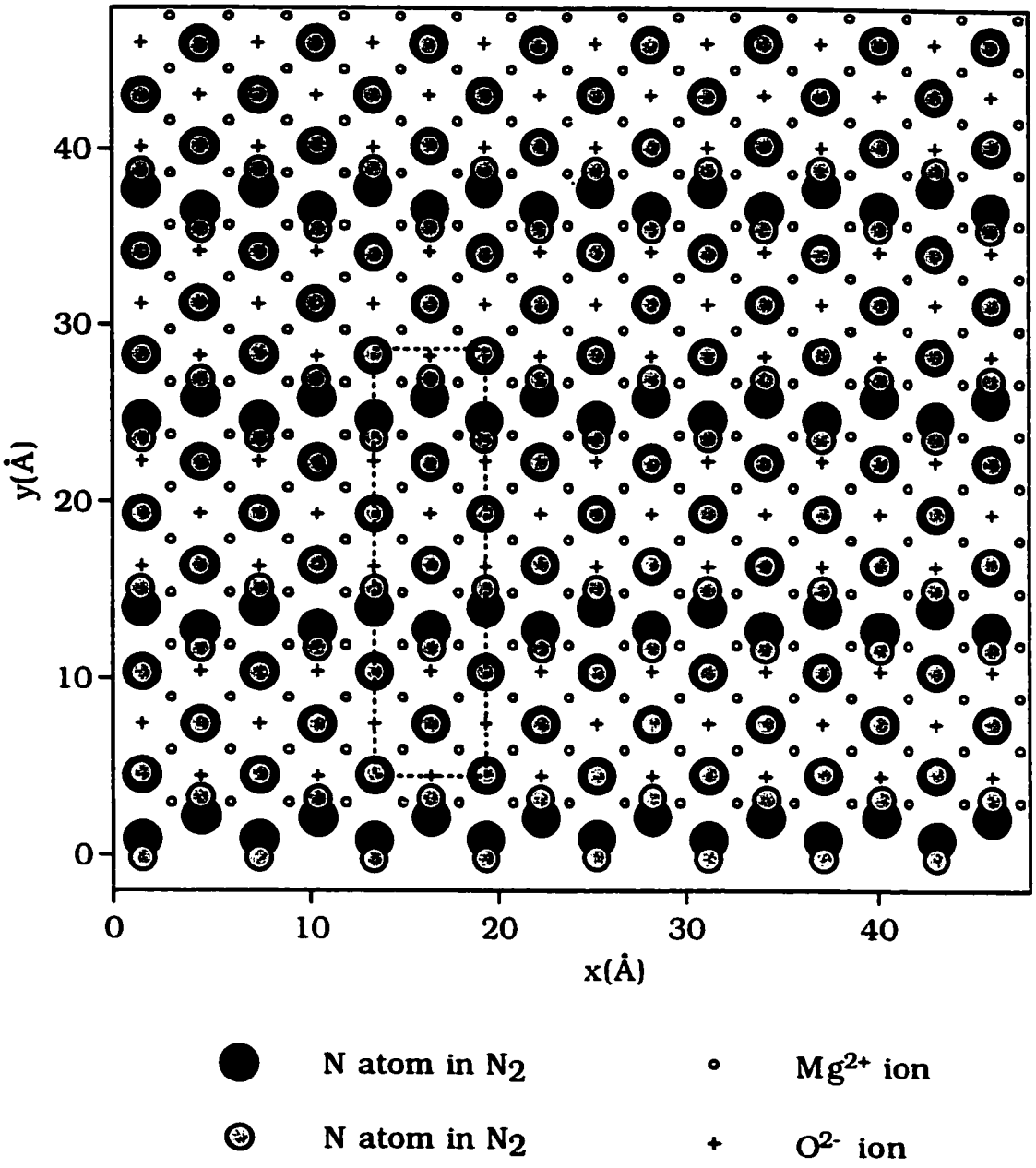

Figure 5.9. A top view of the MgO(001) surface covered with 160 N_2 molecules at 1 K. The resulting *c*(8x2) unit cell is shown (dot lines).

6. N_2 adsorbed on NaCl(001) surface

The NaCl(001) substrate, like MgO(001), has a cubic structure. The main difference occurs in the ionic charges. The ions of NaCl have a formal charge of ±1 e whereas the ions of the MgO have formal charge of ±2 e. Also NaCl has a lattice constant of 5.64 Å, which is much larger than that of MgO (4.20 Å). This means that NaCl has more space available for adsorbed molecules like N_2 and CO molecules than MgO(001). Because the lattice constant of solid N_2 is similar to that of the NaCl surface we expect that nitrogen molecules will occupy every available adsorption site. As CO molecules form an ordered structure on NaCl(001) at low temperature and undergo an order-disorder phase transition at higher temperatures, so we expect that the N_2/NaCl system will behave in the same way. The primary difference between these systems is that the CO molecule has a permanent dipole moment whereas N_2 is a nonpolar molecule. The presence of the dipole moment in the case of CO molecules, can lead to long relaxation times for energy and order parameter equilibration since it has a long range interaction of the order of r^{-3}. In the case of N_2 only quadrupole-quadrupole interactions (r^{-5}) are present and hence N_2 molecules are substituted for CO molecules to overcome the above problem.

The vibrational spectrum for N_2 on NaCl(001) is found to be similar to that of CO adsorbed on NaCl(001) [80]. Due to the intense electric field of the NaCl surface, dipoles are induced in the N_2 molecules and are infrared active [82]. According to polarization studies the nitrogen molecules were found to adsorb perpendicular to the surface directly over the Na^+ ions [80][82].

6.1 Potentials and simulations method

The potentials and methods used are similar to those used in the simulations of the CO/MgO(001) and N_2/MgO(001) systems of the previous chapters. Besides the repulsion and dispersion interactions, point dipoles have been assigned to each of the atomic sites of N_2 to mediate the electrostatic interactions. The construction of the N_2-NaCl surface potential has been discussed in chapter 2 where a modified Buckingham potential was used to describe the non-electrostatic interactions between individual atom-ion pairs. The values used for the dispersion and repulsion coefficients for the various atom-ion pairs are given in Table 2.6. The parameters for the N_2-N_2 interactions are presented in Tables 2.2 and 2.4.

To simulate a monolayer of nitrogen on NaCl(001), (L×L) arrays (L=10,20,30,40,60) of molecules were placed in the NaCl surface potential. Periodic boundary conditions with a cutoff radious of 16.5 Å

(up to four lattice sites) for molecule-molecule interactions were imposed. The nitrogen molecules were allowed random moves (translations and rotations). The Monte Carlo simulations (discussed in chapter 3) were run for 1-2 Mcycles at each of the temperatures sampled in the range of 1-50 K. For a given temperature, the first 200-500 kcycle were discarded to ensure that the system had reached equilibrium and statistical data for the variables of interest collected for the last 700 kcycle to 1.5 Mcycles.

6.2 Simulations results

6.2.1 Single molecule

Energy minimization using the steepest descent method, is used to find the geometry and binding energy for a single N_2 adsorbed on the NaCl(001) surface at 0 K. Besides providing information valuable to experiments, this study of a single molecule allowed us to fine tune our potential surface parameters. In agreement with experiments, it was found that an N_2 molecule sits perpendicular to the surface over top of a Na^+ ion with a height of 2.65 Å (distance between the bottom N atom and the surface) above a cation site.

The Monte Carlo simulations were also preformed for a single molecule. In these simulations a single N_2 molecule was placed in the

NaCl surface potential. This molecule is given initially a random position and orientation. The final configuration at 1 K shows that the nitrogen molecule sits perpendicular to the surface over top of an Na^+ ion with a surface binding energy of -2.88 kcal/mol, which is in agreement with the experimental values corrected to 1 K. The polar angle distribution shows a gaussian-like distribution centered on $\theta=0°$ and a uniform distribution in the azimuthal angle. Finite temperature simulations show that on average the molecule remains oriented perpendicular to the surface over top of the cation site with no preferred azimuthal orientation.

6.2.2 Monolayer N_2 on NaCl(001)

A monolayer of nitrogen molecules adsorbed on NaCl(001) was simulated by placing an ensemble of 100 molecules (10×10 system) in the NaCl surface potential with every site of Na^+ ions occupied by an N_2 molecule. This system was tested at each temperature over the range of 1-60 K. The initial configuration at 1 K had all molecules perpendicular to the surface. The final configuration after 60 kcycle contained multiple domains of $p(2\times1)$ structure. When the MC simulation was started with an initial structure of a single domain of a $p(2\times1)$ structure at 1 K, the final configuration was an ordered $p(2\times1)$ structure (top panel of Fig. 6.1) similar to that observed in CO/NaCl(001) system, where columns of

adsorbed nitrogen molecules with the same tilt angle are found. The molecules in the adjacent columns have the same tilt angle with respect to the surface normal but are azimuthally oriented in the opposite direction. As seen in Fig. 6.2 the tilt angle distribution at 10 K shows a sharp peak at a tilt angle of 29°. The azimuthal angle distribution shown in Fig. 6.3 at 10 K, shows two sharp peaks at $\varphi=\pm 90°$. The unit cell of this structure contains 2 molecules (Fig. 6.1). The binding energy is found to have a value of -3.09 kcal/mol per molecule.

The $p(2\times1)$ structure remains thermally stable and ordered up to 25 K. As seen in the snap shot shown in the bottom panel of Fig. 6.1 (at 30 K), this structure becomes orientationally disordered, where the long-range azimuthal order has been lost. Some degree of short range order still exists in the form of small domains of the $p(2\times1)$ structures and the occurrence of vortex-antivortex pairs. The vortices seem to appear in the transition region below and above the transition temperature similar to the X-Y model where the they appear at temperatures leading up to the Kosterlitz-Thouless (K-T) transition. The vortices rotating in the clockwise and counterclockwise directions are formed by groups of four neighbouring molecules whose molecular axes have azimuthal orientations of ±45°, ±135° and form the sides of a "diamond" shape. The sense of rotation is provided by imagining the molecular axis having a directional arrow pointing from the lower nitrogen (black) to the upper

nitrogen (gray). The molecules forming a clockwise vortex thus have a sequence of azimuthal angles of +45, -45, -135, +135, moving around the vortex while the counterclockwise vortex has the reverse sequence. The appearance of the vortices might be an indictor of K-T type behaviour. Even though the $p(2\times1)$ structure becomes disordered above 25 K the molecules remain localized above the Na^+ ions with no desorption. This is an indicator that this phase is of the order-disorder type. In order to further determine the type of this phase transition (first order or continuous type) we performed a quantative analysis for the data obtained from the Monte Carlo simulations and is explained in the next sections.

6.2.3 Order disorder phase transition

6.2.3.1 Azimuthal angle distribution analysis

In order to show the destruction of the orientational order of the $p(2\times1)$ structure more quantitatively, the azimuthal angle (φ) distribution for several temperatures below and above 25 K (10 K, 20 K and 30 K) are plotted (see Fig. 6.2). At 10 K the distribution has two sharp peaks at $\varphi=\pm90°$. As the temperature is increased e.g. T=20 K, the distribution also has two peaks at the same positions but they are broader. The distribution becomes uniform around 25 K. This feature show that the $p(2\times1)$ structure loses its long range order and an order-

disorder phase transitions occurs. The same behaviour was found in the CO/NaCl system but it occurred at a different transition temperature.

6.2.3.2 Polar angle distribution analysis

As shown in Fig. 6.3, at all of the tested temperatures the nitrogen molecules adsorbed on NaCl(001) were tilted from the surface normal by 29° on average, although thermal broadening occurred. That is, as the temperature is increased the polar angle distribution broadened but maintained a gaussian-type distribution centered on θ= 29°. In the N_2/NaCl system the molecular tilt is accompanied by a displacement of the nitrogen molecule off of the Na^+ site by 0.15 Å in the same direction as the tilt. No evidence of the molecules untilting or acquiring a perpendicular orientation at or past the transition region was found. On average, the molecules in the disordered phase remain tilted by the same angle of 29° that they have in the ordered phase. This indicates that there is no untilting of the molecules, which might lead to a structural transformation as opposed to an order-disorder transition. The constancy of the average molecular tilt supports the interpretation of the transition being of the order-disorder type in contrast to the N_2/graphite system where a change in molecular tilt leads to a weak first order transition. So, in light of the maintenance of the molecular tilt through the phase transition and the fact that the molecules on average remain localized near the Na ions, it seems probable that the transition is truly

an order-disorder transition of the continuous type and thus exhibits critical behaviour.

6.2.3.3 Energy results

To confirm that the transition is of the continuous type the average energy E per molecule is plotted as a function of temperature in Fig. 6.4 for the 20×20 system. We should note that the energy autocorrelation function (see chapter 3) is used to determine how often (every 10 cycles) we should sample the available data to find the average energy. The energy was obtained after equilibration for 200 kcycle to 500 kcycle and averaging for 1 to 2 Mcycle every 10 cycles. The equilibration number of cycles was obtained by monitoring the energy as a function of cycles. Equilibration occurred when the energy stopped drifting and settled into fluctuations around an average. The average energy curve (Fig. 6.4), as a function of temperature, shows the expected linear increase with temperature below and above the transition region with a continuous sigmoidal curve centered at a transition temperature of T_C= 25.3 K. No discrete jump in the energy was detected. The absence of any discrete jump in the energy is strong indication that the type of the phase transition is a continuous one.

6.2.3.4 Heat Capacity results

6.2.3.4.1 Heat Capacity as a function of temperature

The heat capacity is determined from the energy fluctuations as calculated from $\langle E^2 \rangle - \langle E \rangle^2$ (see Eq. 3.1). The temperature dependence of the heat capacity presented in Fig. 6.5 for a wide range of lattice sizes shows that the shape of the heat capacity displays the Greek letter lambda (λ) divergence, where the heat capacity begins to gradually grow before the transition temperature. This continuous variation of the heat capacity as a function of temperature strongly suggests the occurrence of a continuous phase transition similar to that found by Wiechert *et al.* [152] and Feng *et al.* [58] in their examinations of the CO/graphite system. The heat capacity curves show a sharp peak at the transition temperature (T_c=25.3 K). This value of the transition temperature is similar to that (26 K) of a broad orientational ordering transition observed in the CO/graphite system [152][58] and is also comparable to the transition temperature (27 K) of nitrogen adsorbed on graphite [19][153]. Our data shows that as the lattice size increased the peak height of the heat capacity goes to a higher value and its position is slightly shifted toward a lower transition temperature. This result agrees well with the theoretical work by Ferdinand *et al.* [154] for finite systems with periodic boundary conditions. Away from the transition temperature the heat capacity approaches its baseline value of 2.5 R.

This value is due to the presence of three translational (x, y, z) and two rotational (θ,φ) modes for each molecule, and hence there are five vibrational modes that contribute to the total potential energy. From these results there is a strong indication that the transition is indeed continuous.

6.2.3.4.2 Heat Capacity direct critical exponent

The logarithmic divergence of the heat capacity C with $|t|$ can be written as the following general model function,

$$C^{\pm} = A^{\pm}\cdot\ln(t) + B^{\pm} \qquad (6.1)$$

where the (+) sign refers to temperatures above the transition temperature and (–) sign refers to temperatures below the transition temperature.

In Fig. 6.6 the heat capacity C as a function of the logarithm of the reduced temperature, $\ln(t)=\ln(|(T_C-T)/T_C|)$, is plotted for temperatures above and below T_c=25.1 K for the 60×60 size of the N_2/NaCl(001) system. These data are fitted with a linear regression program (Cricket graph). In both cases, there is a linear dependence of C on ln(t) which can be expressed as,

$$C^{-}/R = -0.256\cdot\ln(t) - 0.158 + 2.5 \qquad \text{for } T < T_C \qquad (6.2)$$

$$C^{+}/R = -0.250\cdot\ln(t) - 0.200 + 2.5 \qquad \text{for } T > T_C \qquad (6.3)$$

where the background heat capacity of 2.5 R is shown explicitly.

Within the error limits of 0.006 and 0.04 in $A^{\pm}$ and $B^{\pm}$ respectively, the amplitude A is the same above and below the transition temperature. The values of $A^{\pm}$ are half of that of the isotropic 2D Ising model on a square lattice $A^{-}=A^{+}=0.4945$ [155]. Contrary to the Ising result for the isotropic 2D Ising model on a square lattice the values of the intercept B^{+} and B^{-} are not the same above and below T_C, the offset of the two heat capacity lines shown in Fig. 6.6. Below T_C the intercept B^{-} has a value approximately one half that of the Ising [155] value (B_{Ising} = 0.3063) whereas above T_c the intercept B^{+} is about 60% of the Ising result. The relative error assigned to the intercepts is large because their values are sensitive to the value of T_c (which is only known to within 0.05 K) used to construct the reduced temperature variable "t". By varying T_c the values of B^{+} and B^{-} can be made equal but only at the unacceptable expense of losing the equivalence of A^{+} and A^{-}. The simulation thus indicates that there is a difference between B^{+} and B^{-} for this system. The origin of this difference might be due to the anisotropic interactions, which can vary the values of the critical amplitudes due to the averaging of the molecular orientations in the disordered phase. Once again it should be noted that the values of A and B are not required to match those of the Ising or four state clock models. Indeed, recent experiments

on similar two dimensional systems exhibiting Ising-like behaviour also yield deviations from the standard values of the coefficients. In particular, measurements of the heat capacity of the CO/graphite system yield values of A^-=0.340 and A^+= 0.344 and B^-=0.157 and B^+=160 for the head-tail disordering transition at T_c = 5.18 K [152] while work on the pinwheel to disorder transition found values of A = 0.940 and B=0.344 with a transition temperature of T_C = 35.2 K [19].

The heat capacity amplitude ratio is are equal to unity, but the intercept ratio is not, viz.

$$\frac{A^+}{A^-} = 0.99 \pm 0.02 \qquad \frac{B^+}{B^-} = 1.26 \pm 0.2 \tag{6.4}$$

Onsager's exact solution [155] of the 2D Ising model obtained unity for both of the above ratios. This result and the logarithmic divergence of the heat capacity (α=0.0) indicate, at this stage, that the phase transition is Ising-like. However, there is a discrepancy in that the ratio $\frac{B^+}{B^-}$ is not 1 as predicted for the Ising model [155].

We should note that the fit of the heat capacity data to a power law was not as good as the logarithmic one (see Fig. 6.7) but was nonetheless possible. The heat capacity critical exponent obtained from the power law fit has a value of α=0.076±0.010.

6.2.3.5 Order parameter results

6.2.3.5.1 Order parameter as a function of temperature

The definition of the order parameter was presented in section 3.2, where the order parameter Φ is constructed from the x and y components of the orientation vector of the nitrogen molecules. After the standard transformations (see chapter 3, section 3.2) needed to account for the antiferroelectric ground state are applied, the orientations were summed over all the molecules in the system. As may be seen in Fig. 6.8 for several system sizes, the order parameter decreased at low temperatures (1-20 K) in a linear manner with an increase in temperature according to the following relation [156][157]

$$\Phi(T) = 1.0 - \frac{1}{2} G_0 T \tag{6.5}$$

This is due to the librational waves in the monolayer, which are analogous to spin waves in magnetic systems.

The factor (G_0) shows no size dependence and has a value of $5 \times 10^{-3} K^{-1}$ ($\pm 2 \times 10^{-3}$), which is half the value found for planar dipoles on a square lattice. Note that the order parameter has a value close to unity at 1 K, which implies that the system is well ordered. The order parameter drops precipitously as the temperature approaches the transition temperature with the larger system showing a sharper drop than the smaller system. The order parameter of the largest system

(60×60) has the sharpest drop and levels out to a baseline value of 0.05, where the system is fully disordered. No break is detected in the curve of the order parameter as a function of temperature, this again leading to the conclusion that the transition is continuous.

6.2.3.5.2 Order parameter direct critical exponent

The critical exponent β was determined by plotting ln(Φ) versus ln(t) as in Fig. 6.9 for the 60×60 system. By fitting this curve to a linear function using (Cricket graph) software we found that there is a linear portion in the transition region ($24.4 \leq T \geq 25.0$). The fitting function has the following form,

$$\ln(\Phi) = \beta \ln(t) + \ln(D) \qquad (6.6)$$

where β is the order parameter critical exponent with value β = 0.62, and the amplitude is $D = 6.11$. These values are significantly higher than the Ising value of β=0.125 and D=1.22. The transition temperature T_c=25.1 used to calculate the reduced temperature "t", was obtained from the location of the peak of the susceptibility which will be discussed in the next section. The value of β is sensitive to the choice of T_c, *e.g.* if T_c=25.0K then β = 0.44 and if T_c = 25.2 K then β = 0.80, but both of these examples still differ significantly from the Ising value. Hence, even with a liberal error estimate of ±0.20, the value of β deviates substantially from the Ising value. Finite scaling analysis will be used to confirm this obtained value of β.

6.2.3.6 Susceptibility results

6.2.3.6.1 Susceptibility as a function of temperature

The susceptibility, as determined from the fluctuations of the order parameter according to the definitions presented in section 3.2, is plotted in Fig. 6.10 as a function of temperature for two system sizes. The susceptibility versus temperature curve for the 20×20 system has a sharp peak at 25.2 K and for the 60×60 system has a sharp peak at 25.1 K. As we have seen in the heat capacity, the maximum and the magnitude of the peak in the susceptibility *vs.* temperature curve depend upon the lattice size. As the system size is increased, the position of the peak of the susceptibility is shifted toward lower values of temperature. This result is typical for finite systems with periodic boundary conditions [154]. Again there is a smooth variation in the susceptibility as a function of temperature. This may be viewed as additional support of our previous findings that the transition in monolayer nitrogen on NaCl(001) is continuous.

6.2.3.6.2 Susceptibility direct critical exponent

In order to obtain the susceptibility critical exponent (γ), we have plotted $\ln(\chi)$ versus $\ln(t)$ above and below the critical temperature, as can be seen in Fig. 6.11, for the 60x60 system, which is the largest

system in size we have used. In the critical region (24.2-25.9 K) the data fits well to the following linear function,

$$\ln(\chi^{\pm}) = \gamma^{\pm} \ln(t) + \ln(G^{\pm}) \tag{6.6}$$

where $\pm$ refers to above and below the transition temperature and $G^{\pm}$ is the amplitude. As shown in the Fig. 6.12, the susceptibility critical exponent (γ) is found to have a values of 0.702 above and 0.708 below the critical temperature (T_c=25.1 K). Varying the critical temperature around 25.1 K yields a large error in the susceptibility critical exponent. The error is assigned a value of ± 0.1 and reflects the sensitivity of γ to the choice of T_c. Eq. 6.6 is equivalent to the following standard form,

$$\chi^{\pm} = G^{\pm} t^{-\gamma^{\pm}} \tag{6.7}$$

The amplitudes $G^{\pm}$ above and below T_c are obtained from the intercepts of the lines in Fig. 6.11, and have values of 0.035 and 0.017 for G^{+} and G^{-} respectively. The values of these amplitudes are non-universal quantities and hence they do not necessarily have to match the numerical estimates of the Ising model *i.e.* $G^{+} = 0.963$ and $G^{-} = 0.0255$.

The values of the critical exponent above and below the critical temperature (T_c=25.2 K) were also estimated from the 20×20 system and found to be similar but yielded a value of 1.5. This value deviates from the Ising value of 1.75 but not nearly as much as the 60×60 system.

As we mentioned previously, our goal is to determine which of the several existing theories for critical behavior is valid for our system N_2/NaCl and which universality class the system falls into. Since the obtained critical exponents for the order parameter and susceptibility strongly deviate from the Ising critical exponents, our simulations predict that the order-disorder phase transition of the N_2/NaCl(001) system fall into the universality class of the XY model with cubic anisotropy. Only this model has non-universal critical exponents.

The obtained values of α, β and γ is used to check the validity of Rushbrooke's relation, $\alpha+2\beta+\gamma\geq 2$. If the heat capacity is regarded as having a logarithmic divergence with α assigned the nominal value of zero, then the sum $\alpha+2\beta+\gamma=1.95$ falls short of satisfying the relation. However, if the power law result for the heat capacity ($\alpha=0.076$) is used then $\alpha+2\beta+\gamma=2.03$ and the relation is valid. In either case, the Rushbrooke relation is satisfied as an equality within the error limits.

6.3 Finite size scaling

The previous analysis is based on the assumption that the 60×60 system is close to the thermodynamic limit, *i.e.* the system is sufficiently large that the results are close to the results for an infinite system. To

fully verify these results a finite size scaling analysis should be performed.

Finite size scaling analysis provides a powerful tool to calculate the order parameter and susceptibility critical exponents for an infinite system from the behaviour of these thermodynamical observables as a function of the system size. To perform the finite size scaling analysis for the order parameter and susceptibility we should know the transition temperature T_c and correlation length critical exponent (ν).

6.3.1. The Binder fourth order cumulant to obtain Tc

To find the transition temperature T_c of an infinite system (thermodynamic limit), we plot the variation of the Binder fourth order cumulant (U_L) (see section 3.2) as a function of temperature for various system sizes in Fig. 6.12. The transition temperature T_c is located at the intersection of these curves and is found to have a value of T_c=25.087. We should point out that the curves in Fig. 6.12 do not exactly intersect at a fixed point and hence an error of ±0.004 should be assigned to the transition temperature T_c.

The quantity (U_L) at the transition temperature is found to have a value of U_L=0.556 which is different from the two-dimensional Ising value U_L^{Ising}=0.611 [158]. This result provide another strong indication that

the universality class associated to the phase transition of this system N_2/NaCl(001) is different from the Ising universality class.

6.3.2. Correlation length critical exponent ν

The correlation length critical exponent (ν) can be estimated by using the relations between the finite size transition temperature $T_c(L)$ and the infinite critical exponent T_c, [159] viz.

$$T_c(L) = T_c + \zeta L^{-1/\nu} \tag{6.8}$$

where ζ is a constant. Provided that we know T_c and $T_c(L)$ we can have a good estimate of (ν). As shown in Fig. 6.13 the finite transition temperature $T_c(L)$ is plotted as a function of $L^{-\frac{1}{\nu}}$ with T_c=25.087 K, ν was found to vary from 0.9 to 1.2 and the intercept lie in the range between 25.083 K and 25.04 K . The uncertainty in the finite transition temperature $T_c(L)$ should be included in the estimation of the error in calculating the critical exponent ν. Thus the value of ν is estimated to be 1±0.2, the large error is due to the uncertainty in the transition temperature $T_c(L)$.

6.3.3 Finite size scaling for the order parameter

The scaling relation given in chapter 1 (Eq. 1.5) is used to perform finite scaling analysis for the order parameter. In Fig. 6.14 we plot

$\Phi(L)L^{\beta/\nu}$ *vs.* $tL^{1/\nu}$ for the (30×30), (40×40) and (60×60) systems. The curves all lie on a single line, and the slope of this line was found to have a value of 0.620±0.1. This matches the previous result obtained from the direct analysis of the 60×60 system. Since the data collapses onto a single straight line the critical temperature and critical exponents are well chosen (T_c=25.087, ν=1.0 and β=0.620). For small values of $tL^{1/\nu}$ the function $\Phi(t)L^{\beta/\nu}$ approached a constant value of 1.0,

6.3.4 Finite size scaling for the susceptibility

Eq. (1.6) is used to perform the scaling analysis for the susceptibility. The best results that could be obtained are presented in Fig. 6.15 where $\ln(\chi(T,L)L^{-\gamma/\nu})$ versus $\ln(tL^{1/\nu})$ are plotted above and below the transition temperature T_c. It is clear that the data scale very well in the critical region and yielded a susceptibility critical exponent of $\gamma^- = 0.701 \pm 0.06$ below T_c. The error was obtained by varying the transition temperature and the critical exponent ν. Above T_c the susceptibility critical exponent was found to have a value of $\gamma^+ = 0.706 \pm 0.04$. Within the margin of error γ^+=γ^- and is the same as that found by examining the 60×60 system directly.

6.4 Conclusions

Monte Carlo simulations of the N_2/NaCl(001) system using detailed and realistic interaction potentials, predict that nitrogen molecules below 25.3 K will form uniform monolayer with an ordered p(2x1) structure on the (001) face of a NaCl surface with a unit cell that consists of two tilted molecules (θ=29°). This ordered monolayer is found to undergo a continuous order-disorder phase transition into an azimuthally disordered phase.

The energy curves displayed a continuous sigmoidal shape in the transition region with no discrete jump. The heat capacity is found to exhibit a logarithmic divergence similar to the Ising behaviour but with amplitude values different from the Ising values. Also the heat capacity is found to have a very weak power law divergence ($\alpha = 0.076$) as an alternative to the logarithmic divergence.

The critical exponents of the order parameter and susceptibility were found to have non-universal values and deviate significantly from the two dimensional Ising values. This result supports the prediction of José *et al.* [55], that a class of phase transition exists where the critical exponents are not universal but instead depend on the strength of an external anisotropy. The finite size scaling analysis was performed to

obtain reliable critical exponents and was similar to those obtained by the direct way. Even though the critical exponents β and γ were found to have nonuniversal values, they still obey Rushbrooke's scaling law, $\alpha+2\beta+\gamma=2$. The correlation length critical exponent has the value $\nu = 1$ and thus the Josephson hyperscaling law, $d\cdot\nu = 2 - \alpha$, is also satisfied.

In the end we should note that some of the results of this chapter were already published previously as a rapid communication in Physical Review B [160].

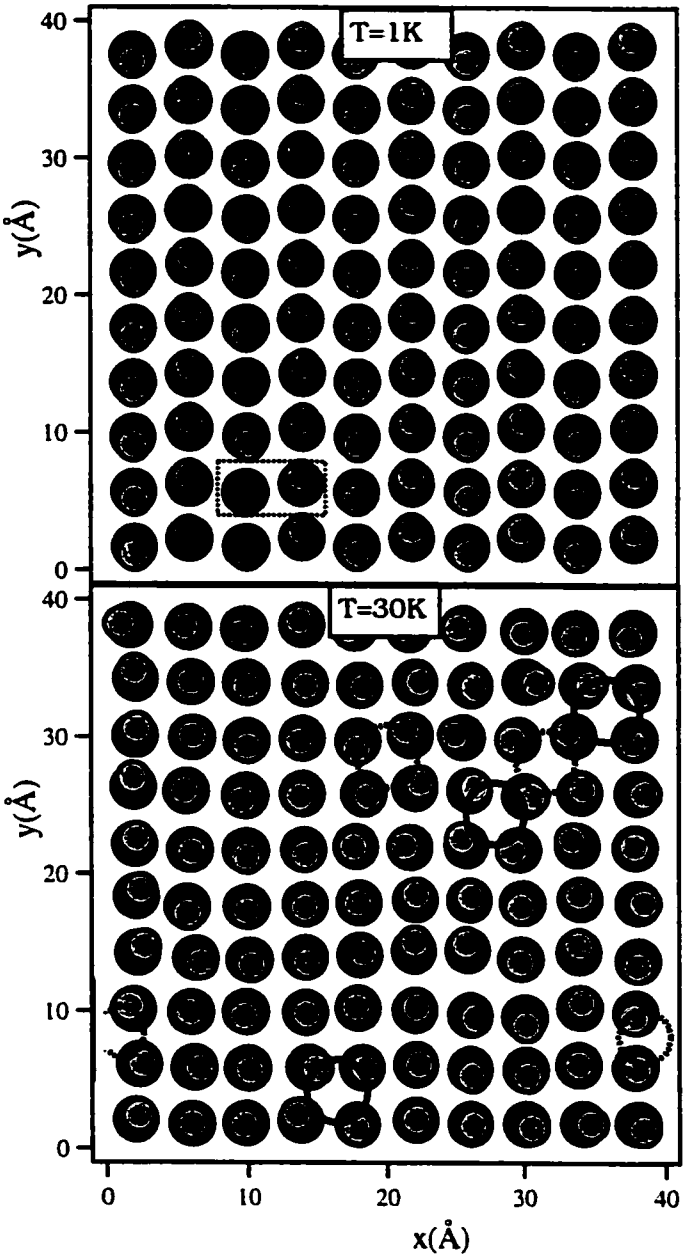

Figure 6.1. An overview of a typical configuration of 100 N_2 molecules at 1 K (top panel) and 30 K (bottom panel). The nitrogen atoms closest to the surface are shown as black and the upper nitrogen atoms as gray. Clockwise(counterclockwise) vortices are denoted by the solid (dashed) circles.

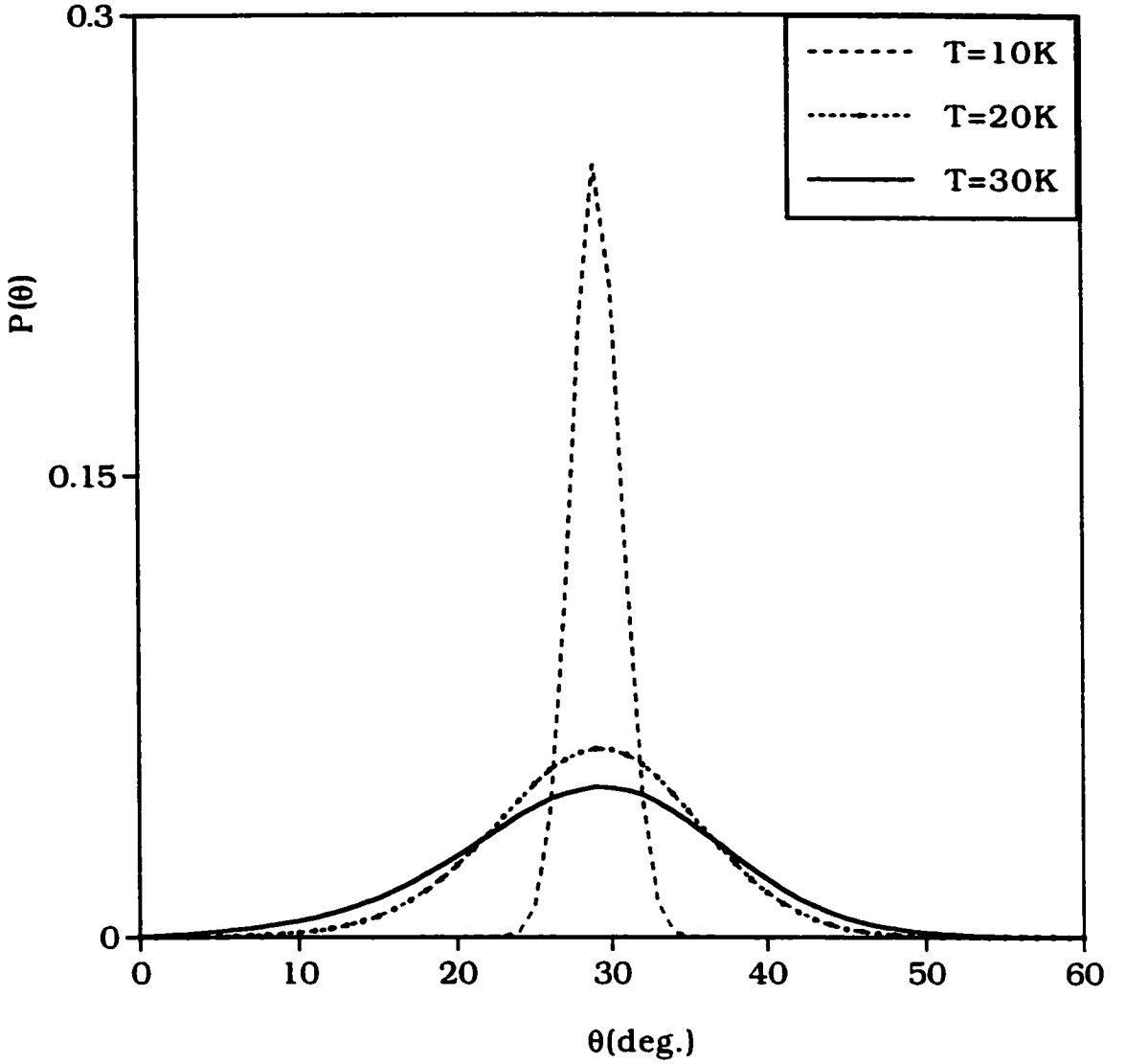

Figure 6.2 The tilt angle (θ) distribution for N_2/NaCl(001) system. Note that the average tilt angle does not change with temperature.

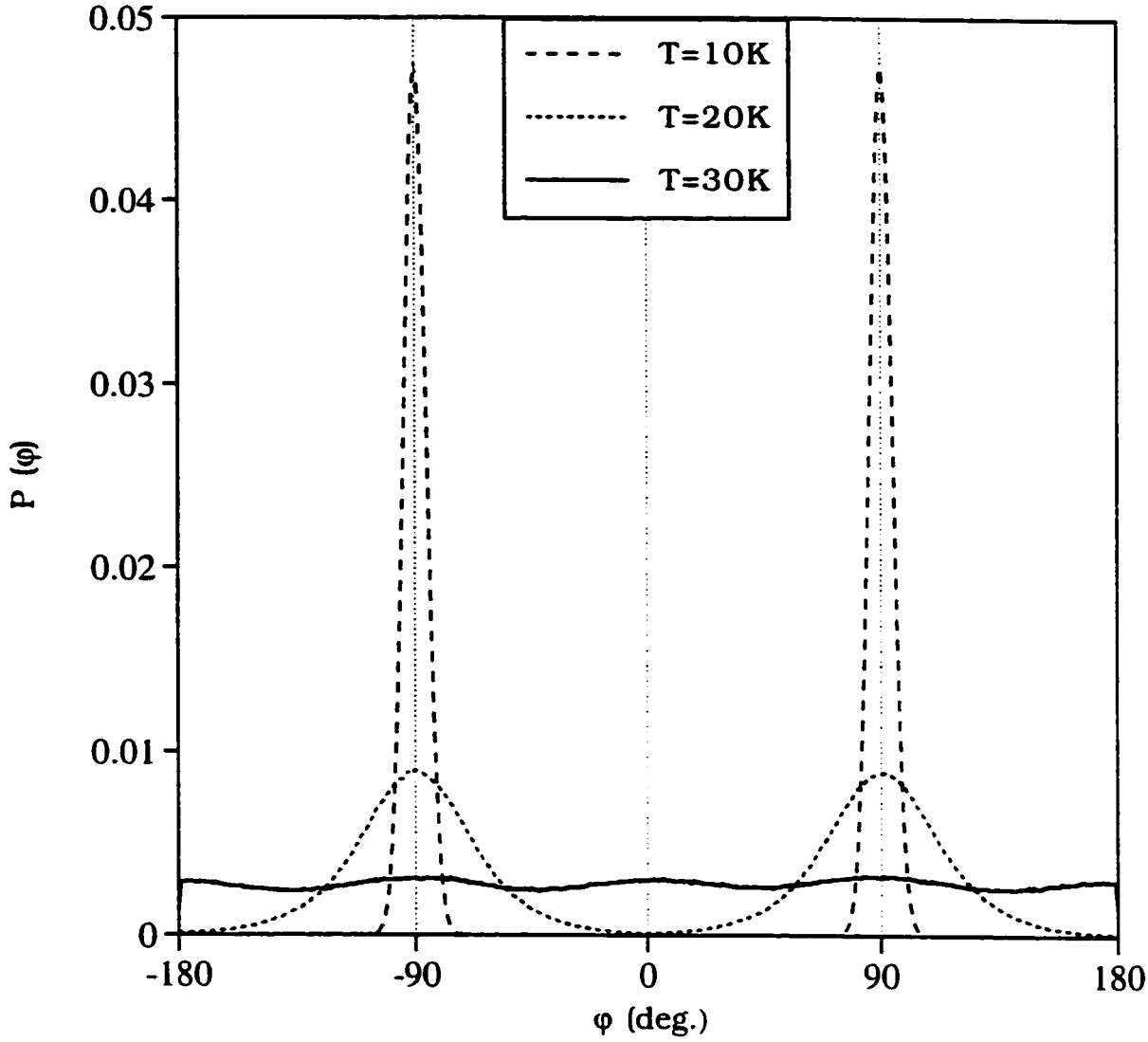

Figure 6.3. The azimuthal angle (j) distribution for T=10 K (dashed), 20 K (dotted), 30 K (solid). Note that at 30 K other than a minor residual preferential orientation, the probability is uniform.

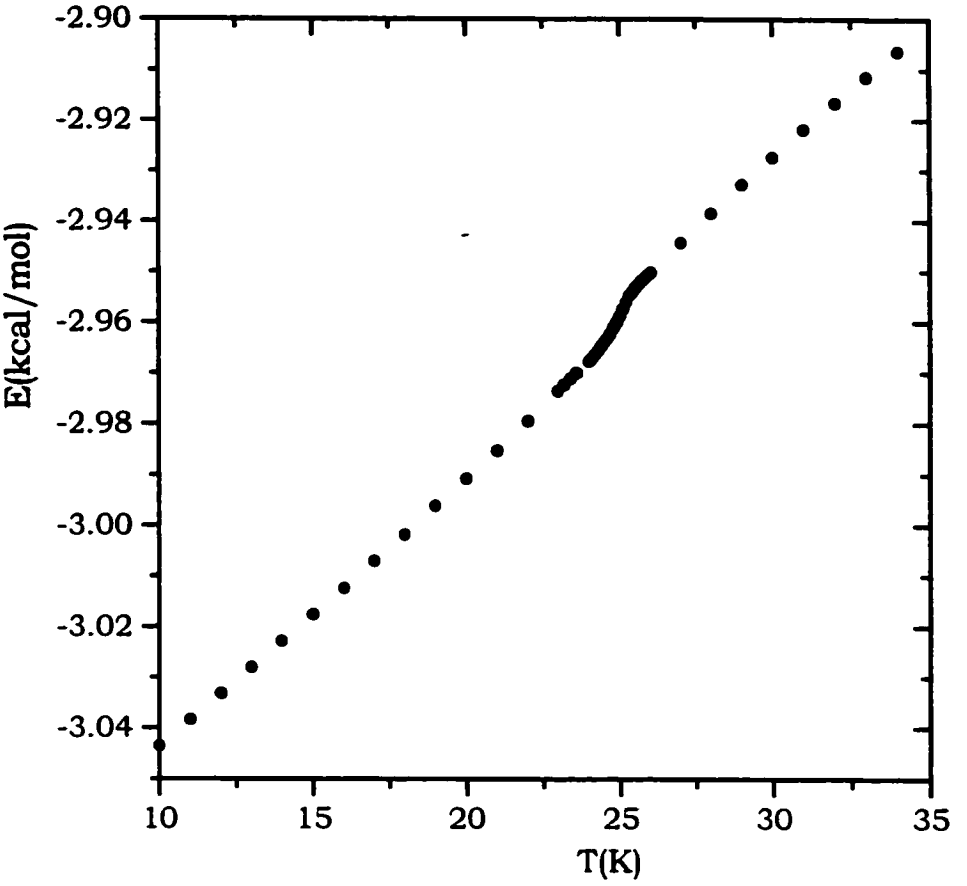

Figure 6.4. Plot of energy as a function of temperature for (20x20) system.

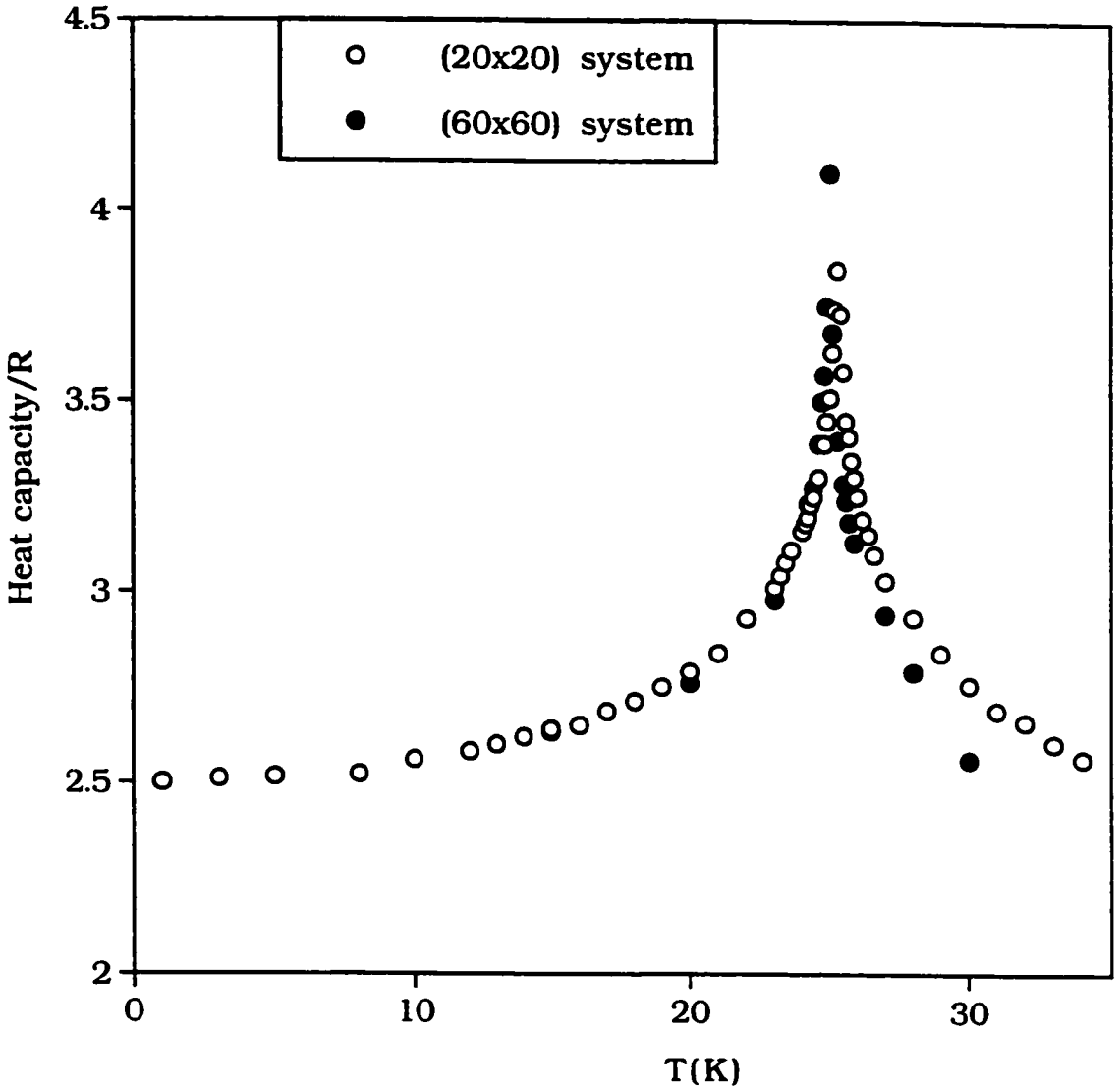

Figure 6.5. The heat capacity as a function of temperature for (20x20) and (60x60) systems. The peak for (20x20) system occurs at T_c=25.3 K while for (60x60) system occurs at T_c=25.1 K.

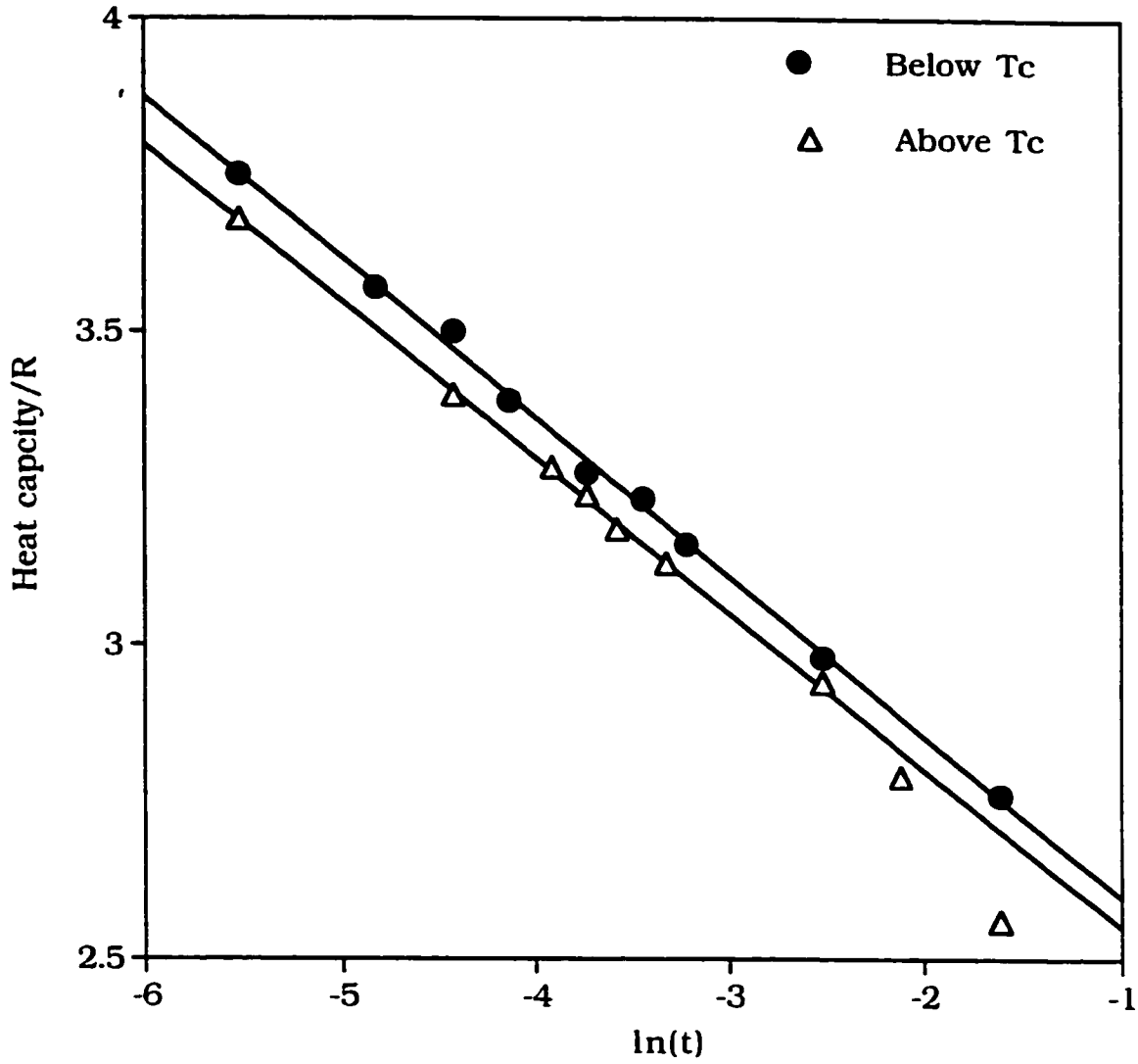

Figure 6.6. Plot of the heat capacity as a function of ln(t) where "t" is reduced temperature (N=3600).

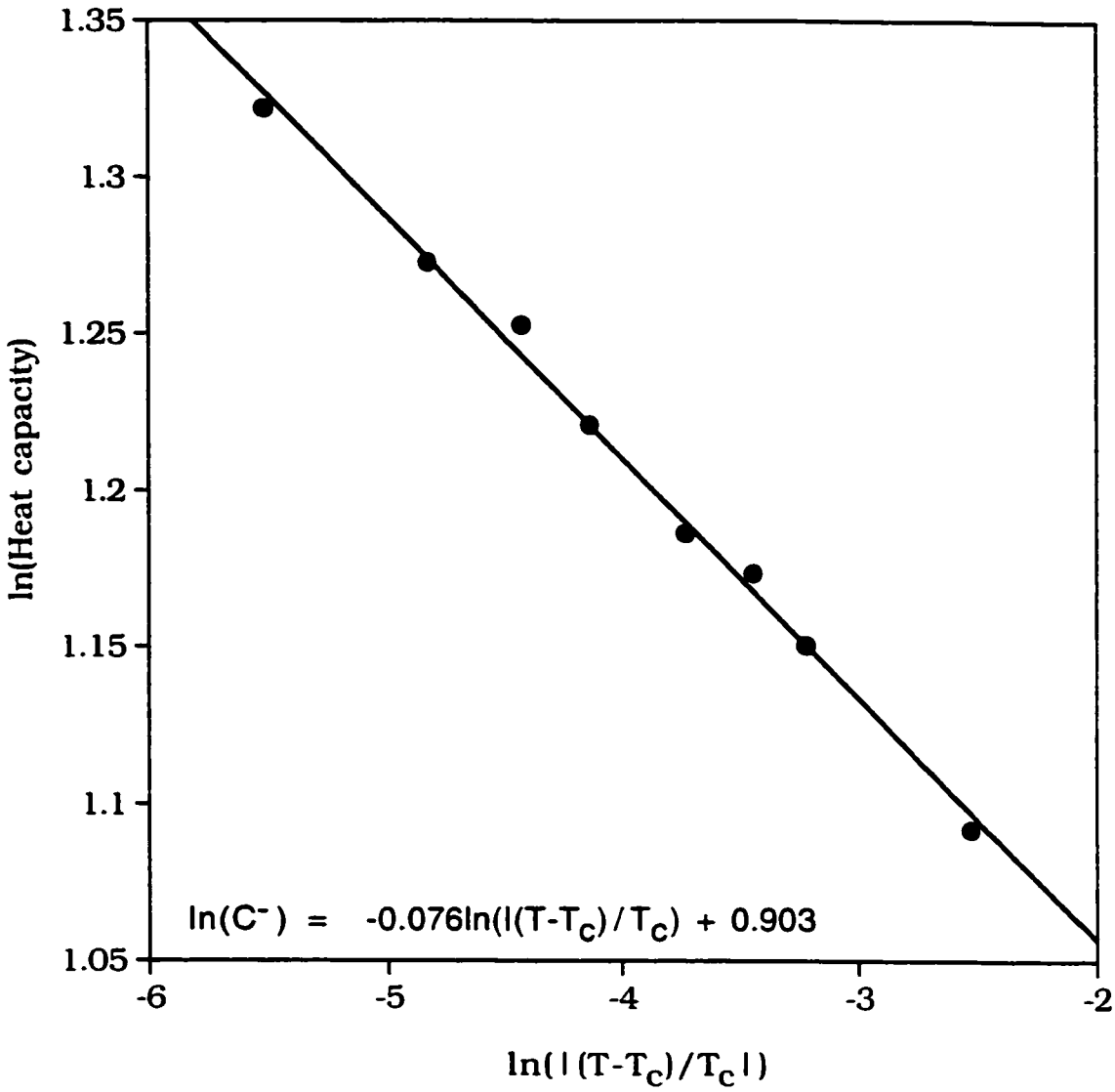

Figure 6.7. Log-log plot of the heat capacity as a function of reduced temperature for (60x60) system below the transition temperature. The small value of the heat capacity critical exponent (α=0.076) indicates that a logarithmic form for the heat capcity divergence is more appropriate rather than a power law.

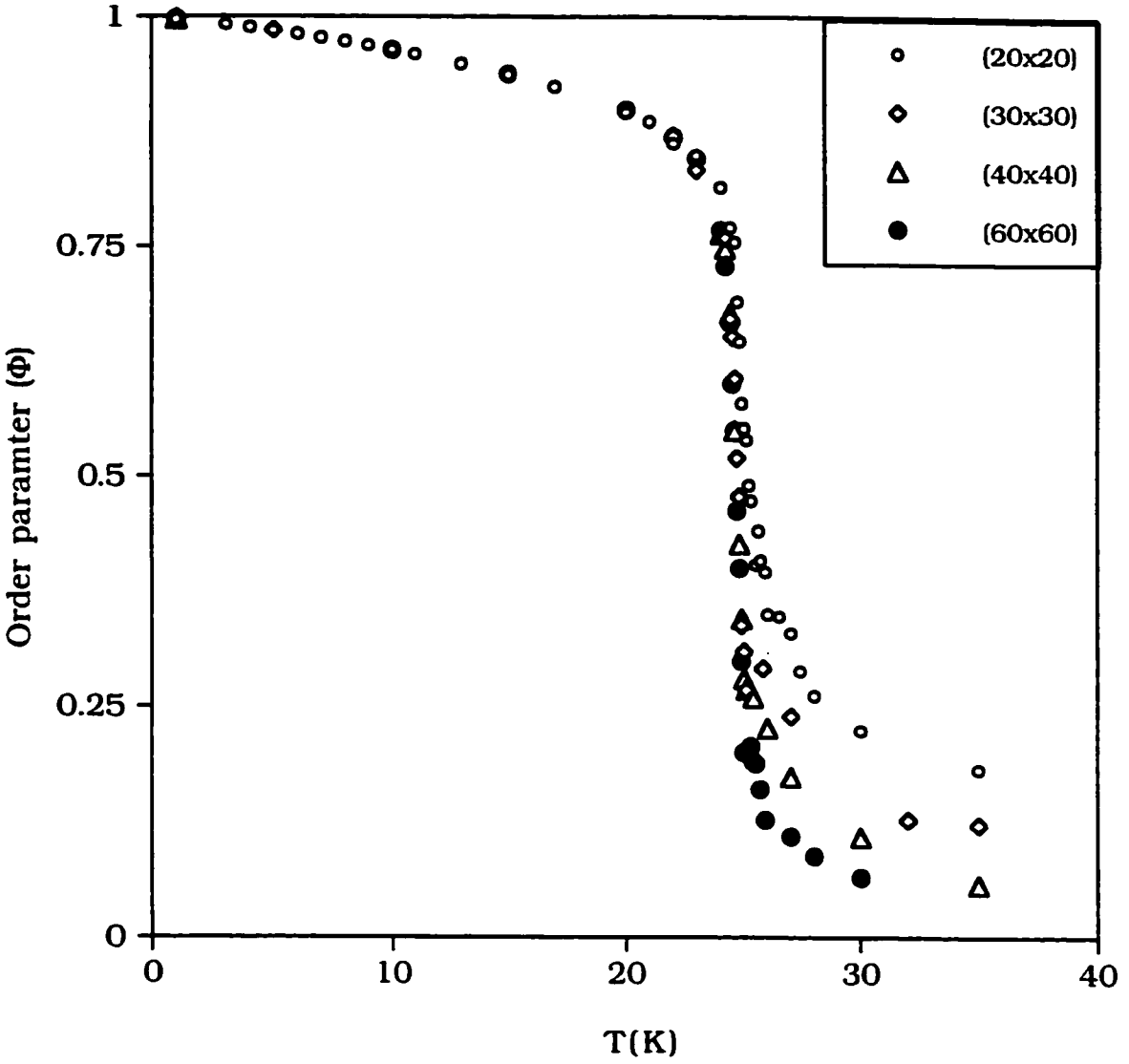

Figure 6.8 The order parameter as a function of temperature for several systems of nitrogen adsorbed on NaCl(00). The order parameter Φ is constructed from the azimuthal angle of the individual molecules.

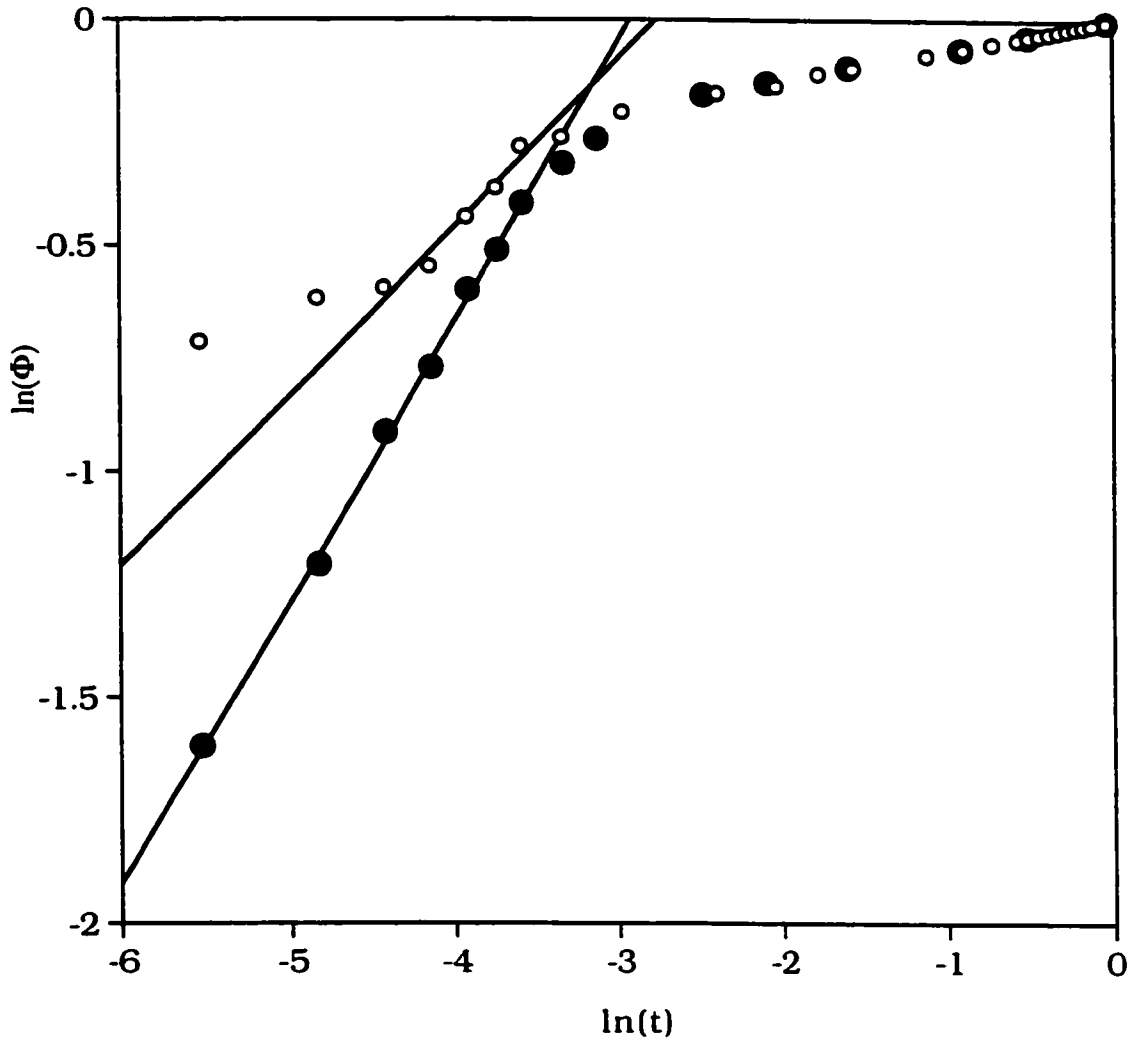

$\ln(\Phi) = 0.374\ln(t) + 1.036$ for (20x20) system (o)

$\ln(\Phi) = 0.620\ln(t) + 1.814$ for (60x60) system (●)

Figure 6.9. Log-log plot of the order parameter as a function of reduced temperature for (N=400) and (N=3600). The value of the critical exponent β is given by the slope of the curve and found to have a value (β = 0.374) for (20x20) system and (β = 0.620) for the (60x60) system which differ significantly from the Ising value (β = 0.125).

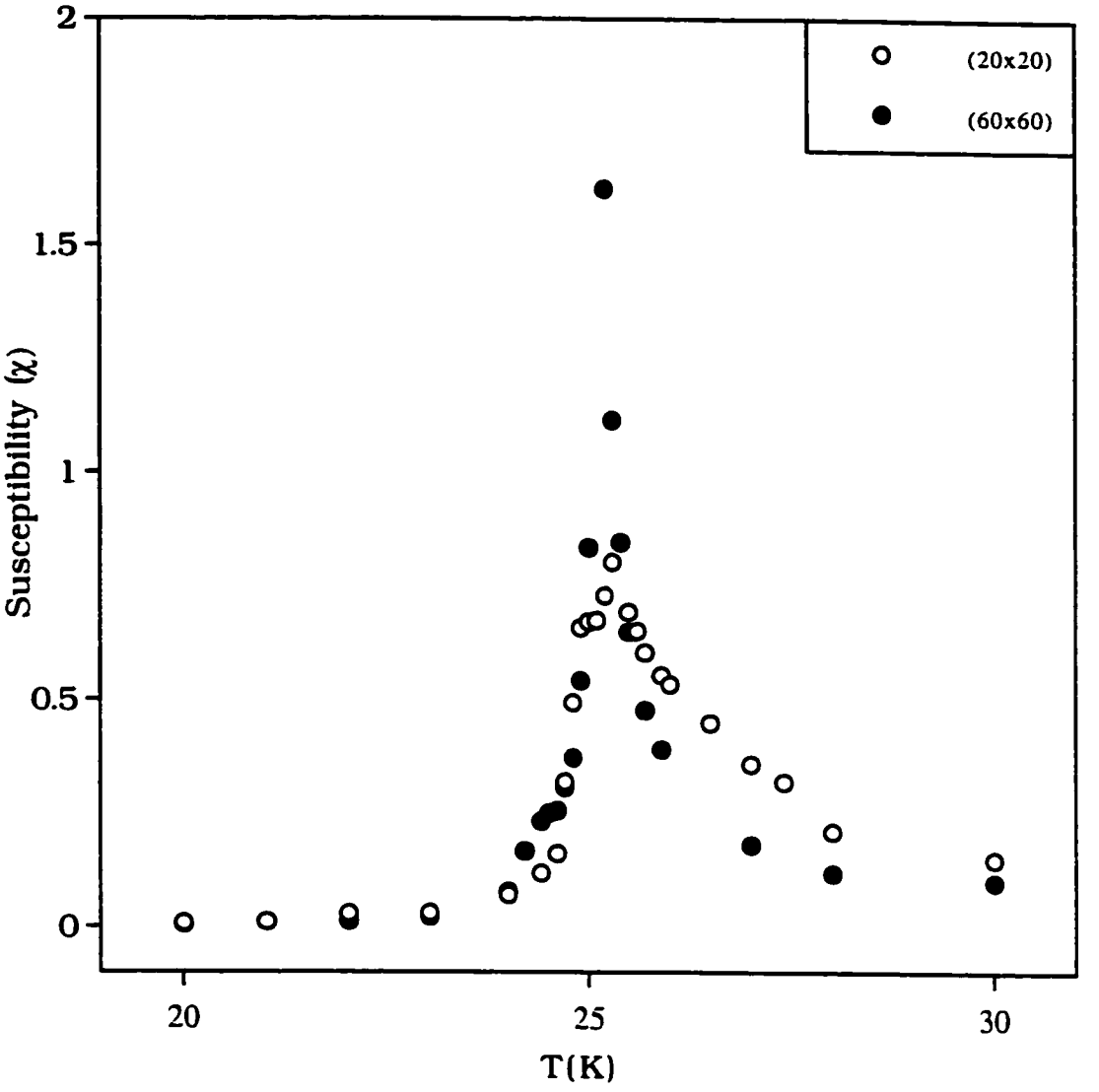

Figure 6.10. The susceptibility (χ) as a function of temperature for (20x20) and (60x60) systems

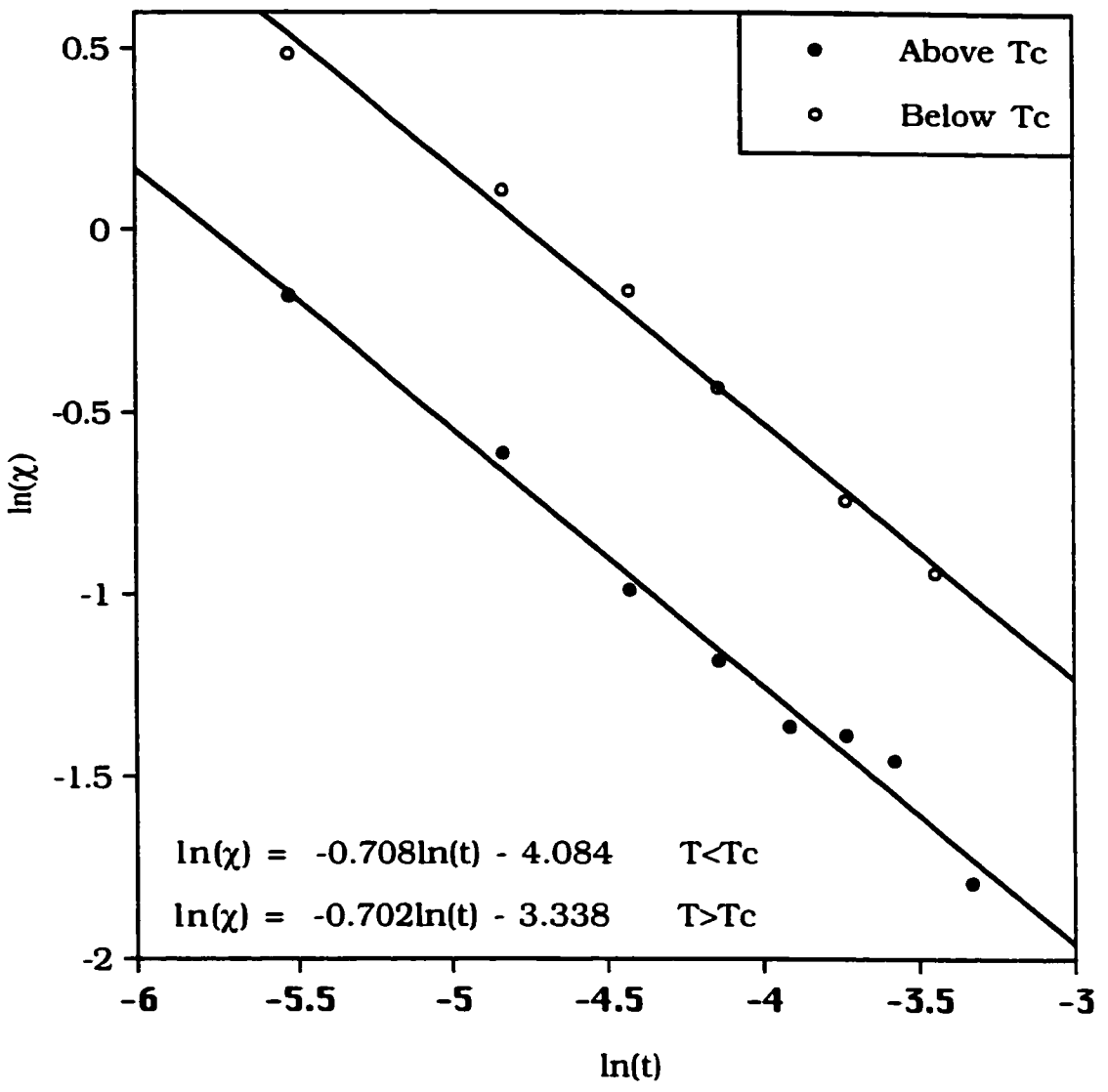

Figure 6.11. Log-log plot of the susceptibility as a function of reduced temperature below and above T_c (N=3600). The two lines have almost identical slopes (γ=0.708, 0.725) which differ significantly from the Ising value (γ = 1.75). The offset of the curves above and below T_c indicates that the prefactors above and below T_c are not the same.

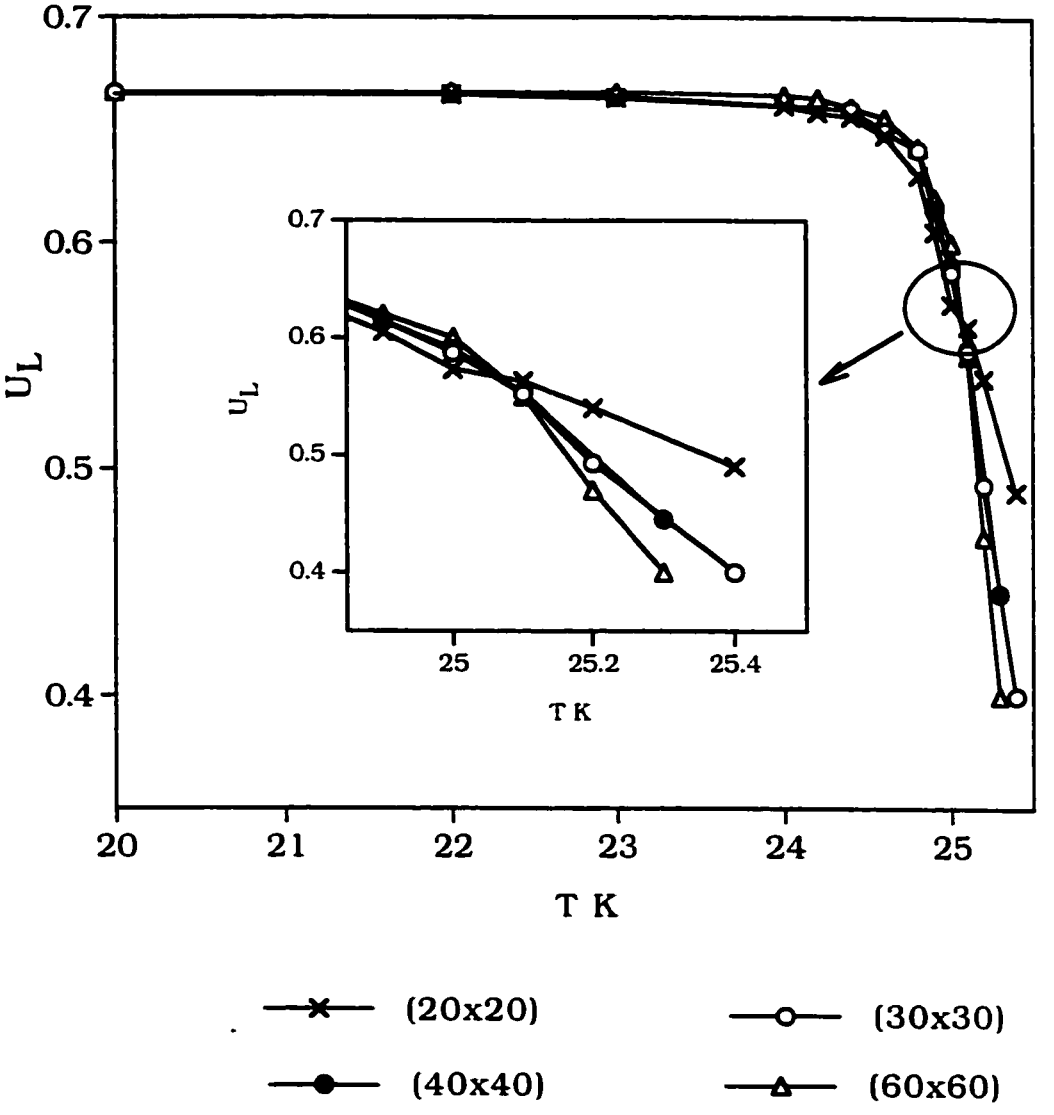

Figure 6.12. Binder fourth order cumulant $U_L(T)$ as a function of temperature T for several values of the lattice size L. The critical temperatures is T_c = 25.087 ±0.004 in units of K.

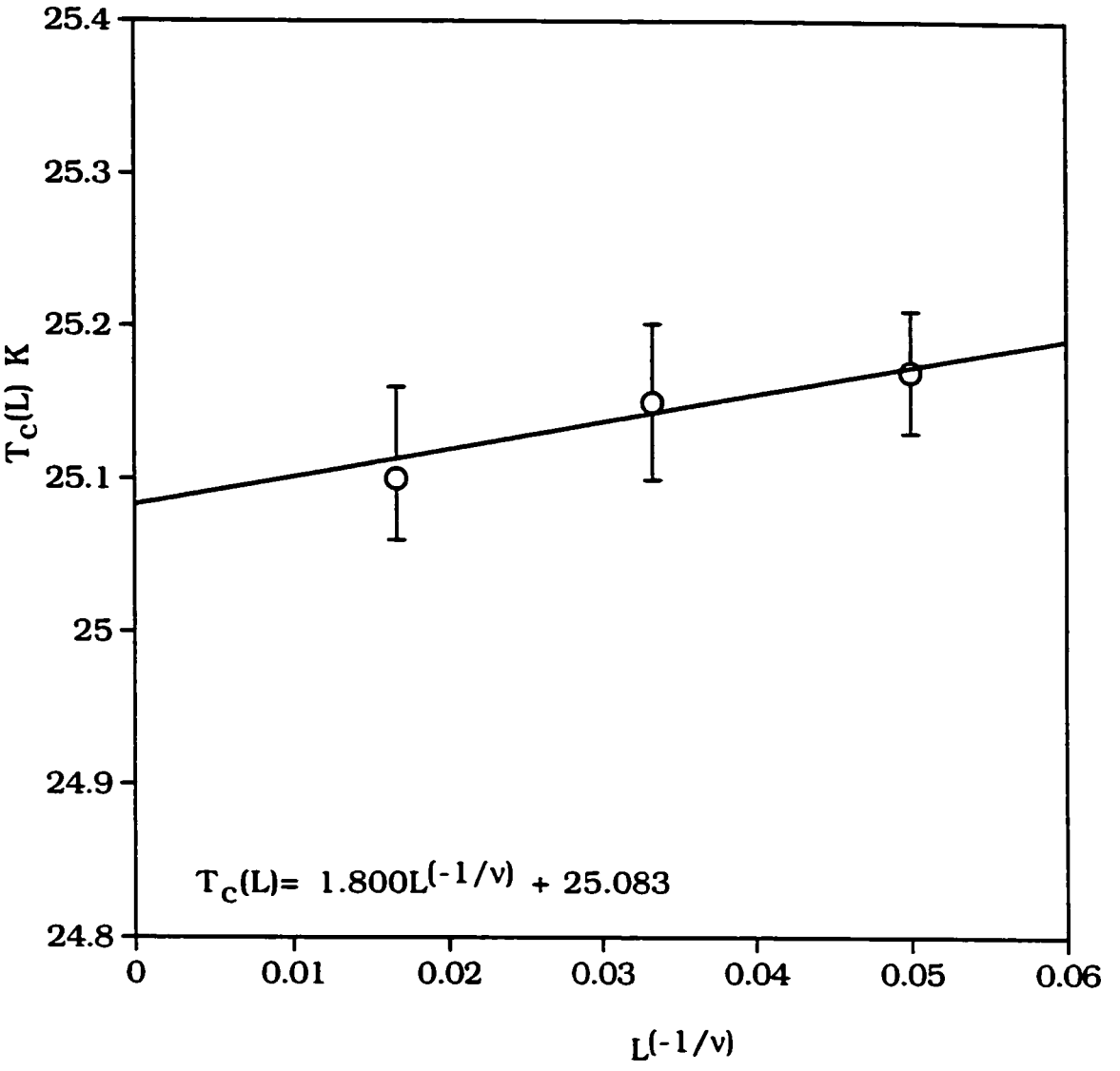

Figure 6.13. The finite critical temperatures $T_c(L)$ versus $L(-1/\nu)$ with $\nu=1.0$ and $T_c=25.08K$.

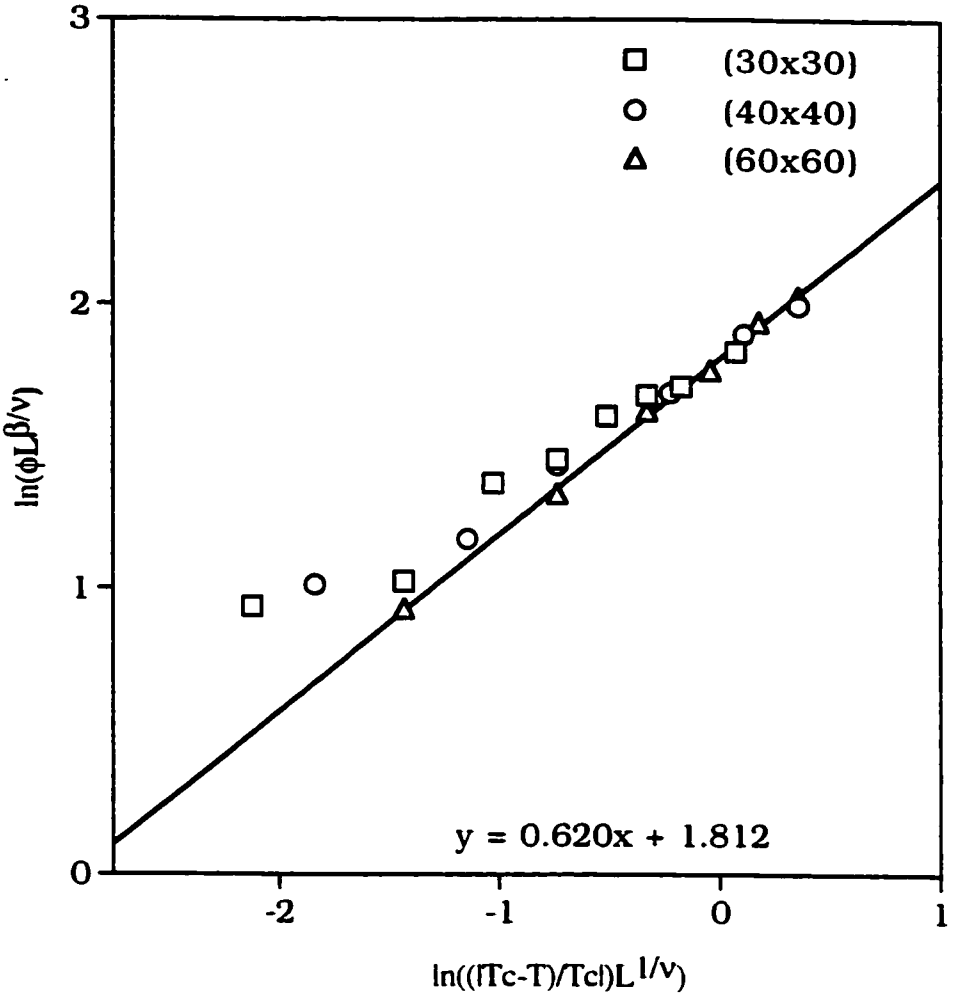

Figure 6.14. Log-log plot of finite size scaling for the order parameter of N_2/NaCl(001) system with periodic boundary conditions above and below T_c.

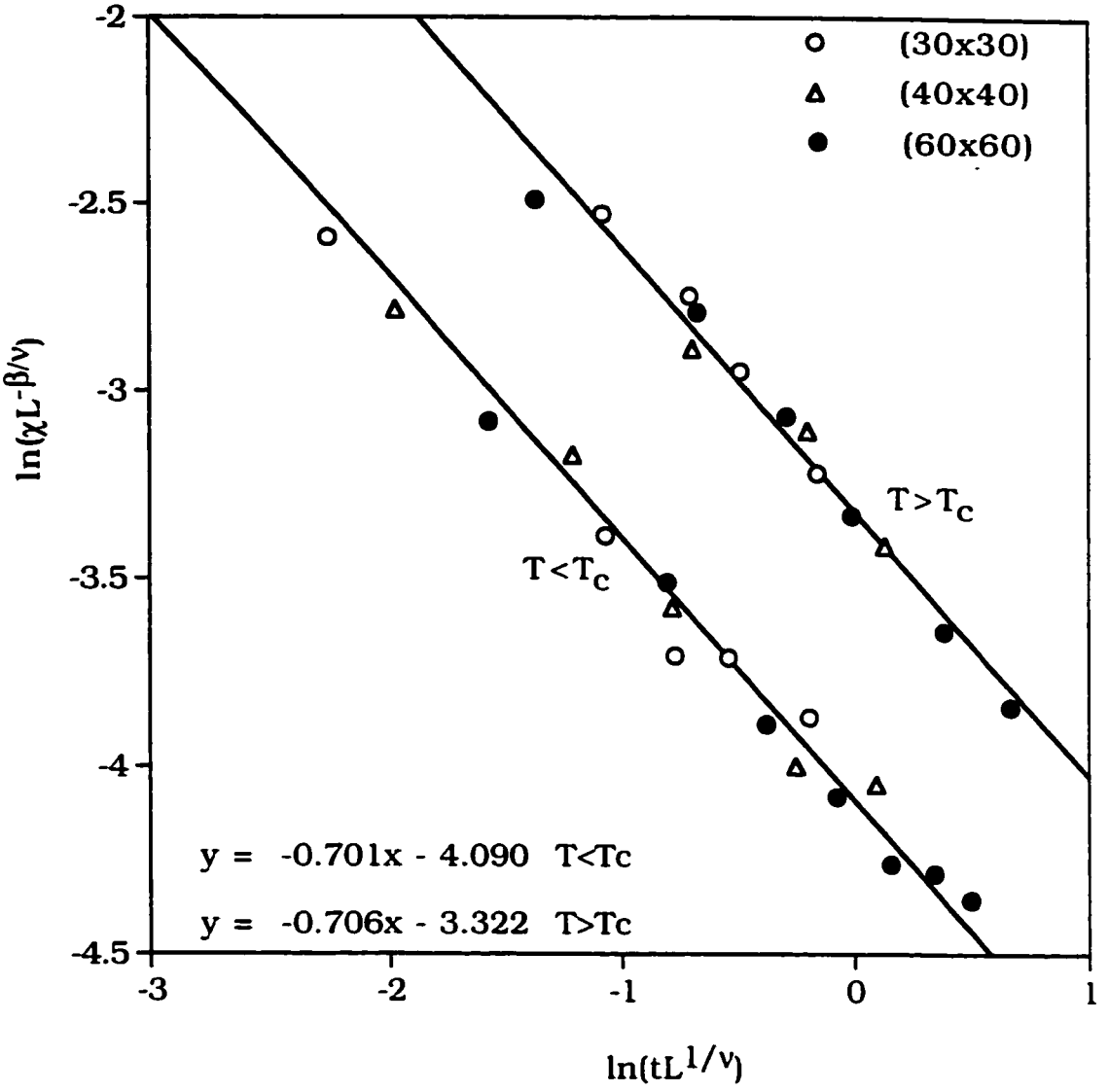

Figure 6.15. log-log plot of the finite size scaling for the susceptibility of N_2 /NaCl(001) with periodic boundary conditions above and below T_c.

7.0. Conclusions

This work is concerned with an understanding of adsorption energy, geometry, adsorbate orientation and phase transitions of two-dimensional structures of small molecules (CO and N_2) physisorbed on ionic surfaces, *i.e.* NaCl(001) and MgO(001). Attempts have been made in this work to understand the manner in which ordering, orientation and phase transitions depend on both the underlying substrate and overlaying adsorbate (by varying them), as well as the effects of coverage, pressure, and temperature.

Monte Carlo simulations, using realistic interaction potentials, have been used to accomplish the objectives of this work. The molecule-molecule and molecule-surface interactions employ the two-body approximation and use the Tang-Toennies and Buckingham potentials for non-electrostatic interaction. The electrostatic interactions are mediated by point charges and point dipoles assigned to each of the two atom sites of the adsorbed molecules. Polarization effects have also been included.

For the first time, finite temperature ($T<60$ K) simulations have been used to determine the geometry and stability of layers of these molecules adsorbed on the MgO(001) and NaCl(001) ionic substrates.

The results obtained from these simulations agree well with the experimental data reported from LEED, HAS and PIRS experiments [30-38]. These simulations also reconcile some of the seemingly contradictory experimental results [35-37]. In addition, the simulations predicted novel behaviour in the form of examples of the devil's staircase (CO/MgO & N_2/MgO) and critical phenomena with nonuniversal behaviour (N_2/NaCl).

For all of these systems, a single adsorbed molecule was found to sit perpendicular to the surface over top of a cation site. In the case of CO, the carbon atom is down. The adsorption energies were found to be similar to the recent experimental values [32][79][82] for the three cases and as expected most of the adsorption energy comes from the electrostatic interactions.

For the CO/MgO system the CO molecules are found to form a *c(4×2)* structure (with rows of tilted molecules (θ=31°) separated by rows of untilted molecules). This structure was found to be the most stable structure below 41K. Above this temperature the *c(4×2)* structure became unstable and transformed into either a disordered phase or a *p(3×2)* structure. To determine the conditions under which this cases occurred, a model that allowed the study of the relative stability between *c*(4×2) and *p*(3×2) structures was developed. This model revealed that at

low pressure the $c(4\times2)$ structure undergoes a transition into a disordered phase. In both cases the phase transitions are accompanied by the desorption of some of the molecules. These results show that the phase transitions of $c(4\times2)$ structure into either a $p(3\times2)$ structure or disordered (1×1) phase depend on the partial CO pressure as well as the temperature and hence reconciles some of the results of the LEED experiment with those of the HAS & PIRS experiments. Other structures with an even lower density were examined and found to be stable at yet higher temperatures. These structures also consist of rows of tilted molecules separated by a characteristic number of rows of untilted (perpendicular) molecules. As the number of untilted rows increases, the adsorbate density decreases and the thermal stability increases. The process of increasing the number of untilted rows between the tilted rows defines the following sequence of transformations:

$$c(4\times2) \rightarrow p(3\times2) \rightarrow c(8\times2) \rightarrow p(5\times2) \rightarrow \ldots \rightarrow c(2\times2)$$

This proposed sequence might be the series of $(n\times2)$ structures observed experimentally and is an example of the devil's staircase phenomena.

To illustrate the effects of changing the adsorbate the adsorption of N_2 on MgO(001) were studied. Although CO and N_2 molecules have almost the same physical properties they were found to adopt different geometries on the MgO surface. This may be due to the difference in their quadrupole moment (CO is larger) and the fact that CO possesses a

permanent dipole moment. This certainly accounts for the fact that CO molecules bind more strongly to the MgO surface than N_2. Nonetheless, nitrogen molecules are also found to form a sequence of structures. At temperatures below 20 K the molecules adopt a $(\sqrt{13}x\sqrt{13})$ structure. Above 20 K molecules desorb from this structure and in all likelihood evolve into a less dense $(\sqrt{25}x\sqrt{25})$ structure. The $(\sqrt{25}x\sqrt{25})$ structure is stable up to 25 K, in agreement with HAS results. This system might also prove to be an example of the devil's staircase phenomena.

The success of our simulations in reproducing most of the experimental data reported on the above two systems (N_2 and CO on MgO(001)) is indeed a strong indication that the parameters and the electrostatic models used in this work are well chosen. This led us to extend this study to include the interesting N_2/NaCl(001) system. In agreement with experiments, we found that nitrogen molecules occupy every adsorption site and a uniform film is formed. Our simulations predict that the N_2 molecules form an ordered structure with p(2x1) symmetry at low temperatures (below 25.3 K). The molecules in this structure have a tilt angle of 29°. This ordered p(2x1) structure is found to undergo a phase transition into an orientationally (azimuthally) disordered phase at 25.087 K and falls into the universality class of the XY model with cubic anisotropy. This universality class is of interest because it predicts that the critical exponents have nonuniversal values.

The MC simulations of this system predict that two critical exponents are indeed nonuniversal ($\beta = 0.62$ and $\gamma = 0.704$) and show strong deviations from the Ising exponents, while two others retain their Ising values ($\alpha = 0$ and $\nu = 1$). Nonetheless, the exponents still obey Rushbrooke's scaling law, *viz.* $\alpha+2\beta+\gamma=2$, and Josephson's hyperscaling law, $d\cdot\nu = 2 - \alpha$. We thus identify the N_2/NaCl(001) system as a candidate for experimental studies that could test the properties of this unusual universality class.

Overall, the molecular systems are well reproduced and yield an accurate description of the adsorbate structures, along with their thermal stability and phase transitions. This is in part due to the detailed and accurate interaction potentials that are used. The success of our simulations in reproducing most of the experimental data reported on the above systems is indeed a strong indication that the parameters and the electrostatic models used in this work are well chosen. The adjustment made in the atom-ion repulsion parameters to give agreement between the calculated and the experimental binding energy, shows that the combining rules for atom-ion repulsion parameters overestimate the values of atom-ion repulsion parameters and hence these parameters should be adjusted in the same way in any future work on similar systems. Also, using point charges and point dipoles to model the electrostatic interaction of the adsorbed molecules was proven to be essential in these kinds of simulations.

In closing I would like to make some suggestions for future work.

1) Since the number of molecules changes in the CO/MgO(001) and N_2/MgO(001) systems during the transition from one phase to another, the Monte Carlo simulations using the grand canonical ensemble might yield even better results.

2) A simplified model of the N_2/NaCl(001) system might be used to perform more simulations and studies on this system. This model system should make the calculations much faster and hence make studies of the correlation function tractable and allow for a direct determination of the critical exponent ν of the correlation length ξ.

References

[1] A. Lakhlifi and C. Girardet, Surf. Sci., **241,** 400 (1991).

[2] W. A. Steele, *The Interaction of Gases with Solid Surfaces,* 1974, Pergamon Press, Oxford.

[3] S. C. Fain, Jr., M. F. Tony and R. D. Diehl, In *Proceedings of the Ninth International Vacuum Congress and Fifth International Conference on solid Surfaces,* pp. 129, Editor: J. L. Segovia, 1983, Imrenta Modema, Madrid.

[4] S. C. Fain, Jr., Ber. Bunsenges, Phys. Chem., **90**, 211 (1986).

[5] D. Marx, H. Wiechert, Adv. Chem. Phys., **95**, 213 (1996).

[6] G. Dash, *Films on Solid Surfaces,* 1975, Academic, New York; Contemp. Phys. **30**, 89 (1989).

[7] J. Heidberg, E. Kampshoff, R. Kuhnemuth and O. Schonekas, J. Electron Spectrosc. Relat. Phenon., **64/65,** 803 (1993).

[8] J. C. Polany and R. J. Williams, J. Chem. Phys., **88**, 3363 (1988).

[9] J. C. Polanyi and H. Rieley, *Photochemistry in the Absorbed State, in Dynamics of Gase-Surface Interactions,* Editors: C. T. Rettner and M. N. R. Ashfold, 1991, The Royal Society of Chemistry, Cambridge.

[10] M. Bretz, Phys. Rev. Lett., **38**, 501 (1977).

[11] S. Alexander. Phys.Rev. Lett., **54A**, 353 (1978).

[12] M. J. Tejwani, O. Ferreira and O. E. Vilches, Phys. Rev. Lett., **44**, 152 (1980).

[13] G. E. Ewing, International Rev. Phys. Chem., **10,** 394 (1991).

[14] M. A Van Hove and G. A. Somorjai, Surf Sci., **199/300**, 487 (1994).

[15] E. Hulpke. *Helium Atom Scattering from Surfaces,* vol. 27, 1992, Springer, Berlin.

[16] S. A. Safron, Adv. Chem. Phys., **95**, 129 (1996).

[17] J. Heidberg. L. Cahbigon, E. Kampshoff. M. Kandel, R. Kuhnemuth, D. Meine, B. Redlich, O. Schonekas, M. Suhren, H. Weiss and D.

Wetter, In *Adsorption on Ordered Surfaces of Ionic Solids and Thin Films*, pp. 46, Editors: H. J. Freund and E. Umbach, 1993, Springer, Berlin.

[18] D. Marx, Phys. Rep., **125**, 1 (1985).

[19] M.H. W. Chan, A. D. Migone,K. D. Miner, Z. R. Li, Phys. Rev. B, **30**, 2681 (1984)

[20] M.P. Allen and D. J. Tildesley, *Computer Simulation in Chemical Physics*, 1993, Kluwer Academic Publishers, Dordrecht.

[21] M.P. Allen and D. J. Tildesley, *Computer Simulation of Liquids*, 1987, Clarendon Press, Oxford.

[22] B. Hetenyi and B. J. Berne, J. Chem. Phys., **114**, 3674 (2001).

[23] B. Kuchta and R. D. Etters, J. Computational Phys., **108**, 353 (1993)

[24] O. G. Mouritsen, *Computer Studies of Phase Transitions and Critical Phenomena*, 1984, Springer-Verlag, Berlin Heidelberg.

[25] W. Hu, M.-A. Saberi, A. Jakalian, and D. B. Jack, J. Chem. Phys., **106**, 2547 (1997).

[26] K. Binder, D. W. Hermann, *Monte Carlo Simulations in Statistical Physics an Introduction*, 1992, Springer-Verlag, Berlin.

[27] N. –T. Vu and D. B. Jack, J. Chem. Phys., **108**, 5653 (1998).

[28] M. E. J. Newman and G. T. Barkema, *Monte Carlo Methods in Statistical Physics*, 1999, Clarendon Press, Oxford.

[29] O. Engkvist and Anthony J. Stone, J. Chem. Phys., **112**, 6827 (2000).

[30] T. Angot and J. Suzanne, In: *The Structure of Surfaces III*, Editors. S. Y. Tong, M. A. Van Hove, K. Takayanagi and X. D. Xie, Vol. 24, 1991, Springer, Berlin.

[31] K. Madih, PhD Thesis, University d' Aix-Marseille 2, 1986.

[32] M. Trabelsi, K. Madih and J. P. Coulomb, Phase transitions, **30**, 103 (1991).

[33] P. Audibert, M. Sidoumou and J. Suzanne, Surf. Sci. Lett., **273**, L467 (1992).

[34] M. Trabelsi, J. P. Coulomb, D. Degenhardt, and H. Lauter, Surf. Sci., **377-378**, 38 (1997)

[35] V. Panella, J. Suzanne, P.N.M. Hoang and C. Girardet, J. Phys. (Paris), **4**, 905 (1994).

[36] R. Gerlach, A. Glebov, G. Lange, J.P. Toennies and H. Weiss, Surf. Sci., **331-333**, 1490 (1995).

[37] J. Heidberg, M. Kandel, D. Meine and U. Wild, Surf. Sci., **331-333**, 1467 (1995).

[38] F. Trager, PhD thesis, Max-Planck-Institut für Strömungsforschung, Göttingen, Germeny (2001)

[39] S. Aubry, In *Solitons and Condensed Matter Physics*, pp.264, Editors: A. R. Bishop and T. Schneider, 1978, Springer, Berlin.

[40] P. Bak, Rep. Prog. Phys., **45**, 587 (1982).

[41] G. A. Somorjai, *Introduction to Surface Chemistry and Catalysis*, 1994, John Wiley and Sons, New York.

[42] V. Bortolani, N.H. March, and M. P. Tosy, *Interaction of Atoms and Molecules with Solid Surfaces*, 1990, Plenum press, New York.

[43] Hans Luth, *Surface and Interfaces of Solids*, 1993, Springer-Verlag, Berlin Heidelberg. Germany.

[44] Gabor A. Somorjai, *Introduction to Surface Chemistry and Catalysis*, 1994, John Wiley and Sons, Inc.

[45] P. W. Atkins, *Physical Chemistry*, 1990, W. H. Freeman and company.

[46] J.Estel,H. Hoinkes, H. Kaarmann, H. Nahr, and H. Wilsch, Surf. Sci., **65**, 393 (1976).

[47] J. Villain and M. B. Gordan, J. Phys. C: Solid State Phys. **13**, 3117 (1980).

[48] D. P. Woodruff and T. A. Delchar, *Modern Techniques of Surface Science*-Second Edition, 1994, Cambridge University Press.

[49] M. Prutton, *Introduction to Surface Physics,* 1994, Clarendon Press, Oxford.

[50[P. Zeppenfeld, U. Becher, K. Kern and G. Comsa, Phys. Rev. B., **45**, 5179 (1991).

[51] H. Kawamura and Y. Sakamoto, Phase Trans., **53** 165 (1995).

[52] H. E. Stanley, *Introduction to Phase Transitions and Critical Phenomena*, 1971, Oxford University Press.

[53] J. M. Yeomans, *Statistical Mechanics of Phase Transitions,* 1992, Clarendon Press, Oxford.

[54] L. D. Roelofs and P. J. Estrup, Surf. Sci., **125**, 51 (1983)

[55] J. V. José, L. P. Kadanoff, S. Kirkpatrick, and D. R. Nelson, Phys. Rev. B, **16**, 1217 (1977).

[56] G. Y. Hu and S. C. Ying, Physica, **140A**, 585 (1987).

[57] A. M. Brashan and H. Gonrad, *Vibration at Surfaces*, 1987, Elsevier, Amsterdam.

[58] Y. P. Feng and M. H. W. Chan, Phys. Rev. Lett., **71**, 3822 (1993).

[59] O. G. Mouritsen and A. J. Berlinsky, Phys. Rev. Lett., **48**, 181 (1981)

[60] L. W. Bruch and F. Y. Hansen, Phys. Rev. B, **57**, 9285(1997)

[61] J. C. Polanyi, R. J. Williams and S. F. O'Shea, J. Chem. Phys., **94**, 978 (1991).

[62] M. Bienfait, in: *Dynamics of Molecular Crystals, Proceedings of the 41st International Meetingof Physical Chemistry*, 1987, Elsevier, Amsterdam.

[63] P. N. M. Hoang, S. Picaud, and C. Girardet, Surf. Sci., **360**, 261 (1996).

[64] C. Minot, M. A. van Hove, J.-P. Biberian, Surf. Sci., **346**, 283 (1996).

[65] K. Jug and G. Geudtner, J. Chem. Phys., **105**, 5285 (1996).

[66] G. Pacchioni, Surf. Rev. Lett., **7**, 277 (2000).

[67] J. A. Snyder, D. R. Alfonso, J. E. Jaffe, Z. Lin, A. C. Hess and M. Gutowski, J. Phys. Chem. B, **104,** 4717 (2000).

[68] R. Wichtendahl, M. Rodriguez-Rodrigo, U. Hartel, H. Kuhlenbeck and H. -J. Freund, Phys. Stat. Sol. (a) **173**, 93 (1999)

[69] S. Furuyama, H.Fujii, M. Kawamura, and T. Morimoto, J. Phys. Chem., **82**, 1028 (1978).

[70] E. A. Paukshtis, R. I. Soltanŏv, and N. E. Yurchenko, Reaction Kinet. Catal. Lett., **16**, 93 (1981).

[71] C. R. Henry, C. Chapon, and C. Duriez, J. Chem. Phys., **95**, 700 (1991).

[72] J.-W. He, C. A. Estrada, J. S. Corneille, M.-C. Wu, and D. W. Goodman, Surf. Sci., **261**, 164 (1992).

[73] R. Dovesi, R. Orlando, F. Ricca, and C. Roetti, Surf. Sci., **186**, 267 (1987).

[74] C. Pisani, R. Dovesi, R. Nada, and S. Taniro, Surf. Sci., **216**, 489 (1989).

[75] G. Pacchioni, G. Cogliandro and P. S. Bagns, Surf. Sci., **255**, 344 (1991).

[76] S. A. Pope, I. H. Hillier, M. F. Guest, E. A. Colbourn and J. Kendrick, Surf. Sci., **139**, 299 (1984).

[77] M. A. Nygren, L. G. M. Pettersson, Z. Barandiaran and L. Seijo, J. Chem. Phys., **100**, 2010 (1994).

[78] K. M. Neyman, S. Ph. Ruzankin and N. Rosch, Chem. Phys. Lett., **246**, 546 (1995).

[79] Thesis work of M. Kandel as communicated by H. Weiss (08/98).

[80] W. Steele, Chem. Rev., **93,** 2355 (1993).

[81] J. P. Coulomb, In *Phase Transitions in Surface Films* 2, Editors: H. Taub, G. Torzo, H. J. Lauter, C. S. Fain, Jr., 1991, Nato ASI 267, Plenum Press, New York.

[82] D. J. Dai, *J. Chem. Phys.*, **104**, 2461 (1996).

[83] M. Bojan and W. A. Steele, *Langmuir*, **3**, 116 (1987).

[84] A. Inaba, T. Shirakami, and H. Chihara, *surf. Sci.*, **242**, 202 (1991).

[85] H. You and S. C. Fain, Jr., Surf. Sci., **151**, 361 (1985).

[86] J. Piper, J. A. Morrison, and C. Peters, Mol. Phys., **53**, 1463 (1984).

[87] T. A. Scott, Phys. Rep., **C27**, 89 (1976).

[88] D. E. Stogryn and A.P. Stogryn, Mol. Phys., **11**, 371 (1966).

[89] A. Terlain and Y. Larher, Surf. Sci., **93**, 64 (1980).

[90] J. Heidberg, E. Kampshoff, and M. Suhren, J. Chem. Phys., **95**, 9408 (1991)

[91] D. Schmicker, J. P. Toennies, R. Vollmer, and H. Weiss, J. Chem. Phys., **95**, 9412 (1991).

[92] N.-T. Vu, PhD thesis. Concordia University (in preparation)

[93] N.-T. Vu, A. Jakalian, and D. B. Jack, J. Chem. Phys., **106**, 2551 (1997).

[94] E. Bayong, and H. T. Diep, Phys. Rev. **B59**, 11919 (1999).

[95] G. Pacchioni, G. Cogliandro and P. S. Bagus, Int. J. Quant. Chem., **42**, 1115 (1992).

[96] S. Picaud, P. N. M. Hoang, C. Girardet, Surf. Sci., **294**, 149 (1993).

[97] A. Zangwill, *Physics at Surfaces*,1988, Cambridge University Press.

[98] V. J. Barcaly, D. B. Jack, J. C. Polanyi, and Y. Zeiri, J. Chem. Phys., **97**, 9458 (1992).

[99] R. William, WMIN, *A Computer Program to Model Molecules and Crystals in Terms of Potential Energy Functions*, 1981, Oak Ridge National Laboratory Oak Ridge, Tennessee 37830.

[100] J. E. Gready, G. B. Backsay, and N. S. Hush, Chem. Phys., **31**, 375 (1978).

[101] W. D. Cornell, P. Cieplak, C. I. Bayly, I. R. Gould, K. M. Merz Jr., D. M. Ferguson, D. C. Spellmeyer, T. Fox, J. W. Caldwell, P. A. Kollman, J. Am. Chem. Soc., **117**, 5179 (1995).

[102] C. A. Burrus, J. Chem. Phys., **28**, 427 (1958).

[103] C. Graham, J. Pierrus and R. E. Raab, Molec. Phys., **67**, 939 (1989).

[104] G. H. F. Diercksen and A. J. Sadlej, Chem. Phys., **96**, 17 (1985).

[105] N. J. Bridge and D. Buckingham, Proc. R. Soc., **295A**, 334 (1966).

[106] A. J. Stone, Mol. Phys., **56**, 1065 (1985).

[107] H. Hettema, P. E. S. Wormer and A. J. Thakkar, Mol. Phys., **80**, 533 (1993).

[108] W. J. Meath, and A. Kumar, Int. J. Quantum Chem., **S24**, 501 (1990).

[109] A. Kumar and W. J. Meath, Theor. Chim. Acta., **54**, 131 (1992).

[110] G. D. Zeiss and W. J. Meath, Mol. Phys., **33**, 1155 (1977).

[111] M. A. Saberi, M. Sc. Thesis, Concordia University (1996).

[112] Westerhoff et al. Z. Phys. B, **100**, 417 (1996).

[113] H. J. Boham and R. Ahlrichs, Mol. Phys., **55**, 1159 (1985).

[114] M. Karplus and R. N. Porter, *Atoms and Molecules*, 1970, Benjamin/Cummings, Menlo Park.

[115] F. Mulder, G. F. Thomas, and W. J. Meath, Mol. Phys., **41**, 249 (1980).

[116] C. Hattig and B. A. Hess, J. Chem. Phys., **105**, 9948 (1996).

[117] A. W. Meredith and A. J. Stone, J. Chem. Phys., **104**, 3058 (1996).

[118] J. E. Lennard-Jones and B. M. Dent, Trans. Farad. Soc., **24**, 92 (1928).

[119] K. T. Tang and J. P. Toennies, Z. Phys. D, **1**, 91 (1986).

[120] Habitz, P., Tang, K. T., Toennies, J. P., Chem. Phys. Lett., **85**, 461 (1982).

[121] C. Douketis, G. Scoles, S. Marchetti, M. Zen, and A. Thakkar, J. Chem. Phys., **76**, 3057 (1982).

[122] P.W. Fowler, P. J. Knowles, and N. C. Pyper, Mol. Phys., **56**, 83 (1985).

[123] N. C. Pyper, and P. Popelier, J. Phys.: Condens. Matter., **7**, 5013 (1995).

[124] U. Öpik, Proc. Phys. Soc. London, **92**, 566 (1967).

[125] R. R. Freedman and D. Kleppner, Phys. Rev. A, **14,** 1614 (1976).

[126] A. D. McEachran, A. D. Stauffer, and S. Greita, J. Phys. B **12**, 3119 (1979).

[127] M. Matsui, J. Chem. Phys., **91**, 489 (1989).

[128] E. Escalona-Platero, D. Scarano, G. Spoto, and A. Zecchina, Faraday Discuss. Chem. Soc., **80**, 183 (1985).

[129] N. C. Pyper and P. Popelier, Proc. R. Soc. London, Ser. A, **398**, 377 (1985).

[130] H. M. Kelly and P. W. Fowler, Mol. Phys., **80**, 135 (1993).

[131] M. Matsui and W. R. Busiig, Phys. Chem. Minerals, **11**, 55 (1984).

[132] P. W. Fowler and P. A. Madden, Phys. Rev. B, **29**, 1035 (1984).

[133] P. W. Fowler and N. C. Pyper, Proc. R. Soc. A, **398**, 377 (1985).

[134] R. P. McEachran, A. D. Stauffer and S. Greita, J. Phys. B, 12,3119 (1979)

[135] P. W. Fowler and N. C. Pyper, Mol. Phys., **59**, 317 (1986).

[136] N.-T. Vu and D. B. Jack (unpublished).

[137] V. J. Barclay, D. B. Jack, J. C. Polanyi, and Y Zeiri, J. Chem. Phys., **97**, 9458 (1992).

[138] T. L. Gilbert, J. Chem. Phys., **49**, 2640 (1968).

[139] T. L. Gilbert, O. C. Simpson, and M. A. Williamson, ibid, **63**, 4061 (1975).

[140] F. T. Smith, Phys. Rev. A, **5**, 1708 (1972).

[141] N. Metropolis, A. W. Rosenbluth, M. N. Rosenbluth, A. H. Teller, and E.Teller, J. Chem. Phys., **21**,1078(1953).

[142] J. J. Binney, N. J. Dowrick, A. J. Fisher and M. E. J. Newman, *The Theory of Critical Phenomena an Introduction to the Renormalization Group*, 1992, Oxford University Press.

[143] D. Nicholson and N. G. Parsonage, *Computer Simulation and Statistical Mechanics of Adsorption*, 1982, Academic Press, New York.

[144] W, Hu, M.Sc. Thesis, Concordia University (1997).

[145] A. B. MacIsaac, J. P. Whithead, K. De'Bell, and P. H. Poole, Phys. Rev. Lett., **77**, 739 (1996)

[146] K. De'Bell, A. B. MacIsaac, I. N. Booth, and J. P. Whitehead, Phys. Rev. B, **55**, 15108 (1997).

[147] K. Binder, Annu. Rev. Phys. Chem., **37**, 401 (1992).

[148] K. Binder, Phys. Rev. Lett., **47**, 693 (1981).

[149] A. K. Sallabi and D. B. Jack, J. Chem. Phys., **112**, 5133 (2000)

[150] M. C. Desjonquères and D. Spanjard, *Concepts in Surface Physics*, (2nd ed.), 1996, Springer, Berlin.

[151] C. Girardet, P.N. M. Hoang, and S. Picaud, Phys. Rev. B, **53**, 16615 (1996).

[152] H. Wiechert and K. D. Kotmann, Surf. Sci., **441**, 65 (1999).

[153] A. D. Migone, H. K. Kim, M. H. W. Chan, J. Talbot, D. J. Tildesley, and W. A. Steele, Phys. Rev. Lett., **51**, 192 (1983).

[154] A. E. Ferdinand and M. E. Fisher, Phys. Rev., **185**, 832 (1969).

[155] L. Onsager, Phys. Rev., **65**, 117 (1944).

[156] K. De' Bell, A. B. MacIsaac, I. N. Booth, and J. P. Whithead, Phys. Rev. B, **55**, 15108 (997).

[157] J. Tobochnik and G. V. Chester, Phys. Rev. B, **20**, 3761 (1979).

[158] G. Kamieenarz and H. W. J. Blote, J. Phys. A, **26**, 201 (1993).

[159] D. Loison and P. Simon, Phys. Rev. B, **61**, 6114 (2000).

[160] A. K. Sallabi and D. B. Jack. Phys. Rev. B, **62**, R4841 (2000).